Institut für Verfahrenstechnik der
Technischen Universität München

Prediction of Adsorption Equilibria of Gases

Ugur Akgün

Vollständiger Abdruck der von der Fakultät für Maschinenwesen der
Technischen Universität München zur Erlangung des akademischen Grades eines

Doktor-Ingenieurs

genehmigten Dissertation.

Vorsitzender:	Univ.-Prof. Dr.-Ing. Weuster-Botz
Prüfer der Dissertation:	1. Univ.-Prof. Dr.-Ing. A. Mersmann, emeritiert
	2. Univ.-Prof. (komm. L.) Dr.-Ing. J. Stichlmair, emeritiert

Die Dissertation wurde am 25.10.2006 bei der Technischen Universität München
eingereicht und durch die Fakultät für Maschinenwesen am 21.12.2006 angenommen.

Acknowledgments

I would like to express my deep and sincere gratitude to my supervisor, Professor Dr.-Ing. Alfons Mersmann, em. His wide knowledge and his logical way of thinking were of great value for me. His understanding, encouraging and personal guidance provided an ideal basis for the present thesis.

I am deeply grateful to Professor Stichlmair, who was member of my committee. My sincere thanks are to Professor Weuster-Botz for acting as chairman of my examination. I especially thank Professor Lercher and Dr. Staudt for the help extended to me and the valuable discussion that I had with them during my research.

Special thanks are to Dr.-Ing. PhD Walter Roith for his guidance. Only people like him, who have walked the same rocky way, can understand the efforts we made and the happiness we received.

For giving me the impetus to restart the thesis after a break of several years I would like to thank Dr.-Ing. Axel Eble.

I am grateful to Dr.-Ing. Lutz Vogel for the experiences we shared on the bus route 53 in Munich, Dr.-Ing. Björn Braun for Schafkopfen, Dr.-Ing. Frank Stenger for listening, Dr.-Ing. Lydia Günther for Rock and Roll, Dr.-Ing. Carsten Mehler and Dr.-Ing. Michael Löffelmann for enjoying life in Munich. Especially I would like to thank Carsten Sievers and Manuel Stratmann from the Lehrstuhl für Technische Chemie 2 at the Technische Universität München and Andreas Möller from the Institut für Nichtklassische Chemie e.V. at the Universität Leipzig for investing their limited time in adsorption experiments.

I thank all students and staff at the Lehrstuhl für Feststoff- und Grenzflächenverfahrenstechnik whose presence and spirit made the otherwise gruelling experience tolerable. Especially, I would like to thank Wolfgang Lützenburg and Ralf-Georg Hübner for soccer.

I thank the company Grace Davison for providing zeolite material.

Last but not least I am grateful to my wife Özlem for the inspiration and moral support she provided throughout my research work and for her patience. Without her loving support and understanding I would never have completed my present work.

Apollo and Daphne (1622-1625) from Gian Lorenzo Bernini

For my daughter *Ilayda Defne* Ingolstadt, 2006, Ugur Akgün

Table of Contents

Notation and Abbreviations

Latin Symbols

$A_{i,j}$	-	dimensionless interaction parameters
$\left(\frac{Al}{Si}\right)_j$	-	ratio of aluminium to silicon atoms in the zeolite molecule
C	-	parameter in isotherm prediction equation
C	-	absorption strength in the IR and UV range
C	J*m^6	interaction constant
C	mol/ m^3	overall concentration of gas
D	m	diameter of a particle sphere
D_{ax}	m^2/s	axial dispersion coefficient in a pipe
E	V/m	field intensity
E	J	potential energy between two molecules or particles
F	N	force
H_{Ads}	J/mol	specific enthalpy of adsorption
H_L	J/mol	specific heat of liquefaction
He	mol/(kg*Pa)	*Henry* coefficient
Ha	J	*Hamaker* constant
I	A	electrical current
I	J	ionisation energy of a molecule
IP	-	interaction parameter
K	-	effective isotherm slope in concentration pulse method
K_L	1/Pa	*Langmuir* constant
K_T	(1/Pa)^m	*Toth* constant

L	m	length of a pipe or pore capillary
M	kg/mol	molar mass
N	mol	number of moles
$\dot{N}$	mol/s	molar flow
N	$1/m^3$	number density of dipole moments in a volume element
N	-	partial loading in *Langmuir* isotherm
N_A	1/mol	*Avogadro* constant = $6{,}0225*10^{23}$ 1/mol
P	C/m^2	electrical polarisation
Q	$C*m^2$	quadrupole moment
R	-	parameter defined by equation (6.10)
R´	-	parameter defined by equation (8.14)
$\Re$	J/(K*mol)	universal gas constant = 8,3143 J/(K*mol)
R_m	m^3/mol	molar refraction
$R_{m,i}$	m^3/mol	molar refraction of the atom or ion
S	m^2	surface
S_{BET}	m^2/kg	specific surface of the adsorbent
T	K	temperature
V	m^3	volume
V	m^3	total volume of gas adsorbed on a solid surface
$\dot{V}$	m^3/s	volumetric flow rate
W	J	work
a	m/s^2	acceleration
a	-	integration parameter
a_{mol}	m^2/number	average area occupied by a molecule of adsorbate in the BET monolayer

a_i	$mol/(m^2*s*Pa)$	BET constant
a	-	slope
b	-	electronic overlap parameter
b	kg/mol	intercept of the linear form of the BET isotherm
b_i	$mol/(m^2*s)$	BET constant
b	-	interception value
c_0	m/s	speed of light in vacuum= 299792456.2 m/s
c	-	BET constant
c	J/(kg*K)	heat capacity
c	mol/m^3	gas concentration
d	m	tube inner diameter or pore diameter
d	m	distance (e.g. between particles)
e	C	charge of one electron = $1,60*10^{-19}$ C
f	Hz	oscillator strength
$f_{i,j}$	-	potential factor
g	Pa	BET constant
h	J*s	*Planck*'s constant = $6,6256*10^{-34}$ J*s
i	-	complex number $\sqrt{-1}$
k	J/K	*Boltzmann* constant = $1,3804*10^{-23}$ J/K
l	m	distance between positive and negative charges
m	kg	mass
m	kg/mol	slope of the linear form of the BET isotherm
m	-	*Toth* parameter, $0 < m < 1$
m_e	kg	mass of one electron = $9,11*10^{-31}$ kg
n	-	refractive index

$\bar{n}$	-	mean refractive index
n	mol/kg	loading
n_a	-	number of atoms in a formal solid molecule
n_c	-	number of positive charges in a formal solid molecule
p	Pa	pressure
p^0	Pa	saturation pressure
p_1	-	parameter of the analytical *Henry* function
p_2	-	exponential parameter of the analytical *Henry* function
q	C	charge
r	m	distance
r	m	pore radius
s	-	average number of bonding electrons per solid atom
$s_{cations}$	-	average number of positive charges per solid atom
ss	-	sum of square error of the method of *Margules*
t	s	time
t	nm	statistical thickness of the adsorbed multilayer in the t-plot
u	-	substitution parameter for the Lambert function
v	-	number of valence electrons of the cation in the stoichiometric formula of a zeolite
v	m^3/kg	specific volume
v_b	m^3/mol	molar volume of adsorptive at normal boiling point
v_{micro}	m^3/kg	micropore volume
v_{N2}	m^3/kg	micropore volume measured with nitrogen adsorption
v_{vdW}	m^3/mol	*van-der-Waals* volume of a gas molecule
w	m/s	velocity

x	-	reduced distance
x_1	-	diameter ratio
x_i	-	stoichiometric coefficient of matter i
y	mol/mol	molar fraction
y_1	-	diameter ratio
z	m	distance of the adsorptive from the adsorbent surface

Greek Symbols

Φ	J	potential of adsorption between an adsorptive molecule and the solid continuum
Ψ	–	differential function of *Toth*
α	$(C^{2}*m^{2})/J$	polarisability
α'	m^3	volumetric polarisability
$\overline{\alpha}$	$(C^{2}*m^{2})/J$	average polarisability
$\beta(T)$	m^3/mol	molar volume of adsorbate
β	–	affinity coefficient in *Dubinin* theory
β	Grad	contact angle
β	$J*m^6$	*London* constant
$\overline{\beta}$	$J*m^6$	average *London* constant
χ	–	porosity
ε	J/mol	adsorption potential of *Polanyi*
$\varepsilon(\omega)$	–	frequency dependent dielectric response function
ε_0	C/(V*m)	permittivity of free space = $8,854*10^{-12}$ C/(V*m)
ε_r	-	relative permittivity

ε	C/(V*m)	permittivity of a medium
φ	Grad	orientation angle of an adsorption pair to each other
φ	–	porosity
φ	–	ratio of partial pressure to saturation pressure
γ	–	material dependent constant
γ	N/m	surface tension
κ	–	function of the distribution of volume of the pores
λ	W/(m*K)	thermal conductivity
μ	J	chemical potential
μ	C*m	dipole moment (1 debye = $3{,}34*10^{-30}$ C*m)
μ_0	(V*s)/(A*m)	permeability of free space = $1.257*10^{-6}$ (V*s)/(A*m)
μ_r	–	relative permeability of a medium
μ	(V*s)/(A*m)	permeability of a medium
ν_0	1/s	frequency of the electron in the ground state
ν_e	1/s	main electronic absorption frequency = $3*10^{15}$ 1/s
ν_i	1/s	orbiting frequency of the molecule electrons
π	-	circle number = 3.1416
ρ	kg/m^3	density
ρ_{app}	kg/m^3	apparent density of the adsorbent
ρ_s	kg/m^3	true density of the adsorbent
$\rho_{j,at}$	$1/m^3$	average number density of solid atoms per volume
σ	C/m^2	charge density
σ	m	van-der-Waals diameter
τ	s	mean retention time
τ_D	s	mean system dead time

ω	Hz	frequency
ξ	Hz	imaginary frequency

Super- and Subscripts

A	*Avogadro*
BET	*Brunauer, Emmet, Teller*
C	Carrier gas
G	Gas
L	*Langmuir*
L	Liquid
L	*London*
LG	Liquid-Gas
S	Solid
SG	Solid-Gas
SL	Solid-Liquid
at	atom
app	apparent
ads	adsorption
adsads	adsorbate – adsorbate
adsorb	adsorbate
adsorp	adsorptive
aft	after
b	bulk
bef	before

c	critical
calc	calculated
dipcha	permanent dipole - electrical charge
dipind	permanent dipole – induced dipole
e	electron
exp	experimental
f	free
i	layer i
i	atom or ion i
i	adsorptive i
ij	interaction of adsorptive i with adsorbent j
indcha	induced dipole - electrical charge
indind	induced dipole – induced dipole
j	adsorbent j
jj	interaction of adsorbent j with itself
m	mole
max	maximum
mic	microporosity
micro	micropore
mix	mixed
mol	molecule
mon	monolayer
pred	predicted
quadind	permanent quadrupole – induced dipole
quadcha	permanent quadrupole – electrical charge

r	reduced
rel	relative
ref	reference
s	saturation, solid
stand	standard
vdW	*van-der-Waals*
0	layer 0
0	vacuum
∞	infinite
*	reduced

Abbreviations

BC	before *Christ*
COSMO-RS	conductor like screening model for real solutions
Δ_f	free place
DFT	density functional theory
G	gas molecule
GCMC	grand canonical Monte Carlo
IAST	ideal adsorbed solution theory
IR	infra red
IUPAC	International Union of Pure and Applied Chemistry
LTA	Linde type A zeolite
MD	molecular dynamics
MPRAST	multiphase predictive real adsorption theory
NP	number of data points
OP	occupied places
PBU	primary building unit
SBU	secondary building unit

SP	sorption place
UV	ultra violett
ZLC	zero length column

Dimensionless Numbers

$A_{indind} = \frac{3}{4}\sqrt{\frac{2Ha_j}{\pi\sigma_j^3 p_C}}\frac{T_C}{T_{Ads}}$ interaction parameter for the induced dipole – induced dipole potential

$A_{indcha} = \frac{\alpha_i s^2 e^2 \rho_{j,at}}{8\pi\varepsilon_0^2 (k T_{ads})\sigma_{i,j}}$ interaction parameter for the induced dipole – electrical charge potential

$A_{dipind} = \frac{\mu_i^2 \overline{\alpha_j}\rho_{j,at}}{12\pi\varepsilon_0^2 (k T_{ads})\sigma_{i,j}^3}$ interaction parameter for the permanent dipole – induced dipole potential

$A_{dipcha} = \frac{\mu_i^2 s^2 e^2 \rho_{j,at}}{12\pi\varepsilon_0^2 (k T_{ads})^2 \sigma_{i,j}}$ interaction parameter for the permanent dipole – electrical charge potential

$A_{quadind} = \frac{3Q_i^{\,2}\overline{\alpha_j}\rho_{j,at}}{40\pi\varepsilon_0^2 (k T_{ads})\sigma_{i,j}^5}$ interaction parameter for the quadrupole moment – induced dipole potential

$A_{quadcha} = \frac{Q_i^{\,2} s^2 e^2 \rho_{j,at}}{240\pi\varepsilon_0^2 (kT_{ads})^2 \sigma_{i,j}^3}$ interaction parameter for the quadrupole moment – electrical charge potential

$B = C\frac{T_c}{T_{ads}}\left(\frac{Ha_j}{\sigma_j^3 p_c}\right)^{3/2}$ parameter in the general isotherm

$$B' = \frac{T_c}{T_{ads}}\left(\frac{Ha_j}{\sigma_j^3 p_c}\right)^{3/2}$$ parameter in the general isotherm

$$D_{mic} = \sigma_j S_{BET} \rho_{solid}$$ degree of microporosity

$$E_{Ha}^* = \frac{Ha_j}{\sigma_j^3 p_c}$$ reduced *Hamaker* energy

$$IL = \frac{He \Re T}{\sigma_{i,j} S_{BET}}$$ initial loading

$$N = \frac{n \sigma_i^2 N_A}{S_{BET}}$$ number of molecule layers

$$P^* = \frac{\alpha_{solid} N_A \rho_{solid}}{\varepsilon_0 M_{solid}}$$ solid parameter

$$S^* = \frac{S_{BET} \sigma_i}{v_{micro}}$$ microporosity parameter

$$T_{r\_ads} = \frac{T_{ads}}{T_c}$$ reduced adsorption temperature

$$\beta^*(T) = N_A \sigma_i^3 \beta(\mathrm{T})$$ reduced molar volume of adsorbate

$$n^* = \frac{n}{He\, p}$$ reduced loading

$$n_s^* = \frac{n M_i}{v_{micro} \rho_{adsorb}} = \frac{n \beta(T)}{v_{micro}}$$ saturation degree or pore filling

$$1 - n_s^* = 1 - \frac{n M_i}{v_{micro} \rho_{adsorb}}$$ residual capacity

$$x = \frac{z}{\sigma_{ij}}$$ reduced distance

1. Introduction

The term adsorption denotes the mass transfer of substances from a fluid phase towards a solid surface. Thus, adsorption is a surface effect on solid phases. Accordingly one or more components (adsorptives) of a fluid (liquid or gas) are attached as adsorbate onto solids (adsorbents). The opposite effect is called desorption. Adsorption is a mass transfer mechanism in the two phase system solid/fluid [47]. At a given temperature this mass transfer leads to a thermodynamic equilibrium at which the concentrations of adsorptives and adsorbates remain constant. In the dilute region the solid adsorbate loading is proportional to the partial pressure of the adsorptive. The proportional constant is called *Henry* coefficient. At higher pressures the loading achieves saturation.

The ability of porous solids to reversibly adsorb large volumes of vapour was detected in the eighteenth century [48]: *Lowitz* studied in 1785 the effectiveness of charcoal in decolorizing various aqueous solutions and, in particular, its commercial application to the production of tartaric acid. *De Sussure* reported in 1812 on adsorption experiments of different gases onto porous substances whereas he also described the heat of adsorption. In 1876 *Gibbs* thermodynamically derived the law of adsorption by describing the relation of surface loading with gas or liquid concentration. Advances towards a quantitative description of the adsorption mechanisms were made in the twentieth century. Besides *Freundlich* and *Toth, Langmuir,* in particular, has to be mentioned. In 1916 he derived the theory of monomolecular covering of adsorbed surfaces. This concept was expanded to the theory of multilayer adsorption by *Brunauer*, *Emmet* and *Teller* (BET) in 1938. In 1914 *Polanyi* introduced the adsorption potential to describe the dependency of the adsorption equilibrium on temperature [24]. *Dubinin* extended this potential theory in 1959.

The laws of equilibrium thermodynamics, firstly applied to adsorption by *Prausnitz* in the nineteen sixties, were adopted to gas mixtures by *Myers*. He developed the theory of ideal adsorbed solutions (IAST) [24]. The developments are still ongoing. A

good example is the multiphase predictive real adsorption theory (MPRAST), by which *Markmann* described the equilibrium of a non-ideal adsorbate mixture with an energetically non-homogenous solid surface [8].

Some modern concepts have to be mentioned also. With the *Hellman-Feynman*-Theorem it is possible to specify intermolecular interactions. The basic idea is that the interaction correctly and completely can be described with the help of electrodynamic approaches if the charge distribution of the molecules is known [49]. The charge distribution itself can be calculated by applying the density functional theory as in the COSMO-RS-approach.

Mehler [50] found that it is still not possible to describe real solid surfaces using only theoretical quantum mechanical calculations. Surfaces seem to be too complex and unknown. On the contrary, he used adsorptive molecules with known properties as probes to characterize the solid surface. The interaction of these probes with the adsorbent is the basis in COSMO-RS for calculating the energy distribution of the solids. He quantified the interaction potentials of the solids via the *Henry*-coefficients determined by adsorption experiments.

It seems that *Henry*-coefficients are very important not only for describing the adsorption itself but also for characterizing the solid surfaces. The basis of all adsorption processes and theories is the single-component adsorption equilibrium and especially the *Henry*-coefficient. *Maurer* established an innovative way for a priori calculating *Henry*-coefficients, based only on gas and solid properties. He analysed very successfully the interaction of gases with energetically homogenous microporous adsorbents like activated carbon.

Nevertheless, there is no general model for the description of adsorption of any polar or nonpolar gases on any polar or nonpolar microporous adsorbent. After removing this deficiency it would be possible to improve the prediction not only of multicomponent adsorption problems which are real engineering tasks. Also the characterisation of solid surfaces with density functional theories would be one important step closer.

2. Objective

Hydrogen plays an eminent role in the processing of fuels and can become important for engines in motorcars with respect to CO_2-emissions. An important task is the design of a new unit for the purification of a contaminated hydrogen gas in a petrochemical plant. This gas is used in heterogeneous hydrogenation reactors with fixed bed catalysts. The separation of the contaminants from hydrogen leads to a very pure hydrogen feed to the reactors resulting in an improved selectivity. The tail gas of the separation no longer burdens the capacity of the whole petrochemical plant and can be burned as recycled fuel gas in the cracking furnaces. A feasible process is a pressure swing adsorption unit to purify the hydrogen stream. When planning this new separation process an engineer has to consider the two main general aspects

- phase equilibrium and
- mass transfer dynamics.

Understanding the mass transfer dynamics aids the calculation of the time required for the process. In the above example it is the time until the adsorption beds are on the verge of a breakthrough of contaminated hydrogen feed. For continuous operation it is necessary to switch the feed from this loaded adsorber to a second one which is fresh regenerated. In modern concepts automated programs control the switching matrix of the adsorber valves. The dynamics of the process yields the information when to switch the valves so that the whole capacity of the adsorbers can be used without letting contaminated gas through.

The first aspect is the equilibrium of the materials in the separation process itself. It gives the engineer information about the amount of adsorbent required to remove the impurities in hydrogen stream and to calculate the size of the apparatus. In combination with the dynamics of the process two general engineering challenges can be optimised: Maintaining a constant high quality of the product and reducing expenses.

In adsorption processes or adsorption steps of physical, chemical or biological reactions the adsorption isotherm is the most used description method of the phase equilibrium. Knowledge of phase equilibria is the key for understanding complicated processes. Engineers need these isotherms in the planning of production processes. On the other hand it consumes both time and manpower to determine the isotherms by costly experiments.

Besides engineering aspects the scientific viewpoints of adsorption are of great interest when developing new materials and processes. The physical behaviour of complex systems of gases and solids often depends on the adsorption of the educts. For instance, in heterogeneous catalysis gas molecules adsorb on the catalyst surface, and reactions in the adsorbed monolayer lead to products which are desorbed from the surface.

Many processes and reactions in the chemical industry and in chemical science are based upon heterogeneous catalysis. Three important questions of these processes are the understanding of the reaction, the development of the catalyst and the design and optimisation of the reactor. All aspects can benefit from a rigorous and accurate kinetic modell. Especially the competition for adsorption sites is very important for the kinetics of a heterogeneous catalytic reaction if it is the rate determining step. It refers then to the slowest step of the reaction process and controls the activity [123]. A prerequisite for kinetic modelling is the knowledge of adsorption equilibria.

Therefore, the adsorption equilibrium of the gaseous educts with the catalyst surface is related to the reaction rate and also the amount of molecules occupying the free adsorption sites. In both main model mechanisms of heterogeneous catalysis (*Langmuir-Hinshelwood* and *Elay-Rideal*) the adsorption isotherm is needed to calculate the effective reaction rate in dependence of the partial pressures of the reactands. Therefore adsorption equilibria are not only eminent for the understanding of the process of heterogeneous catalysis but also for the development of novel catalysts and adsorbents.

In the literature the isotherm of interest is not always available. Concepts like COSMO-RS are very promising but to complex for daily engineering work. Also adaptations on the isotherm data like *Langmuir* and *Toth* can not always be extrapolated to other gas-solid systems. There is no general model to describe the adsorption of any polar or nonpolar gas by any polar or nonpolar microporous adsorbent.

The objecitve of this study is driven by this demand. First, the fundamentals of adsorption will be examined in this work. The engineer and scientist will get an overview over microporous adsorbents, methods of measurement and the different isotherm descriptions. There will be a Section about characterisation of solid surfaces. Because there is a lack of data regarding *Hamaker* constants of microporous solids an advanced *Hamaker-de Boer* model will be introduced to calculate this dispersion coefficient.

Henry coefficients of adsorption will a priori be calculated based on gas and solid properties of the molecules. In the case of nonpolar gas – nonpolar solid, polar gas – nonpolar solid and nonpolar gas – polar solid an analytical equation will be introduced to directly calculate the *Henry* coefficients. This approach will be expanded to the fourth case of polar gas – polar solid so that the whole spectrum of possibilities is covered. A novel model for predicting the complete adsorption isotherm based only on the molecular properties will be introduced. The model will be verified with own experimental and literature data.

After a discussion of the experimental and theoretical results there will be a conclusion and an outlook to future demands. The experimental methods and materials of the work will be explained in the appendix together with lists of the properties of the examined adsorptives and adsorbents.

3. Fundamentals of Adsorption

3.1. Introduction

Although adsorption has been known as a physical process since the 18th century new aspects are generated through the demands of modern engineering and science in the 21st century.

On the one hand the industry, especially the chemical one, has to improve itself permanently. The understanding of adsorption is a key for future improvements. To withstand the global competition the industry has to enhance its effectiveness continuously. Manpower and invests need to be adopted very carefully at the right time. So modern engineers need powerful instruments to base their decisions on solid technical fundamentals. These instruments need to be economic, usable in a wide range of applications and easy to learn. This study provides such an instrument for the field of adsorption.

On the other hand science also has made great advances and still continues to. Adsorption seems to be a fundamental physical step in a wide range of research fields. For example in medical biochemistry the interaction of cells with biomaterials is dependent on the adsorption layer of proteins [51]. Another example is the storage of hydrogen through reversible adsorption in metallic hydrides. Also the adsorption step of reactants on solid surfaces is eminent for the field of heterogeneous catalysis.

The aim of Chapter 3 is to give a brief overview on the state of research and the literature regarding adsorption science and processes.

3.2. Adsorbents

Development and application of adsorption cannot be considered separately from development of the technology of manufacture of adsorbents applied both on the laboratory and industrial scales. These sorbents can take a broad range of chemical

forms and different geometrical surface structures. This is reflected in the range of their applications in industry, or helpfulness in the laboratory practice [52]. Table 3.1 shows the basic types of industrial adsorbents.

Table 3.1: Basic types of industrial adsorbents.

Carbon adsorbents	**Mineral adsorbents**	**Other adsorbents**
Activated carbons	Silica gels	Synthetic polymers
Avtivated carbon fibres	Activated alumina	Composite adsorbents: (complex mineral_carbons, X_elutrilithe, X_Zn, Ca.)
Molecular carbon sieves	Oxides of metals	Mixed sorbents
Mesocarbon microbeads	Hydroxides of metals	
Fullerenes	Zeolites	
Heterofullerenes	Clay minerals	
Carbonaceous nanomaterials	Pillared clays	
	Porous clay hetero-structures (PCHs)	
	Inorganic nanomaterials	

In this work emphasis is laid on microporous adsorbents like activated carbon and zeolites, especially aluminosilicates. These sorbents play an important role in industry.

3.2.1. Activated carbon

Since our early history active carbon has been the first widely used adsorbent. Its application in the form of carbonised wood (charcoal) was described as early as 3750 BC in an ancient Egyptian papyrus [52].

Nowadays commercial sources for activated carbons include biomass materials (wood, coconut shell and fruit pits) and fossilized plant matter (peats, lignites and all ranks of coal) or synthetic polymers [53]. Activated carbon is normally made by thermal

decomposition of carbonaceous material followed by activation with steam or carbon dioxide at elevated temperature (700 – 1100°C). The activation process essentially involves the removal of tarry carbonisation products formed during the pyrolysis, thereby opening the pores [48]. It is generally believed that carbon dioxide activation mainly causes the creation of microporosity while steam activation results in the development of mesoporosity to a higher extent. These types of activation are known as the physical methods and are widely used in industries.

Important parameters that determine the quality and yield of activated carbons are the final temperature of activation and dwell time at this temperature [54]. Effects of dwell time and activation temperature on the BET surface area and micropore volume of activated carbons made from pistachio-nut shells are shown in figure 3.1 and in figure 3.2 respectively. Also the CO_2 flow rate and the heat rate have an impact.

The structure of activated carbon consists of elementary micro crystallites of graphite, but these micro crystallites are stacked together in random orientation. The spaces between the crystals which form the micropores. The pore size distribution is typically trimodal [48]. Characteristic properties of activated carbons used for gas purification are listed in table 3.2 [24].

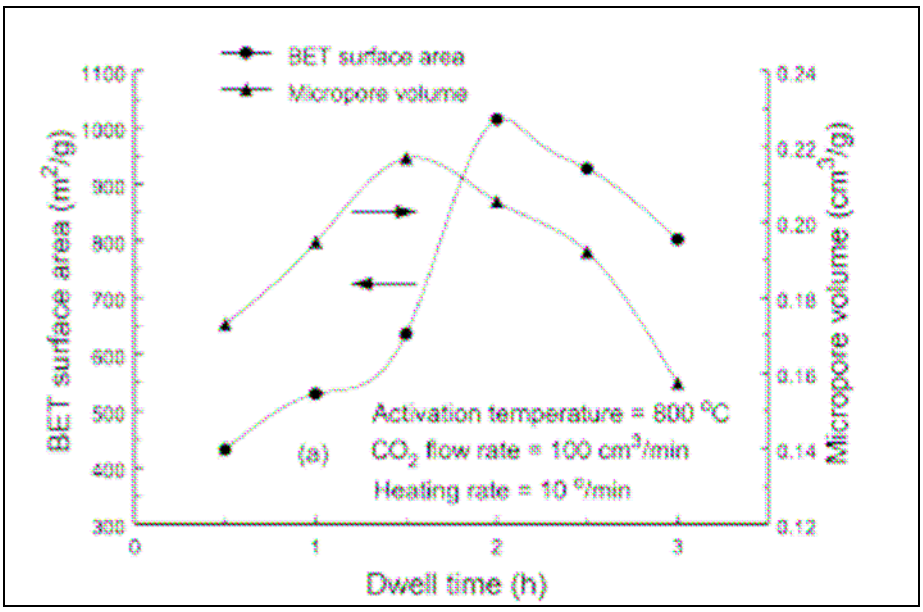

Figure 3.1: Effects of dwell time on the BET surface area and micropore volume of activated carbons made from pistachio-nut shells [54].

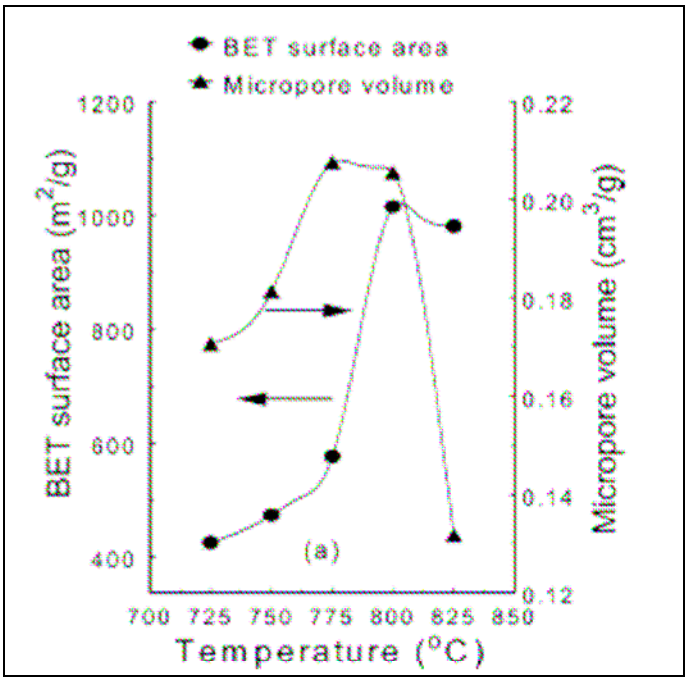

Figure 3.2: Effects of activation temperature on the BET surface area and micropore volume of activated carbons made from pistachio-nut shells [54].

Table 3.2: Data of different activated carbons for gas purification [24].

Characteristic properties	**Numbers**	**Units**
True density ρ	2000	kg/m^3
Apparent density ρ_{app}	600 - 800	kg/m^3
Bulk density ρ_b	350 - 500	kg/m^3
Porosity φ	0,7 - 0,6	-
Specific surface S_{BET}	900.000 - 1.200.000	m^2/kg
Macropore volume d > 50 nm	$0,3*10^{-3}$ - $0,5*10^{-3}$	m^3/kg
Mesopore volume 2 nm < d < 50 nm	$0,05*10^{-3}$ – $0,1*10^{-3}$	m^3/kg
Micropore volume d < 2nm	$0,25*10^{-3}$ – $0,5*10^{-3}$	m^3/kg
Specific heat capacity c	840	J/(kg*K)
Thermal conductivity λ	0,65	W/(m*K)

3.2.2. Zeolites

The main class of microporous adsorbents are zeolites which comprise, according to a recommendation of Structure Commission of the International Zeolite Association, not only aluminosilicates but also all other interrupted frameworks of zeolite-like materials, e.g. aluminophosphates [52]. In this study emphasis is laid on aluminosilicates like MS4A, MS5A, NaX and NaY which are widely used in industry.

The term zeolite was originally coined in the 18^{th} century by a Swedish mineralogist named *Axel Fredrik Cronstedt* who observed, upon rapidly heating a natural mineral, that the stones began to dance about as the water evaporated. Using the Greek words which mean "stone that boils" he called this material zeolite.

The elementary building units of zeolites are SiO_4 and AlO_4^- tetrahedrons. Adjacent tetrahedrons are linked at their corners via a common oxygen atom, and this results in an inorganic macromolecule with a structurally distinct three-dimensional framework. It is evident from this building principle that the net formulae of the tetrahedrons are SiO_2 and AlO_2, i.e. one negative charge resides at each tetrahedron in the framework which has aluminium in its centre. The framework of a zeolite contains channels, channel intersections and/or cages with dimensions from ca. 0.2 to 1 nm. Inside these voids are water molecules and small cations which compensate the negative framework charge [55].

Figure 3.3 shows the principle construction of a zeolite. The smallest unit is the primary building unit (PBU) which consists of SiO_4 or AlO_4^- tetrahedrons. These tetrahedrons are linked together via oxygen ions to secondary building units (SBU). The SBUs can be of cubic form or a hexagonal prism or an octahedron. They are knotted to β-cages which are linked again via the oxygen ions [56].

The chemical composition of a zeolite can, hence, be represented by a formula of the type $M_{x/v}((AlO_2)_x(SiO_2)_y)z*H_2O$ [57] with v the number of valence electrons of the cation M (Na^+, K^+, Ca^{++}, Mg^{++}). The numbers x and y are integers and the ratio y/x is equal or bigger one, z is the number of water molecules in the zeolite unit cell [57].

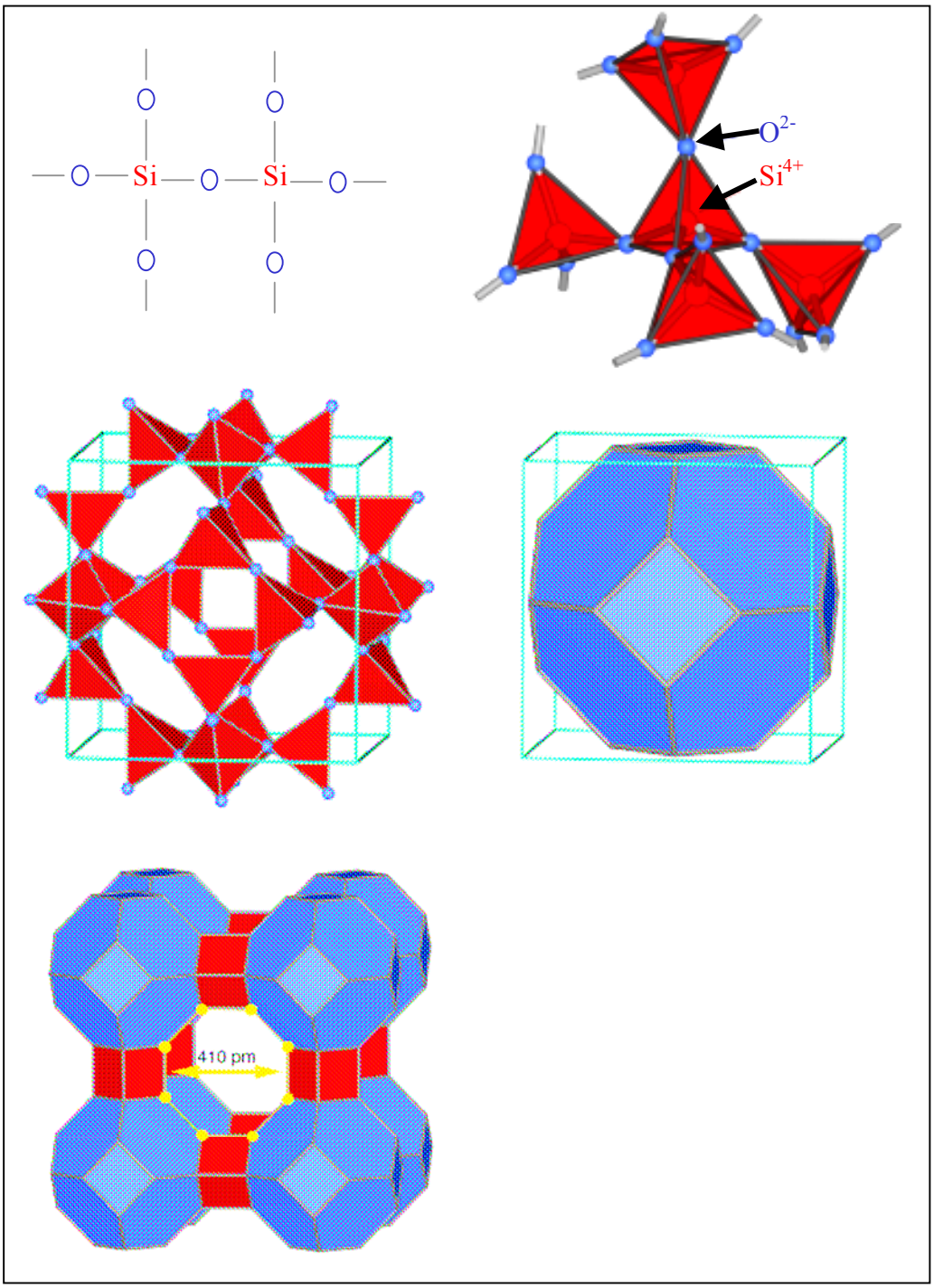

Figure 3.3: Principle construction of a zeolite of LTA type [56].

Until today approximately 40 natural zeolites have been found. As the consequence of successful synthesis work more than 100 new zeolites were produced. Most of the zeolites are manufactured via so-called hydrothermal synthesis. These are reactions in aqueous solution with temperatures above 100°C, similar to the natural conditions. In the laboratory the sources for the reactions are sodium silicate or silica sol as the SiO_2-origin and hydrated aluminium hydroxide or aluminates as the Al_2O_3-origin. The two sources react with strong bases like NaOH or KOH under hydrothermal conditions and pressure in autoclaves. The reaction time can be between several minutes and months [58].

Zeolites are applied in many fields.

- One characteristic property is the ability of ion exchange. Zeolite A can exchange its sodium ions with the calcium ions in water which becomes then “softer”. The calcium enriched zeolites are discharged with the waste water.
- Zeolites can act as acid catalysts in chemical reactions because the alkali metal ions can be exchanged with protons. This happens in the inner cavities, so zeolites can be handled without danger.
- Another application is the use of zeolites as chemical sensors for detecting gases like NH_3 in exhausts of automobiles or power plants. It seems that protons can migrate through the zeolite cavities. This causes a change in the ionic conductibility which is measurable.
- For this work the adsorption of gases or vapours is eminent. As adsorbents they can capture air moisture or solvent vapour. They are used in the clearance of multiple composite glasses or for drying of refrigerants in cooling circuits or brake systems.
- Sterical effects of zeolites are neglected in this study. However they can be very important in many chemical processes like filtering linear hydrocarbons out of petrol to get it knockproof and, in general, separation of mixtures.

3.2.3. Silicalite-1

Silicalite-1 was firstly introduced by *Flanigen* as a new hydrophobic but organophilic polymorph of silica. This new polymorph was topologically very similar to ZSM-5 so it was considered as the aluminium free end member of MFI type zeolites. It contains two types of channel systems with similar size: straight channels and sinuous channels. The diameters of these channels are about 0.54 nm. These two different channels are perpendicular to each other and generate intersection areas which have 0,89 nm of diameter. Silicalite-1 has ten membered oxygen pore openings, and has high thermal and acidic stability. The comparable pore size of silicalite-1 channels with industrially important small organic molecules like methane, n-butane, n-octane and ethanol makes it important for many applications [59]. Silicalite-1 provides a non-polar structure [133]. It is, therefore, considered as a model adsorbent for testing adsorption isotherm models, based on gas-solid molecular interactions [60].

3.3. Characterising microporous solids

Most analysis techniques typically probe a particular aspect of the material and, consequently, a combination of methods is necessary to give a balanced description of complex solids [61]. Microporous adsorbents have very different properties which are fundamental for the process of adsorption. Their properties can influence the equilibrium and/or the dynamics of adsorption. Although this study is mainly about gas adsorption equilibria also dynamical aspects should be mentioned because engineers need both information for planning industrial or laboratory processes. The dynamic and steady state properties of the solids can be found by characterising them through following factors:

- Specific surface
- Porosity
- Density
- Chemical composition
- Refractive index
- Hamaker constant

3.3.1. Specific surface

There are interactions of molecules on every interface between a solid and a fluid – gas or liquid- phase which can lead to attraction or repulsion forces. In the case of attraction a two dimensional interaction phase is composed with the thickness of molecule dimensions. This phenomenon is usable for technical purposes if this interface has sufficient dimensions and if it is accessible for the molecules. The surfaces of microporous adsorbent have magnitudes of several hundred square meter per gram solid [24].

From type II and type IV isotherms, the specific surface area of the adsorbents can be determined by applying the BET method [61]. *Brunauer, Emmett* and *Teller* have derived an equation for the adsorption of gases on solids with n layers [62]:

$$\frac{V_G}{V_{G,mon}} = \frac{c\varphi}{(1-\varphi)} \cdot \frac{1-(n+1)\varphi^n + n\varphi^{n+1}}{1+(c-1)\varphi - c\varphi^{n+1}} \qquad (3.1)$$

where V_G is the total volume of gas adsorbed on the solid surface, $V_{G,mon}$ the volume of gas adsorbed in a monolayer, φ the ratio of pressure to saturation pressure of the gas. The parameter c is a dimensionless constant and dependent from the enthalpy of adsorption in the first layer and the heat of evaporization. The assumption made by *Brunauer, Emmet* and *Teller* is that the evaporation-condensation properties of molecules in the second and higher adsorbed layers are the same as those of the liquid state.

If we deal with adsorption on a free surface, then at the saturation pressure of the gas an infinite number of layers can build up on the adsorbent. $n \to \infty$ one leads to

$$\frac{V_G}{V_{G,mon}} = \frac{c\varphi}{(1-\varphi)} \cdot \frac{1}{1+(c-1)\varphi} \qquad (3.2)$$

With the law of ideal gases and the balance of the mass of the adsorbent equation (3.2) becomes

$$\frac{n}{n_{mon}} = \frac{c\varphi}{(1-\varphi)} \cdot \frac{1}{1+(c-1)\varphi} \tag{3.3}$$

where n is the overall loading of the adsorbent and n_{mon} the monolayer loading. From this the linear form (y = b + m φ) can be derived to obtain the specific surface of the adsorbent due to the BET adsorption isotherm:

$$\frac{\varphi}{n(1-\varphi)} = \frac{1}{n_{mon}c} + \frac{(c-1)}{n_{mon}c}\varphi \tag{3.4}$$

The intercept, b = $\frac{1}{n_{mon}c}$, and the tangent of the gradient angle, m = $\frac{(c-1)}{n_{mon}c}$, permit the calculation of the monolayer loading n_{mon} and the BET constant c:

$$n_{mon} = \frac{1}{b+m} \tag{3.5}$$

$$c = \frac{m}{b} + 1 \tag{3.6}$$

Finally the BET surface area is calculated from

$$S_{BET} = n_{mon}\ a_{mol}\ N_A \tag{3.7}$$

Here a_{mol} denotes the average area occupied by a molecule of adsorbate in the completed monolayer and N_A the *Avogadro* constant [63].

By convention, most surface area determinations are based on the area occupied by a nitrogen molecule. The nitrogen adsorption is measured at the boiling point of nitrogen, 77.4 K. The value of a_{mol} may be estimated following an early suggestion of *Emmett* and *Brunauer* from the density of liquid nitrogen at 77.4 K. The estimate uses

the assumption that the packing density of adsorbed nitrogen on a surface is the same as in the liquid. This leads to the equation

$$a_{mol} = 1{,}091\left(\frac{M}{\rho_L N_A}\right)^{2/3} \tag{3.8}$$

where M is the molar mass of nitrogen (0.028 kg/mol), ρ_L the density of liquid nitrogen (810 kg/m^3) and 1.091 is a packing factor for 12 nearest neighbours in the bulk liquid and six on the plane surface. Insertion of these quantities and of the *Avogadro* constant into equation (3.8) gives $a_{mol}(N_2)$ = 0.162 nm^2 for nitrogen at 77.4 K.

For practical purposes, the average area occupied by other molecules can be determined by comparison of their monolayer capacity with that of nitrogen. Using this method, the areas occupied by argon a_{mol}(Ar) and krypton a_{mol}(Kr) at 77.4 K were then determined to be 0.138 nm^2 and 0.2 nm^2, respectively.

3.3.2. Pore volume distribution

The word pore comes from the Greek word '$\pi o \rho o \sigma$' which means passage. This indicates the role of a pore acting as a passage between the external and the internal surfaces of a solid, allowing material, such as gases and vapours, to pass into, through or out of the solid. Almost all adsorbents used in catalysis or for purification/separation purposes have a high porosity, and this porosity is the only practical method of introducing greatly enhanced surface areas into a solid [64]. Porosity has a classification system as defined by IUPAC which gives a guideline of pore widths applicable to all forms of porosity. Distinctions in porosity classes are not rigorous and they may often overlap in size and definition. The widely accepted IUPAC classification is as follows:

$$d_{Micropores} < 2 \text{ nm}$$

$$2 \text{ nm} < d_{Mesopores} < 50 \text{ nm}$$

$$d_{Macropores} > 50 \text{ nm}$$

There are several methods to measure pore related parameters of a solid. Here exemplarily the mercury porosimetry and the t-plot method of *de Boer* shall be discussed in detail. The other common methods are listed in Table 3.3 [67]:

Table 3.3: Methods to measure pore related parameters of a solid.

Method	Definition
BJH	The method of *Barrett, Joyner* and *Halenda* is a procedure for calculating pore size distributions from experimental isotherms using the Kelvin model of pore filling. It applies only to the mesopore and small macropore size range.
de Boer t-Plot	The t-Plot method is most commonly used to determine the external surface area and micropore volume of microporous materials. It is based on standard isotherms and thickness curves which describe the statistical thickness of the film of adsorptive on a non-porous reference surface.
MP-Method	The MP method is an extension of the t-plot method. It extracts micropore volume distribution information from the experimental isotherm.
Dubinin Plots	Dubinin plots (*Dubinin-Radushkevich* plot and the more general *Dubinin-Astakhov* plot) relate the characteristic energy of the adsorptive to the micropore structure.
Medek	The *Medek* method uses *Dubinin-Astakhov* plots to determine micropore volume distributions by pore size.
Horvath-Kawazoe technique	This method determines the best fit (in a least squares sense) of a set of single-mode model isotherms to the experimental isotherm. The solution set represents the pore volume distribution by size for the solid on which the isotherm was developed.
DFT plus	Density functional theory provides a method by which the total expanse of the experimental isotherm can be analysed to determine both microporosity and mesoporosity in a continuous distribution of pore volume with respect to pore size.

In mercury porosimetry mercury is injected into the pores of the solid to measure the pore size and the pore volume distribution. The gas is evacuated from the sample cell and mercury is then transferred into the sample under vacuum and pressure is applied to force mercury into the sample. In the theoretical model of *Washburn* [66] all pores are treated as cylindrical pores with an inner radius r. The mercury with the pressure p is balanced with the surface tension γ of mercury. This leads to

$$p\, r = -2\, \gamma \cos \beta \qquad (3.9)$$

with β the contact angle of the mercury with the pore surface. A typical value for β is 140 degrees and for the surface tension 484 mN/m or 0.484 J/m^2.

The *Washburn* equation (3.9) can be derived from the equation of *Yang* and *Dupré* [65]:

$$\gamma_{SG} = \gamma_{SL} + \gamma_{LG} \cos \beta \qquad (3.10)$$

where γ_{SG} is the interfacial tension between solid and gas, γ_{SL} the interfacial tension between solid and liquid, γ_{LG} the interfacial tension between liquid and gas and β the contact angle of the liquid on the pore wall. It is derived from a force balance as seen in figure 3.4 [49].

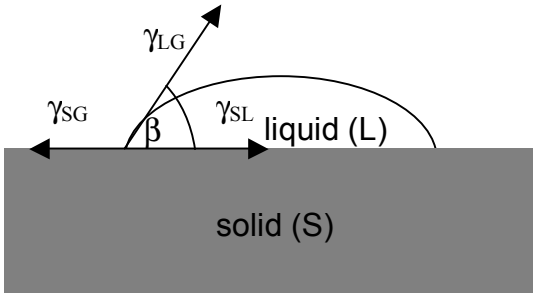

Figure 3.4: Force balance of a mercury drop on a solid surface.

The work, W, required for moving the liquid up the capillary when the solid-gas interface disappears and solid-liquid interface appears is

$$W = (\gamma_{SL} - \gamma_{SG})\Delta S \tag{3.11}$$

where ΔS is the surface of the capillary wall covered by liquid when its level rises. With equation (3.10) it is

$$W = -\gamma_{LG} \cos\beta \, \Delta S \tag{3.12}$$

The work required to raise a column of liquid in a capillary with the radius r is identical to the work necessary to force liquid out of the capillary. If a volume V of liquid is forced out of the capillary with a gas at a constant pressure p, the work W is

$$W = V \; p \tag{3.13}$$

A combination of equations (3.12) and (3.13) gives

$$V \; p = -\gamma_{LG} \cos\beta \, \Delta S \tag{3.14}$$

When the capillary is circular in cross-section, parameters V and ΔS are given by $\pi r^2 L$ and $2\pi rL$, if L is the length of the capillary. Substituting these terms into equation (3.14) yields the *Washburn* equation (3.9), which relates the pressure of the mercury to the radius of the pores via an indirect proportionality.

The interrelationship of the differential volume dV with the differential radius dr is given with a pore volume distribution function f(r)

$$dV = f(r)\, dr \tag{3.15}$$

The *Washburn* equation (3.9) can be rewritten in

$$dr = \frac{-r}{p} dp \tag{3.16}$$

The combination of the equation (3.15) with (3.16) yields

$$f(r) = -\frac{p}{r}\left(\frac{dV}{dp}\right) \tag{3.17}$$

With equation (3.17) the pore radius r is related to the pore volume distribution f(r). Another illustration can be found with the relationship

$$\frac{p}{dp} = -\frac{r}{dr} \tag{3.18}$$

combined with

$$r\ f(r) = -\frac{p}{dp}dV = \frac{d}{dr}dV = \frac{dV}{d\ln r} \tag{3.19}$$

Therefore, the distribution function f(r) and the related volume distribution dV/dlnr can be calculated.

Another method for measuring pore volumes is the t-plot method [63]. The t-plot method is most commonly used to determine the external surface area and micropore volume of microporous materials. It is based on standard isotherms and thickness curves which describe the statistical thickness of the film of adsorptive on a non-porous reference surface.

For a large number of non-porous solids the shape of the nitrogen isotherm can be represented with a single curve, by plotting the ratio $\frac{V_{N_2}}{S}$ as a function of the relative pressure $\frac{p}{p^0}$. V_{N_2} denotes the volume of N_2 adsorbed, S the surface area of the sample, p and p^0 the partial and saturation pressure of nitrogen, respectively. The resulting t-curve reflects the statistical thickness t of the adsorbed nitrogen multilayer and can be calculated according to:

$$t(nm) = 0.1\sqrt{\frac{13.99}{0.034 + \log\left(\frac{p^0}{p}\right)}} \qquad (3.20)$$

Deviations of the t-plot from the ideal behaviour allow the deduction of the nature of pores and the determination of the micropore volume (figure 3.5). Curve a in figure 3.5 is linear and starts at the origin, which indicates an ideal t-material. Therefore, S can be calculated from the tangent. Curve b shows a strong upward deviation from linearity at a certain pressure $\frac{p}{p^0}$, which indicates that starting from t_1 capillary condensation takes places in addition to adsorption. In contrast, if some narrow pores are filled by multilayer adsorption according to curve c further adsorption does not occur in this part, as that surface has become unavailable. At this point the t-plot begins to deviate downwards from the straight line at t_2. This situation is, for instance, encountered in the presence of slit-shaped pores. The presence of micropores is indicated by a positive intercept at the y-axis as shown in line d. A straight line is found and the surface S can be calculated from this tangent. The positive intercept point is caused by a relatively large nitrogen uptake at very low t-values. Such a high nitrogen uptake at very low pressures is due to the strong adsorption in micropores and, hence, allows to calculate the micropore volume v_{micro} from the intercept.

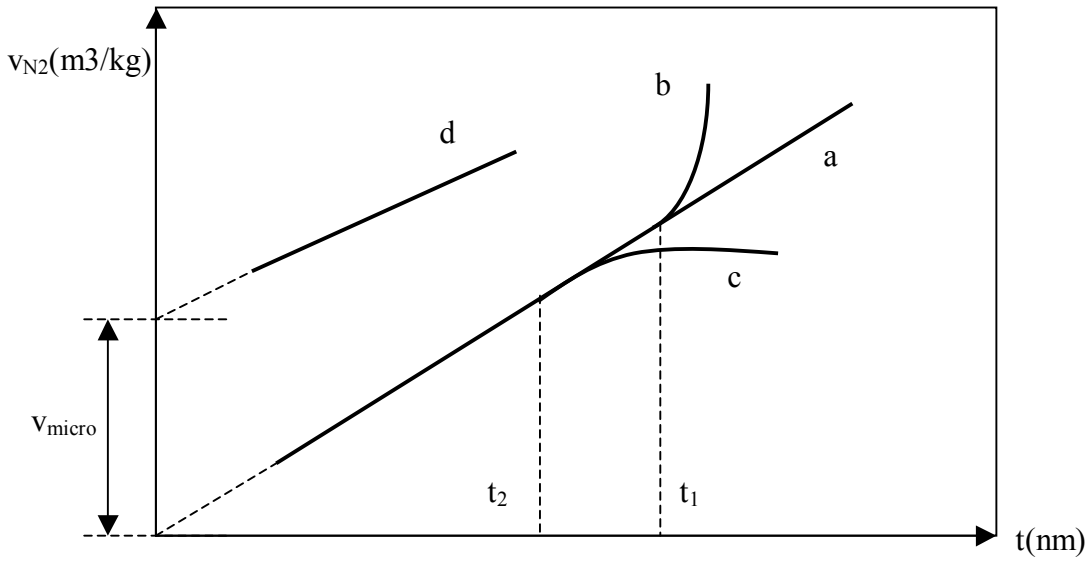

Figure 3.5: Different courses of the t-plot.

For more detailed descriptions and theories to porosity and measurement methods reference should be made to the literature [68].

3.3.3. Density and porosity

The density of a porous solid is the relation of its mass m_S to its volume V_S without the pore volume:

$$\rho_S = \frac{m_S}{V_S} \tag{3.21}$$

Pycnometric density is at the moment the closest approximation of true density [70]. The term pycnometer is derived from the Greek word "πυκνοσ", meaning dense, and meter. With this method the pores are filled with gas molecules [69]. Helium is recommended as probe gas [69] because:

- it is atomic and very close to ideal gas behaviour,
- it is not adsorbed at room temperature,
- its atoms are very small to diffuse also into smallest pores and
- it has a high heat transfer coefficient to adapt the chamber temperature very quickly.

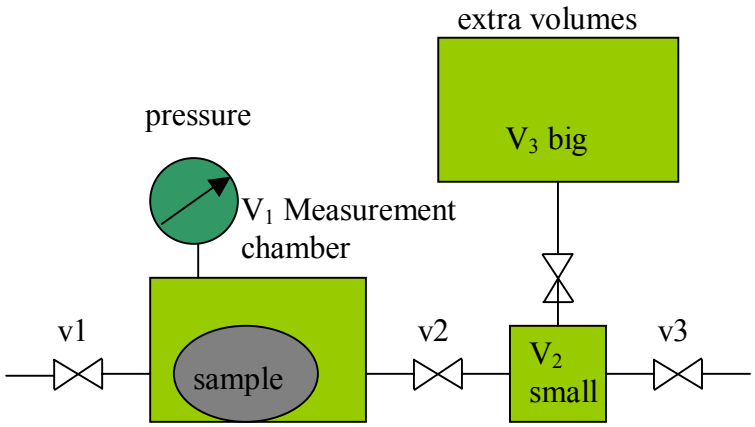

Figure 3.6: Draft of a gas pycnometer.

V_1, V_2 and V_3 are the calibrated volumes of the measurement chamber and the extra volumes for expansion of the measurement gas. V_{gas} is the volume of the gas in the measurement chamber with the sample in it. After weighting the chamber without ($m_{chamber}$) and with the sample ($m_{chamber+sample}$) the mass of the sample can be calculated.

$$m_{sample} = m_{chamber+sample} - m_{chamber} \tag{3.22}$$

In the first step the sampled chamber is filled with a well chosen gas and the pressure p_1 after equilibrium is measured. In the second step the valve v2 between the measurement chamber and the small expansion chamber is opened followed by a second pressure measurement p_2. With the law of ideal gases it follows

$$p_1 V_{gas} = p_2 \left(V_{gas} + V_2\right) \tag{3.23}$$

or

$$V_{gas} = \frac{V_2}{\frac{p_1}{p_2} - 1} \tag{3.24}$$

For the true density it follows:

$$\rho_S = \frac{m_{chamber+sample} - m_{chamber}}{V_1 - \frac{V_2}{\frac{p_1}{p_2} - 1}} \tag{3.25}$$

In order to calculate the volume of the pores the helium in the measurement chamber is moved by a pump. The chamber (with the solid in it) is filled again with mercury under atmospheric conditions. The mercury encapsulates the solid without penetrating into the pores. So it is possible to calculate the pore volume of the sample:

$$V_{pores} = V_{gas} - V_{mercury} \tag{3.26}$$

Finally the porosity of the microporous adsorbent is

$$\varphi = \frac{V_{pores}}{V_{pores} + V_s} = \frac{\frac{V_2}{p_1/p_2 - 1} - V_{mercury}}{V_{gas} - V_{mercury} + V_1 - V_{gas}} = \frac{\frac{V_2}{p_1/p_2 - 1} - V_{mercury}}{V_1 - V_{mercury}} = \frac{V_2/V_{mercury}\left(\frac{1}{p_1/p_2 - 1}\right) - 1}{V_1/V_{mercury} - 1} \tag{3.27}$$

The apparent density of the microporous solid is

$$\rho_{app} = \frac{m_{chamber+sample} - m_{chamber}}{V_{pores} + V_s} = \frac{m_{chamber+sample} - m_{chamber}}{V_1 - V_{mercury}} \tag{3.28}$$

and defined as the ratio of mass of the solid adsorbent to the volume of the solid inclusive the pore volume.

3.3.4. Chemical composition and structure

The chemical composition and the structure of a solid play an important role for polarity and adsorption behaviour similar to the density and the porosity. Zeolites are the main interest of this study so emphasis is laid on composition of aluminosilicates.

The structures of zeolites consist of three-dimensional frameworks of SiO_4 and AlO_4^- tetrahedron. The aluminium ion is small enough to occupy the position in the centre of the tetrahedron of four oxygen atoms, and the isomorphous replacement of Si^{4+} by Al^{3+} produces a negative charge in the lattice. The net negative charge is balanced by exchangeable cations (sodium, potassium, or calcium). The ratio of silicon to aluminium ions cannot be less than one and is infinite in silicalite-1. Zeolite synthesis is already explained in Section 3.2.2. The size of the cage window is determined by the number of oxygen atoms in the ring. A consequence is the physical effect of sieving molecules out of a gas mixture. In table 3.4 important zeolites are listed [24].

Table 3.4: Chemical composition of technical important molecular sieves.

Structure	Cations	Trivial name	Chemical composition	Effective pore opening (10^{-10} m)
A	Na^+	MS4A	$Na_{12}((AlO_2)_{12}(SiO_2)_{12})$	4.2
A	Ca^{2+}	MS5A	$Ca_5Na_2((AlO_2)_{12}(SiO_2)_{12})$	5.0
A	K^+	MS3A	$K_{12}((AlO_2)_{12}(SiO_2)_{12})$	3.8
10X	Ca^{2+}		$Ca_{40}Na_6((AlO_2)_{86}(SiO_2)_{106})$	8
13X	Na^+	NaX	$Na_{86}((AlO_2)_{86}(SiO_2)_{106})$	9 to 10
Y	Na^+	NaY	$Na_{56}((AlO_2)_{56}(SiO_2)_{136})$	9 to 10
ZSM-5	Na^+		$Na_3((AlO_2)_3(SiO_2)_{93})$	6

In Table 3.5 the effect of sieving of zeolites regarding to different gas molecules is listed. The critical molecule diameter in 10^{-10} m is in brackets [24].

Table 3.5: Sieving effect of zeolites.

Zeolite	Effective pore opening in 10^{-10} m	Adsorbed molecules, critical diameter in 10^{-10} m
MS3A	3.8	He (2), Ne (3.2), Ar (3.83), NH_3 (3.8), H_2 (2.4), N_2 (3.0), O_2 (2.8), H_2O (2.6)
MS4A	4.2	Kr (3.94), Xe (4.37), CH_4 (4.0), C_2H_6 (4.44), C_2H_2 (2.4), CH_3OH (3.0), CO_2 (2.8), H_2S (3.6), every of above molecules can be adsorbed
MS5A	5.0	CF_4 (5.33), C_2F_6 (5.33), Cyclopropane (5.0), every of above molecules can be adsorbed
10X	8	SF_6 (6.7), i-C_4H_{10} (5.6), C_6H_6 (6.7), Triophene (5.3), every of above molecules can be adsorbed
13X (NaX)	9 to 10	every of above molecules can be adsorbed
Y (NaY)	9 to 10	every of above molecules can be adsorbed

The molecule diameter can be calculated with the *van-der-Waals* volume v_{vdW} (in m^3/mol) which is defined as [26]

$$v_{vdW} = \frac{\Re\, T_c}{8\, p_c} \tag{3.29}$$

where c relates to critical properties of temperature and pressure and $\Re$ is the universal gas constant. With the assumption that the gas molecule is a sphere the molecule diameter can be calculated. With

$$\frac{v_{vdW}}{N_A} = V_{sphere} = \frac{4}{3}\pi\left(\frac{d}{2}\right)^3 \tag{3.30}$$

it follows for the molecule diameter in m that

$$\sigma_i = \sqrt[3]{\frac{3\,\Re\, T_c}{16\, p_c\, N_A\, \pi}} \tag{3.31}$$

With equation (3.29) and table 3.5 it can be decided whether or not a zeolite is suited for a technical sieving process.

3.3.5. Refractive index

It will be shown later that the refractive index n and the interacting energies $\Phi_{i,j}$ between adsorptive and adsorbent molecules are key parameters in order to calculate adsorption equilibria. Adsorptive molecules can be nonpolar or polar with a dipole moment μ_i and/or a quadrupole moment Q_i. In polar molecules the centres of the positive and negative charge q have the distance l:

$$\mu_i = q_i\, l \tag{3.32a}$$

If two dipoles with counterdirection are effective in an adsorptive molecule a quadrupole Q_i can be effective.

With respect to zeolite molecules the anions and cations lead to an electrical field with the strength E according to

$$E = \frac{q}{4\pi\varepsilon_0 r^2} \tag{3.32b}$$

with ε_0 as the electrical permittivity in vacuum and r is the distance between the charges. In electrical fields a dipole moment $\mu_{i,ind}$ can be induced in an adsorptive molecule according to

$$\mu_{i,ind} = \alpha_i E = \underbrace{\left[\underbrace{(\alpha_0)_i}_{unpolar} + \frac{\mu_i^2}{3kT}\right]}_{polar} E \tag{3.32c}$$

The polarisability $(\alpha_0)_i$ of nonpolar or α_i of polar molecules are definded by this equation. The interaction energies $\Phi_{i,ind}$ according to induced dipoles, $\Phi(\mu_i)$ according to permanent dipoles $\mu_{i,ind}$ and $\Phi(Q_i)$ due to a quadrupole moment Q_i are

$$\Phi_{i,ind} = -\frac{\alpha_i}{2} E^2$$

$$\Phi(\mu_i) = -\mu_i E \quad and \tag{3.32d}$$

$$\Phi(Q_i) = -\frac{Q_i}{2}\frac{\partial E}{\partial r}$$

As mentioned above the refractive index is one of the important parameters describing the optical properties of solid materials. In general it is difficult to obtain a quantitative relation between the refractive index and the structure as well as composition of materials. It seems that the refractive index is dependent on atomic parameters like mass, radius and electric charge of the ions constituting the material [71]. According to classical dielectric theory, the refractive index depends on the density and on the polarisability of the atoms in a given material [72]. The polarisability of a microporous adsorbent determines its disperse properties and,

thus, it is possible to calculate the *Hamaker* constant from knowledge of the refractive index [41]. In [73] refractive indices of multicomponent silicate melts containing alumina have been determined employing a high temperature elipsometer. The data were used to propose a predictive equation for the refractive indices of silicate melts. In [72] 13 SiO_2 polymorphs with topologically different tetrahedral frameworks have been investigated in order to find a relationship between refractive index and density. The mean refractive indices of the guest free porosils were determined by the immersion method using the Na_D line. One example is the ZSM-5 type zeolite silicalite-1 examined by *Marler* [72]. Another possibility is the method of *Becke* lines. A *Becke* line is a bright halo near the boundary of a transparent particle, which moves with respect to that boundary when the microscope is moved up and down. The halo will always move up the higher refractive index medium as the position of the focus is raised. The halo crosses the boundary to the lower refractive index medium when the microscope is focused in downward direction. The results are compared with pure, isotropic crystalline solids with known refractive indices (e.g. NaCl, $CaCO_3$). *Van der Hoeven* measured with this method the refractive index of zeolite MS4A [41].

There are several approaches for quantitatively describing the refractive index. Three of them will be explained in this study. Neglecting interactions between the atoms the classical dielectric theory leads to the *Newton-Drude* relation

$$\frac{\overline{n}_{solid}^2 - 1}{\rho_{app}} = \frac{\overline{\alpha}_{solid}\ N_A}{\varepsilon_0\ M_{solid}} = const. \qquad (3.32e)$$

where M_{solid} is the molar mass of the solid in kg/mol, $\overline{\alpha}_{solid}$ the mean average polarisability in $(C^{2}*m^{2})/J$, $\overline{n}_{solid}$ the mean refractive index, ε_0 the permittivity of free space in C/(V*m) and ρ_{app} the apparent density of the solid in kg/m^3.

The second approach takes into account interactions between the atoms and the fact that the dielectricum is not continuous. This is known as the *Lorentz-Lorenz* assumption. It leads to the *Clausius-Mosotti* equation of nonpolar but polarisable molecules (for a detailed derivation of this theory see *Arndt and Hummel*):

$$\frac{\overline{n}^2 - 1}{\left(\overline{n}^2 + 2\right)\rho_{app}} = \frac{\overline{\alpha}_{solid}\ N_A}{3\varepsilon_0\ M_{solid}} \tag{3.33}$$

The assumption of point charges is valid only for ideal ionic solids in which the ions show no overlap of their electron distribution. To overcome this shortcoming *Marler* suggests a general refractivity formula which takes into consideration an overlap field of near-neighbour interactions.

$$\frac{\overline{n}^2 - 1}{\left(4\,\pi + b\left(\overline{n}^2 - 1\right)\right)\rho_{app}} = \frac{\overline{\alpha}_{solid}\ N_A}{4\,\pi\,\varepsilon_0\ M_{solid}} \tag{3.34}$$

with the electronic overlap parameter

$$b = \frac{4\,\pi}{3} - \gamma \tag{3.35}$$

where γ is a material constant resulting from the overlap field. Equation (3.32e) includes as special cases the *Clausius-Mosotti* formula for $b = \frac{4\,\pi}{3}$ if there is no overlap field and the *Newton-Drude* equation for b = 0 if the overlap field compensates for the *Lorentz* field exactly.

In this study the Clausius-Mosotti equation is used for further investigations because by applying this approach the refractive index of structures like aluminosilicates can be calculated a priori from knowledge on the properties of the solid. Therefore, the theory of Clausius-Mosotti will be explained in more detail.

3.3.5.1. The *Clausius-Mosotti* equation

The electrical field $\vec{E}$ can be expressed by the force which results from a small point charge in this field. The field intensity $\vec{E}$ is a vector in direction of the force vector $\vec{F}$, the charge q is a scalar quantity [95]. It is

$$\vec{E} = \frac{\vec{F}}{q} \tag{3.36}$$

For the displacement of a charge q in a homogenous field between two charged parallel plates of distance d and voltage U the work

$$W = F\,d = U\,I\,t = U\,q \tag{3.37}$$

is necessary where t is the time and I the current. With equation (3.36) if follows

$$E = \frac{U}{d} \tag{3.38}$$

The charges bonded on a loaded matter (e.g. the plates of a condenser) determine the quantity of the field intensity. The charge density σ is defined as the ratio of the matter's charge q to its loaded surface S with

$$\sigma = \frac{q}{S} = \varepsilon_0 E \tag{3.39}$$

where ε_0 denotes the permittivity of free space, $\varepsilon_0 = 8.85 \cdot 10^{-12}$ C/(V*m). If an electrical nonconducting material is inserted into the electrical field the charge density rises with a factor ε_r which is the relative permittivity. It is then

$$\sigma = \varepsilon_r\,\varepsilon_0\,E \tag{3.40}$$

The difference of the charge densities after and before inserting the so-called dielectric into the electrical field is the electrical polarisation P with

$$P = \varepsilon_r\,\varepsilon_0\,E - \varepsilon_0\,E = \varepsilon_0\,E(\varepsilon_r - 1) \tag{3.41}$$

Through the polarisation the charges of the dielectric are separated with the results of a dipole moment μ. With the number density ρ_j of dipole moments in an examined volume element the polarisation also can be written as [94]

$$P = \rho_j \, \mu \tag{3.42}$$

It is common knowledge that the number density ρ_j of particles in a volume element can be calculated via

$$\rho_j = \frac{N_A \rho_{app}}{M} \tag{3.43}$$

where N_A is the *Avogadro* constant, M the molar mass and ρ the density. Inserted into equation (3.42) a relation between a molecular property, the dipole moment, and a macroscopic measurable quantity, the polarisation P is obtained with

$$P = \frac{N_A \rho_{app}}{M} \mu \tag{3.44}$$

The induced free surface charges are the consequence of three processes in the molecular area which occur in presence of an outer electrical field. The polarisation is then the sum of three different parts with

$$P = P_e + P_a + P_\mu \tag{3.45}$$

where P_e is the electronic polarisation, P_a the atomic polarisation and P_μ the orientational polarisation. The electronic polarisation is evident in all atoms and molecules. It is based on the fact that the charge centre of core frame and electronic shell is dispersed through the outer electrical field in different directions. The atomic polarisation occurs at all polar molecules and is based on the changes of bonding distances and bonding angles. These two polarisation parts are combined under the term of displacement polarisation. The induced dipole moment is the consequence of it. The orientational polarisation occurs only at polar molecules with permanent dipole

moment. It is based on the partial arrangement of the molecular dipole moments in direction of the electrical field.

In the following a molecule is considered which is not an electrical dipole in an electrical field. Due to displacement of its charge centre it gets an induced dipole μ_{ind} which is proportional to the electrical field intensity E with

$$\mu_{ind} = \alpha E \tag{3.46}$$

where α is the molecular polarisability in ($C^{2*}m^2$)/J, a measure for the ability of the molecule to deform. With equation (3.44) it follows that

$$P = \frac{N_A \rho_{app}}{M} \alpha E \tag{3.47}$$

If the medium consists of polar molecules the molecules are influenced not only by the outer electrical field E_{outer} but also by an inner electrical field E_{inner}. *Lorenz* [128] and *Lorentz* [129] independently derived the overall field E inside a spherical volume element according to

$$E = E_{outer} + E_{inner} = E_{electrical} + \frac{1}{3}\frac{P}{\varepsilon_0} \tag{3.48}$$

With equation (3.47) it follows that

$$P = \frac{N_A \rho_{app}}{M} \alpha \left(E_{electrical} + \frac{1}{3}\frac{P}{\varepsilon_0} \right) \tag{3.49}$$

With equation (3.41) we obtain

$$P = \frac{N_A \rho_{app}}{M} \alpha \left(\frac{P}{\varepsilon_0 (\varepsilon_r - 1)} + \frac{1}{3}\frac{P}{\varepsilon_0} \right) \tag{3.50}$$

This equation is independent of the polarisation and can be rewritten as the *Clausius-Mosotti* equation:

$$\frac{N_A \alpha}{3\varepsilon_0} = \frac{M}{\rho_{app}} \frac{(\varepsilon_r - 1)}{(\varepsilon_r + 2)} \tag{3.51}$$

With this relationship and the relative permittivity the polarisability of the material can be calculated or vice versa. The aim of the next Section is to derive a new relationship in order to calculate the refractive index of solids like zeolites. It is based on the theory of *Maxwell*.

3.3.5.2. Refractive index of zeolites

Electromagnetic waves are generated when charged particles accelerate. Their existence was predicted in 1865 by *James Clerk Maxwell* on theoretical grounds. They were first produced and studied in 1888 by *Heinrich Rudolf Hertz*. The *Maxwell* equations are a group of equations which centralise the basic laws of electric and magnetic appearances to one package. Only the last of four equations has been derived by *Maxwell* but he was the first to draw the right conclusions from them [96].

He found that the electromagnetic waves spread out with a velocity:

$$c_0 = \frac{1}{\sqrt{\varepsilon_0 \mu_0}} \tag{3.52}$$

With equation (3.52) *Maxwell* has unified the permittivity of free space ε_0, the permeability of free space μ_0, and the speed of light in vacuum, which was found to be c_0.

In the general case the spreading speed of the electromagnetic wave in a medium is:

$$w = \frac{1}{\sqrt{\varepsilon \mu}} \tag{3.53}$$

where ε is the permittivity of the medium and μ the permeability of it. It is

$$\varepsilon = \varepsilon_r \, \varepsilon_0 \qquad \text{and} \tag{3.54}$$

$$\mu = \mu_r \, \mu_0 \tag{3.55}$$

where ε_r and μ_r are the relative permittivity and the relative permeability of the medium respectively. With equation (3.53) it follows:

$$w = \frac{1}{\sqrt{\varepsilon_r \varepsilon_0 \, \mu_r \mu_0}} \tag{3.56}$$

Especially for visible light μ_r can only approximately be 1 because matters with a big μ_r, e.g. ferromagnetics like iron and nickel, are intransparent. Zeolites are assumed in this work not to be magnetic. With equation (3.52) and the above assumption it follows:

$$w = c_0 \frac{1}{\sqrt{\varepsilon_r}} \tag{3.57}$$

The relation of this equation with the refractive index n can be found by using the law of *Snel*. *Willebrord Snel van Royen*, a Dutch mathematician and geodesist, discovered in the early 1600s the law of refraction. If an electromagnetic wave trespasses the frontier of two media it changes with its velocity also its spreading direction. The wave will be refracted like in figure 3.7.

The law of refraction predicats that the ratio of the angles α and β are equal to the ratio of the wave velocities in the different media, therefore

$$\frac{\sin(\alpha)}{\sin(\beta)} = \frac{w_1}{w_2} = n \tag{3.58}$$

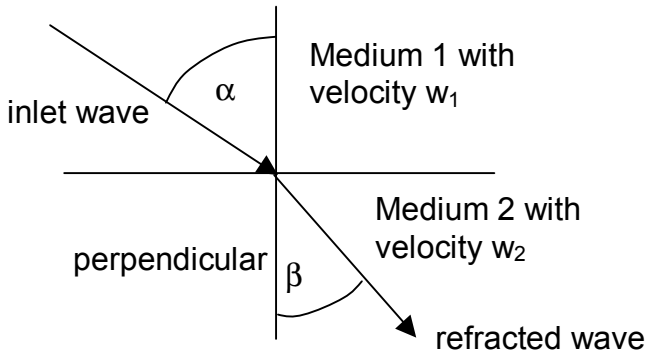

Figure 3.7: *Snel*'s law of refraction.

This ratio is defined as the refractive index n. With equation (3.57) and $w_1 = c_0$ in this special case and with w_2 as the wave velocity in the medium, it is

$$n = \frac{w_1}{w_2} = \frac{c_0}{w} = \sqrt{\varepsilon_r} \tag{3.59}$$

known as the relation of *Maxwell*. If the *Maxwell* equation

$$\varepsilon_r = n^2 \tag{3.60}$$

is inserted in the *Clausius-Mosotti* equation (3.51) the *Lorenz-Lorentz* relationship between the refractive index n of a medium and the polarisability α is obtained:

$$\frac{N_A \alpha}{3\varepsilon_0} = \frac{M}{\rho_{app}} \frac{\left(n^2 - 1\right)}{\left(n^2 + 2\right)} \tag{3.61}$$

The aim of this Section is to derive a formulation to calculate the refractive index of solids like zeolites. Therefore, the polarisability of the adsorbent or the left side of equation (3.61) has to be known. This left side is also defined as the molar refractivity R_m with

$$R_m = \frac{N_A \alpha}{3\varepsilon_0} = \frac{M}{\rho_{app}} \frac{\left(n^2 - 1\right)}{\left(n^2 + 2\right)} \tag{3.62}$$

where R_m is in m^3/mol [98]. The refractive index of the solid is then

$$n = \sqrt{\frac{1 + 2\frac{R_m \rho_{app}}{M}}{1 - \frac{R_m \rho_{app}}{M}}} \tag{3.63}$$

The molar refraction of a molecule with the structure $A_{x_A} B_{x_B}$ is

$$R_m = x_A R_{m,A} + x_B R_{m,B} \tag{3.64}$$

where x_A and x_B are the stoichiometrical coefficients and $R_{m,A}$ and $R_{m,B}$ the ionic molar refractions of the matters A and B, respectively. In general it is

$$R_m = \sum_i x_i R_{m,i} \tag{3.65}$$

The ionic molar refractivities $R_{m,i}$ can be calculated via equation (3.62) if the ionic polarisabilities α_i are known. It is therefore

$$R_{m,i} = \frac{N_A}{3\varepsilon_0} \alpha_i \tag{3.66}$$

In the Handbook of Chemistry and Physics [6] the polarisability volumes α_i' are tabulated for the interesting ions of aluminosilicates. The polarisability α_i is related to the polarisability volume α_i' via

$$\alpha_i = 4\pi\varepsilon_0 \alpha_i' \tag{3.67}$$

In table 3.6 the interesting properties are listed. As an example the refractive index of MS5A is calculated.

Table 3.6: Numerical values for the ionic molar refractivities.

Ion	Polarisability volume α_i' in 10^{-30} m^3 [6]	Polarisability α_I in 10^{-40} $(C^2*m^2)/J$ with equation (4.34)	Ionic molar refraction in 10^{-6} m^3/mol calculated with equation (4.33)
Na^+	0.179	0.1991	0.4515
Ca^{2+}	0.470	0.5229	1.1857
Si^{4+}	0.0165	0.0183	0.0416
Al^{3+}	0.0520	0.0578	0.1311
K^+	0.830	0.9235	2.0938
O^{2-}	3.880	4.3171	9.7881

MS5A has the chemical structure $Ca_5Na_2((AlO_2)_{12}(SiO_2)_{12})$. Its molar mass M is calculated due to the molar masses of the involved matters which are listed in table 3.7 with

$$M = \sum_i x_i M_i \tag{3.68}$$

where M and M_i is in kg/mol and x_i the stoichiometrical coefficients. For MS5A it is

$$M_{MS5A} = 1.68 \frac{kg}{mol} \tag{3.69}$$

Sievers [37] measured for MS5A a pellet density of

$$\rho_{app,MS5A} = 1150 \frac{kg}{m^3} \tag{3.70}$$

Table 3.7: Molar masses of interesting matters.

Compound	Molar mass in 10^{-3} kg/mol
Na	22,989
Ca	40,08
Si	28,086
Al	26,981
K	39,102
O	15,999

The molar refractivity of MS5A is calculated with the values of the ionic molar refractivites of table 3.6 with

$$R_{m,MS5A} = 4.79 \cdot 10^{-4} \frac{m^3}{mol} \tag{3.71}$$

Finally the refractive index of MS5A is

$$n_{MS5A} = 1.57 \tag{3.72}$$

Direct measurements for zeolites were only found for MS4A and silicalite-1. Nevertheless the proposed way of refractive index calculation is very straightforward and independent of experimental work. It is an important parameter for the calculation of *Hamaker* constants, e.g. for aluminosilicates, as shown in the next Section.

3.3.6. Hamaker constant

For the characterisation of solid materials their interaction potentials with other solids or fluids are of strong interest. One of the most important parameters for describing the disperse energies of a given system is the so-called *Hamaker* constant of the solid. This constant is also eminent for the calculation of adsorption equilibria of gases on energetically homogeneous and heterogeneous surfaces.

Hamaker constants of organics (solids and liquids) in air have magnitudes of $(6 \pm 1) \cdot 10^{-20}$ J and are reported to be lower than those of inorganic salts ($(9 \pm 3) \cdot 10^{-20}$ J), which are again lower than those of metal oxides ($(13 \pm 4) \cdot 10^{-20}$ J) [41]. *Götzinger* [49] reports in table 3.8 constants of several inorganic and organic matters.

Table 3.8: Hamaker constants of inorganic and organic matters.

Matter	Hamaker constant in 10^{-20} J
Al_2O_3	12.19 – 17.01
TiO_2	16.05 – 22.08
Silicium	20.60 – 22.90
SiO_2	6.28 – 6.90
Polystyrol	6.34 – 8.0
Graphite	12.71 – 28.0
Active carbon	6.0

Van der Hoeven [41] reports two methods for the estimation of Hamaker constants. The first one is based on the macroscopic theory of *Lifshitz*. It requires the knowledge of the absorption spectrum and the dispersion, i.e. the refractive index $n(\omega)$ and the dielectric permittivity $\varepsilon(\omega)$ as a function of frequency. The other method is the *Hamaker-de Boer* microscopic summation approach. This method is based on the subdivision of the inorganic solid molecules into atoms, which all have an average composition and polarisability, identical to that of the solid molecule. The method requires, apart from the refractive indexes and dielectric constants, the molar masses

and the specific densities of the materials involved. A brief description of these two methods and their theories is given in the next sections.

3.3.6.1. Macroscopic approach of Lifshitz

Hamaker [75] experienced in 1937 the existence of adhesive forces between small particles. He ascribed this adhesion for a large part to *London van-der-Waals* forces. In his theory the energy of interaction between two particles containing $\rho_{j,at}$ atoms per m^3 is given by

$$E = -\int_{V_1} dv_1 \int_{V_2} dv_2 \frac{{\rho_{j,at}}^2 \beta}{r^6} \tag{3.73}$$

where dv_1, dv_2, V_1 and V_2 designate volume elements and total volumes of the two particles, respectively, r denotes the distance between dv_1 and dv_2 in m and β is the *London van-der-Waals* constant in $J*m^6$.

The mutual energy of two spheres of diameters D_1 and D_2, with the distance d according to figure 3.8 and containing $\rho_{1,at}$ and $\rho_{2,at}$ atoms per m^3 which interact with an energy $\frac{\beta}{r^6}$ is according to *Hamaker* (see Figure 3.8)

$$E = -Ha \frac{1}{12}\left(\frac{y_1}{{x_1}^2 + x_1 y_1 + x_1} + \frac{y_1}{{x_1}^2 + x_1 y_1 + x_1 + y_1} + 2\ln \frac{{x_1}^2 + x_1 y_1 + x_1}{{x_1}^2 + x_1 y_1 + x_1 + y_1} \right) \tag{3.74}$$

where the variables are defined as

$$Ha = \pi^2 \rho_{1,at}\ \rho_{2,at}\ \beta\,, \tag{3.75}$$

$$x_1 = \frac{d}{D_1} \text{ and} \tag{3.76}$$

$$y_1 = \frac{D_2}{D_1} \tag{3.77}$$

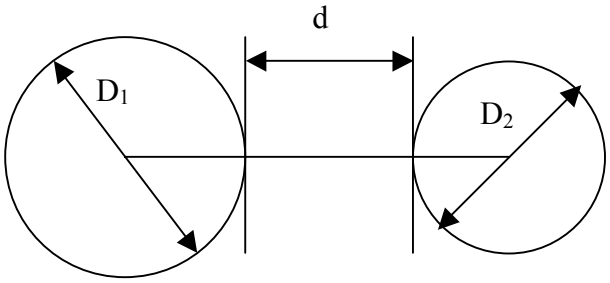

Figure 3.8: Two interacting spheres.

The constant Ha is also known as the Hamaker constant and is defined for like particles with the same atom density $\rho_{j,at}$ as

$$Ha = \pi^2 \rho_{j,at}{}^2 \beta \tag{3.78}$$

When $x_1 << 1$ or $d \rightarrow 0$ equation (3.74) is approximated by

$$E = -Ha \frac{1}{12} \frac{D_2 D_1}{d(D_2 + D_1)} \tag{3.79}$$

Ackler et al. [76] calculated the *Hamaker* constant of muscovite mica, Al_2O_3, SiO_2, Si_3N_4 and rutile TiO_2 from *Lifshitz* theory. He compared these constants to values calculated from physical properties using the *Tabor-Winterton* approximation.

Lifshitz developed a theory for the nonretarded case where the interparticle separations are small enough that the interactions between dipoles is considered instantaneous. The *van-der-Waals* interaction is the result of fluctuations in the electromagnetic field between two macroscopic bodies, modified by the separating media, where the interaction can be referred to the standing waves which only occur at certain frequencies. Hence, the *van-der-Waals* interaction and, thus, the associated *Hamaker* constants can be estimated from the knowledge of the frequency dependent dielectric properties of the interacting materials together with

the intervening medium and the geometry of the bodies. The accuracy of the estimated *Hamaker* constants is directly related to the precision and accuracy of the dielectric spectra and the mathematical representation of this data [77].

The dielectric properties of materials are commonly represented by the frequency dependent dielectric response function

$$\varepsilon(\omega) = \varepsilon'(\omega) + i\varepsilon''(\omega) \tag{3.80}$$

which is a complex function here, $\varepsilon'(\omega)$ is the real part and $\varepsilon''(\omega)$ the imaginary part. For a static applied field ($\omega = 0$), non-conductor materials are characterised by $\varepsilon''(0)$=0, hence $\varepsilon'(0) = \varepsilon(0)$ which is the static dielectric constant. For this case the real part of the dielectric response is directly related to the refractive index n through

$$\varepsilon(0) = \varepsilon'(0) = n^2(0) \tag{3.81}$$

Dielectric data can be obtained with a number of methods including capacitance bridge, optical reflectance and electron loss spectrometry. Most of these techniques yield only one of the components of the complex dielectric response function which often necessitate the transformation from the real to the imaginary component or vice versa. Such a transformation can be performed using the *Kramers-Kronig* relations, one of them defined as

$$\varepsilon'(\omega) = 1 + \frac{2}{\pi}\int_0^\infty \frac{x_1\,\varepsilon''(\omega)}{x_1^{\,2} - \omega^2}\,dx_1 \tag{3.82}$$

However, since the *Kramers-Kronig* relation is formally correct only when $\varepsilon''(\omega)$ is known in the entire frequency range, $0 < \omega < \infty$, this procedure is applicable. *Nimhan* and *Parsegian* showed that by constructing an imaginary dielectric response function, $\varepsilon(i\xi_m)$, a much simpler dielectric representation could be used for the purpose of calculating *Hamaker* constants. In the study of *Bergström* [77] $\varepsilon(i\xi_m)$ is represented for most of the inorganic materials by one UV and IR relaxation through

$$\varepsilon(\mathrm{i}\xi_{\mathrm{m}}) = 1 + \frac{C_{IR}}{1+\left(\frac{\xi}{\omega_{IR}}\right)^2} + \frac{C_{UV}}{1+\left(\frac{\xi}{\omega_{UV}}\right)^2} \tag{3.83}$$

where each material is characterised by four parameters; C_{IR} and C_{UV} are the absorption strengths in the IR and UV range, respectively, and ω_{IR} and ω_{UV} represent the characteristic absorption frequencies in the IR and UV range, respectively. It is

$$C_j = \frac{2}{\pi}\frac{f_j}{\omega_j}\text{, j = IR, UV} \tag{3.84}$$

where f_j is the oscillator strength and ω_j is the relaxation frequency of the absorption band. Now, the non-retarded *Hamaker* constant of two particles 1 and 2 in medium 3 can be derived from the integral

$$Ha_{132} = \frac{3kT}{2}\sum_{m=0}^{\infty}{}'\int_0^{\infty} x_1 \ln\left(1 - \Delta 13\Delta 23\exp(-x_1)\right)dx_1 \tag{3.85}$$

This integral can be solved analytically to yield

$$Ha_{132} = \frac{3kT}{2}\sum_{m=0}^{\infty}{}'\sum_{s=1}^{\infty}\frac{(\Delta 13\Delta 23)^s}{s^3} \tag{3.86}$$

where k is the *Boltzmann* constant and T the temperature in K and with the differences in dielectric response, Δkl, defined as

$$\Delta kl = \frac{\varepsilon_k(i\xi_m) - \varepsilon_l(i\xi_m)}{\varepsilon_k(i\xi_m) + \varepsilon_l(i\xi_m)} \tag{3.87}$$

Bergström [77] used simplified approximations by only retaining a single UV relaxation to represent the dielectric response of each material. His simplifications have been motivated by the important role of the ultraviolet relaxations on the magnitude of the disperse interactions. With such a simple dielectric representation

each material is fully described by three parameters, $\varepsilon(0)$, the characteristic frequency in the ultraviolet, ω_{UV}, and the low-frequency limit of refractive index in the visible UV range, n_0 (since $C_{UV} = n_{vis}^2 - 1$). For example he calculated the *Hamaker* constant Ha_{131} for two identical materials 1, interacting across a medium 3, by using (3.36), neglecting all summation terms s > 1, converting the summation over m to an integral for n > 1, and finally setting $\omega_1 = \omega_3 = \omega$. This results in

$$Ha_{131} = \frac{3kT}{4}\left(\frac{\varepsilon_1(0)-\varepsilon_3(0)}{\varepsilon_1(0)+\varepsilon_3(0)}\right)^2 + \frac{3h\omega}{32\pi\sqrt{2}}\frac{\left(n_1^2-n_3^2\right)^2}{\left(n_1^2+n_3^2\right)^{3/2}} \tag{3.88}$$

Both authors (*Bergström* and *Ackler*) compared their data with the *Tabor-Winterton* approximation for the *Hamaker* constant. Beside the above simplification of ignoring contributions from vibrations in the infrared a second approximation is made that the absorption in the UV occurs within a narrow frequency range. It follows

$$Ha_{131} = \frac{3\,\pi\,h\nu_e}{8\sqrt{2}}\frac{\left(n_1^2-n_3^2\right)^2}{\left(n_1^2+n_3^2\right)^{3/2}} \tag{3.89}$$

where h is the *Planck*'s constant and ν_e the main electronic absorption frequency of about $3*10^{15}$ Hz also called the plasma frequency. Recalling that $n = \varepsilon^2$, it is apparent that the *Tabor-Winterton* approximation enables the calculation of a *Hamaker* constant only from physical properties such as the refractive index or the dielectric constant of the materials of interest and of the medium "3".

In the case of two interacting identiacl macrobodies (index1) in vacuum *Israelachvili* derived the following expression which allows to approximate the *Hamaker* constant [21, 98]:

$$Ha_{11} = \frac{3kT}{4}\left(\frac{\varepsilon_1(0)-1}{\varepsilon_1(0)+2}\right)^2 + \frac{3h\nu_e}{16\sqrt{2}}\frac{\left(n_1^2-1\right)^2}{\left(n_1^2+1\right)^{3/2}} \tag{3.90}$$

In this equation, instead of integration over the whole frequency area, $\varepsilon(\omega)$ and $n(\omega)$ in the original equations of *Lifshitz* are replaced by two static values, one at low frequencies, i.e. the static dielectric constant ε, and one at high frequency, i.e. the refractive index n of the medium in visible light.

In this macroscopic approach the static dielectric constant is not known in many cases or must be measured in a complex way. Considering the large differences in chemical compositions, it is unlikely that inorganic matters all have the same ν_e value of $3 \cdot 10^{15}$ s^{-1}. Nevertheless *Israelachvili* has shown that the results of equation (3.90) are accurate within a few percent when compared with the results of exact computations.

In the next Section the *Hamaker – de Boer* microscopic approach is introduced which is used in this work for the derivation of the *London* interaction forces.

3.3.6.2. Microscopic approach of *Hamaker – de Boer*

The *Hamaker – de Boer* microscopic approach is based on the equation

$$Ha = \pi^2 \rho_{j,at}{}^2 \beta \qquad (3.78)$$

where $\rho_{j,at}$ is the is the number density of solid atoms in $1/m^3$ and β the *London* constant in $J*m^6$ [75]. This approach is strictly speaking valid only for monoatomic solids. If the *Hamaker* constant of multiatomic solids is calculated their chemical structure has to be considered. The proposed route is based on a subdivision of the solid molecule into atoms, which all have a mean concentration and polarisability. The Hamaker constant is then calculated due to these mean polarisabilities. A second assumption is that only the valence electrons of these atoms contribute to the disperse interaction potential. So the average atoms are all bonded by semi-polar bonds and only the bond-forming electrons contribute to the higher energetic waves.

The Hamaker constant for multiatomic solid molecules is then

$$Ha = \pi^2 \rho_{\mathrm{j,at}}^2 \ \overline{\beta} \tag{3.91}$$

where $\rho_{j,at}$ is the number density of solid atoms and $\overline{\beta}$ the London constant. The number density can be calculated via

$$\rho_{j,at} = n_a \frac{N_A \rho_{app}}{M} \tag{3.92}$$

where n_a is the number of atoms in the molecule. M denotes the relative atomic mass related to the same solid molecule with which the number of atoms is calculated. In the following the zeolite MS5A with the chemical structure $Ca_5Na_2((AlO_2)_{12}(SiO_2)_{12})$ is examined. Its molecular mass is given in equation (3.69). The overall number of atoms n_a in this molecule is

$$n_{a,MS5A} = 79 \tag{3.93}$$

With the density in equation (3.70)

$$\rho_{MS5A,at} = 3.27 \cdot 10^{28} \frac{1}{m^3} \tag{3.94}$$

is obtained.

The magnitude of this number density of atoms for zeolite MS5A is comparable to many materials, for example silicon has a number density of $5.0 \cdot 10^{28} \frac{1}{m^3}$ and SiO_2 a number density of $2.2 \cdot 10^{28} \frac{1}{m^3}$ [101].

In 1931 *Slater and Kirkwood* [100] derived an equation for the calculation of the *London* constant. *Van-der-Hoeven* [41] modified this equation by introducing an atomic polarisability. The London constant for macro bodies like zeolites can be calculated by

$$\overline{\beta} = \frac{3}{4}\sqrt{s}\, h\nu_0 \left(\frac{\overline{\alpha}}{4\pi\varepsilon_0} \right)^2 \tag{3.95}$$

The letter s represents the number of electron bondings per atom. It is obtained simply from the summation of the single and double bond forming electrons involved in atomic bonding, divided by the number of atoms in the molecule. The parameter s is only reasonable for the calculation of the Hamaker constant and London dispersion potential, respectively. Later this potential will be introduced as the induced dipole – induced dipole interaction energy.

For example, for zeolite MS5A ($Ca_5Na_2((AlO_2)_{12}(SiO_2)_{12})$) the total number of atoms in the molecule is 79. The number of valence electrons is for calcium 5*2 = 10, for sodium 2*1 = 2, for aluminium 12*3 = 36, for silicon 12*4 = 48 and for oxygen 48*6 = 288, altogether 384 valence electrons. The number of electron bondings is then 192. It follows for s that

$$s_{MS5A} = \frac{192}{79} = 2.43 \tag{3.96}$$

The polarisability of the solid atoms can be calculated from the refractive index using the *Lorenz-Lorentz* equation

$$\overline{\alpha} = 4\pi\varepsilon_0 \frac{M}{n_a \frac{4\pi}{3} N_A \rho} \frac{\left(n^2 - 1\right)}{\left(n^2 + 2\right)} = \varepsilon_0 \frac{3M}{n_a N_A \rho} \frac{\left(n^2 - 1\right)}{\left(n^2 + 2\right)} \tag{3.97}$$

with the already known parameters.

The variable ν_0 is the frequency of the electron in the ground state in 1/s. It is

$$\nu_0 = \frac{e}{2\pi\sqrt{m_e}} \frac{1}{\sqrt{\overline{\alpha}}} \tag{3.98}$$

where e is the charge of an electron (e = $1.60*10^{-19}$ C) and m_e the mass of an electron ($m_e = 9.11*10^{-31}$ kg). With known or calculated values of the refractive index n, the apparent density ρ, the molar mass M and the chemical structure of the solid the *Hamaker* constant for zeolites can be calculated. For MS5A it is:

$$Ha_{MS5A} = 7.66 \cdot 10^{-20} J \qquad (3.99)$$

3.4. Adsorption isotherms

In this study single-component equilibria of gases or vapours with microporous solids are examined. The context does not cover phenomena like chemisorption, hydrogen bonding, steric or formselective effects. Attention is payed only to physisorption only, the adsorptive gas molecules are physically bonded to the microporous surface via potential forces. In this Section the existing types and common descriptions of adsorption isotherms are discussed which are used in this work for different purposes. E.g. measuring the specific surface according to the BET isotherm, calculating Henry coefficients by means of *Langmuir* and *Toth* isotherms.

3.4.1. Types of isotherms

The first classification of physical adsorption isotherms was presented by *Brunauer et al.* [78]. In 1985 the IUPAC Commission on Colloid and Surface Chemistry proposed modifications of this classification by adding a sixth type, the stepped isotherm, to the original five types of *Brunauer et al.*. Type I (the *Langmuir* isotherm) is typical for microporous adsorbents (activated carbons, zeolites). The next two are typical for nonporous materials with strong (type II) and weak (type III) fluid-surface forces. Types IV and V are characteristic for mesoporous materials when capillary condensation occurs (these types exhibit hysteresis loop). Type VI occurs for materials with relatively strong fluid-surface forces, usually when the temperature is near the melting point of the adsorbed gas [79]. Figure 3.9 shows the principle types of adsorption isotherms regarding to IUPAC classification.

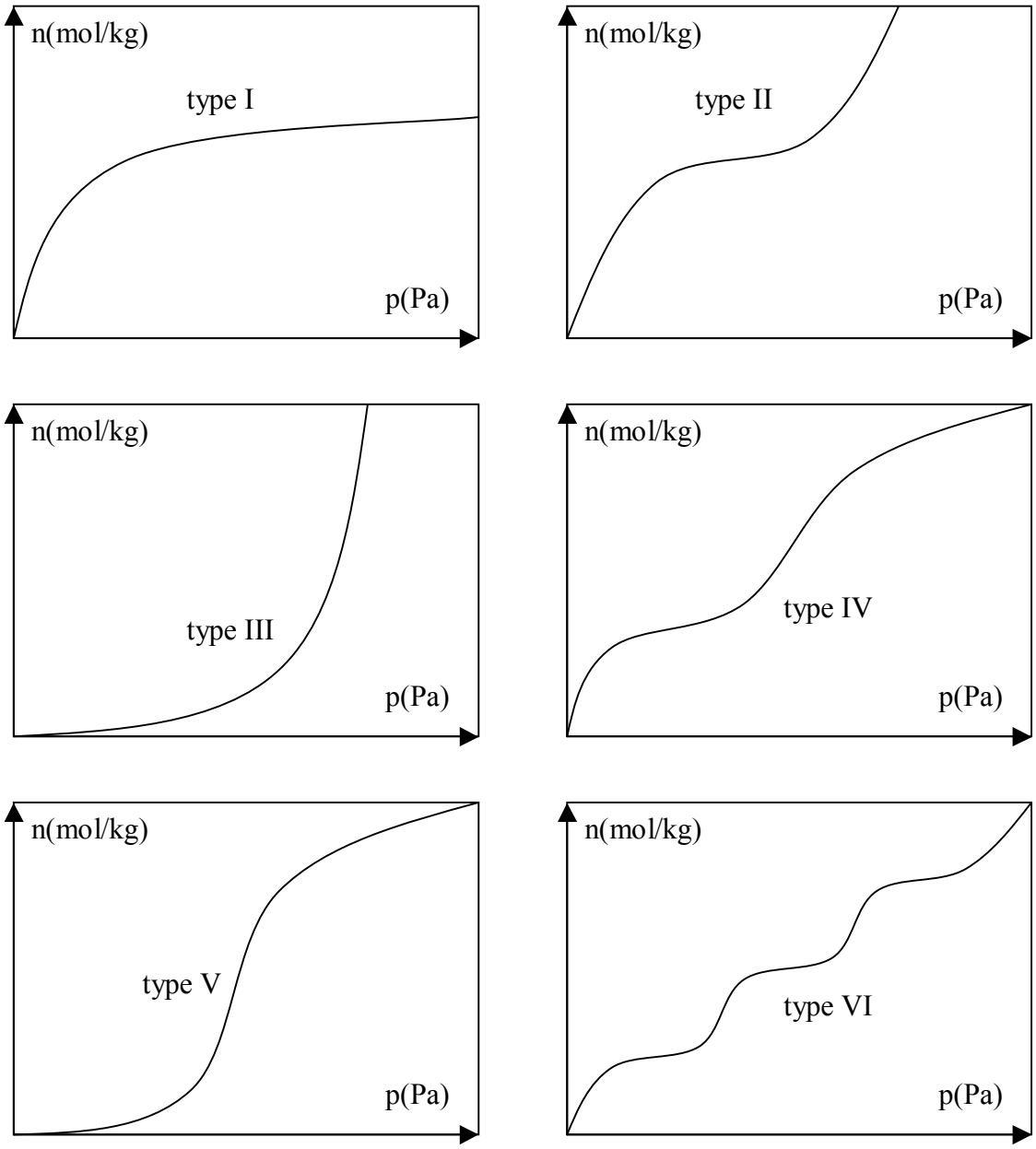

Figure 3.9: Principle types of adsorption isotherms regarding to IUPAC classification.

Nevertheless, the classification of adsorption isotherms in several types is not helpful for the understanding of the decisive physical processes. Also the evaluation of the isotherm types as advantageous or disadvantageous is ambivalent, because an advantageous form for adsorption is at the same time a disadvantageous form for desorption [24]. This work deals mainly with isotherms of type I.

3.4.2. *Langmuir* isotherm

Irving Langmuir developed 1918 a quantitative theory of monolayer adsorption which is simple and ingenious at the same time [80]. Figure 3.10 shows the principle basis of the *Langmuir* model. The assumptions are [82]:

- The molecules are adsorbed on well-defined and localised places.
- Each adsorption place can bind only one adsorptive molecule.
- All adsorption places are energetically equivalent.
- There are no interactions between adsorbed molecules.

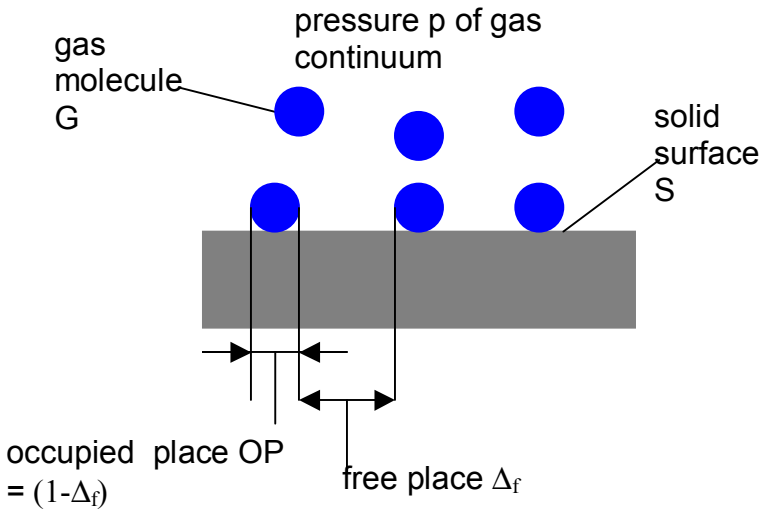

Figure 3.10: Principle of the *Langmuir* model.

For the attachment of molecules with solid surfaces the following reaction is essential:

$$\Delta_f + G \underset{k_{des}}{\overset{k_{ads}}{\leftrightarrow}} OP \qquad (3.100)$$

The adjustment of a sorption equilibrium leads to the equilibrium constant K_L, which is the ratio of the concentration of free gas molecules [G], the concentration of free places [Δ_f] and the concentration of occupied places [OP]:

$$K_L = \frac{[OP]}{[G][\Delta_f]} \tag{3.101}$$

K_L is called the *Langmuir* constant and has the dimension 1/pressure because the concentration of free gas molecules [G] is equivalent to the partial pressure p of the adsorptive. The sum of the concentration of free places and occupied places is the maximum available concentration of sorption places [SP]. It is

$$[SP] = [OP] + [\Delta_f] \tag{3.102}$$

and it follows with

$$[\Delta_f] = [SP] - [OP] \tag{3.103}$$

for the Langmuir constant in equation (3.101)

$$K_L = \frac{[OP]}{[G]([SP] - [OP])} \tag{3.104}$$

After resolution to the concentration of occupied places it follows:

$$[OP] = [SP]\frac{K_L[G]}{1 + K_L[G]} \tag{3.105}$$

The concentrations of occupied and maximum available sorption places are equivalent to the loading n and the maximum available loading n_{mon} of gas molecules on the solid surface. So the *Langmuir* isotherm for monolayer loadings can be immediately written to

$$n = n_{mon}\frac{K_L\ p}{1 + K_L\ p} \tag{3.106}$$

For very low pressures $K_{L*}p$ becomes negligible compared to unity, so that as a first approximation the *Henry* isotherm is obtained:

$$n = n_{mon}\ K_L\ p \tag{3.107}$$

The product of the constants $n_{mon} * K_L$ is equal to the *Henry* coefficient He. These constants are adjustable coefficients to adsorption data. With a linearised form the *Langmuir* coefficients can be derived via a graph with p as the x axis and p/n as the y axis. It is

$$\frac{p}{n} = \frac{1}{n_{mon} K_L} + \frac{1}{n_{mon}} p \tag{3.108}$$

The *Henry* coefficient is then indirect proportional to the intercept point L_i:

$$He = \frac{1}{L_i} = \frac{1}{1 \diagup (n_{mon} K_L)} \tag{3.109}$$

The *Langmuir* isotherm can also be derived from statistical thermodynamics and by using *Gibb*'s isotherm [81].

3.4.3. BET isotherm

The BET isotherm is eminent for the determination of the specific surface of adsorbents. Therefore, the isotherm is derived theoretically in this Section. With the help of a few simplifying assumptions it is possible to carry out an isotherm derivation for multimolecular layers that is similar to *Langmuir*'s derivation for monolayers [62]. *Brunauer, Emmett* and *Teller* look at the surface layers s_i covered by only i layers of adsorbed molecules. Using *Langmuir*'s equation for monolayer adsorption they derive the general equation

$$a_i p s_{i-1} = b_i s_i \exp\left(\frac{-H_i}{\Re T_{ads}}\right) \tag{3.110}$$

where p is the pressure in Pa, H_i the specific heat of the i-th layer in J/mol, a_i a mole rate constant of layer i in mol/(m^2*s*Pa), b_i a mole rate constant of layer i in mol/(m^2*s) and s_i the surface of the molecule layer i in m^2. Equation (3.110) means that the rate of condensation on top of the layer i-1 is equal to the rate of evaporation of the i-th layer. *Brunauer et al*. proposed the following points:

- The specific heat of the first layer is the heat of adsorption H_{ads}.
- The specific heat of the i-th layer is the heat of liquefaction H_L with

$$H_1 = H_2 = ...H_i = H_L \tag{3.101}$$

  This is equivalent to saying that the evaporation-condensation properties of the molecules in the second and higher adsorbed layers are the same as those of the liquid state. This means also that

$$\frac{b_2}{a_2} = \frac{b_3}{a_3} = ...\frac{b_i}{a_i} = g \tag{3.102}$$

  where g is an appropriate constant in Pa.
- At equilibrium the surface layers s_i remain constant.

The total surface S is given by

$$S = \sum_{i=0}^{\infty} s_i \tag{3.103}$$

and the total volume adsorbed is

$$V_G = v_0 \sum_{i=0}^{\infty} i\, s_i \tag{3.104}$$

where v_0 is the volume of gas adsorbed on one square meter of the adsorbent surface when it is covered with a complete monolayer of adsorbed gas. It follows that

$$\frac{V_G}{S v_0} = \frac{V_G}{V_{G,mon}} = \frac{\sum_{i=0}^{\infty} i\, s_i}{\sum_{i=0}^{\infty} s_i} \tag{3.105}$$

where $V_{G,mon}$ is the volume of gas adsorbed when the entire adsorbent surface is covered with a complete monolayer. One can express now s_1, s_2, … s_i in terms of s_0 whereas

$$s_1 = y s_0 \quad where \quad y = \frac{a_1}{b_1} p \exp\left(\frac{H_{ads}}{\Re T_{ads}}\right) \tag{3.106}$$

$$s_2 = \varphi s_1 \quad where \quad \varphi = \frac{p}{g} \exp\left(\frac{H_L}{\Re T_{ads}}\right) \tag{3.107}$$

$$s_i = \varphi s_{i-1} = \varphi^{i-1} s_1 = y \varphi^{i-1} s_0 = c \varphi^i s_0 \quad where \quad c = \frac{y}{\varphi} = \frac{a_1 g}{b_1} \exp\left(\frac{H_{ads} - H_L}{\Re T_{ads}}\right) \tag{3.108}$$

The variable φ can also be understood as the relative saturation, the ratio of the pressure of the gas to its saturation pressure. The variable c is the well known BET constant.

Substituting (3.106), (3.107) and (3.108) into equation (3.105) yields

$$\frac{V_G}{V_{G,mon}} = \frac{c s_0 \sum_{i=1}^{\infty} i \varphi^i}{s_o \left(1 + c \sum_{i=1}^{\infty} \varphi^i\right)} \tag{3.109}$$

If the number of the adsorbed layers cannot exceed a maximum number n, then the summation of the two series in equation (3.109) is to be carried out to n terms only, and not to infinity. It follows then

$$\frac{V_G}{V_{G,mon}} = \frac{c\varphi}{(1-\varphi)} \frac{1 - (n+1)\varphi^n + n\varphi^{n+1}}{1 + (c-1)\varphi - c\varphi^{n+1}} \tag{3.110}$$

which is the well known general BET isotherm. For the determination of the solid surface S_{BET} the summation of the two series has to be carried out to infinity. The denominator sum can be represented as the sum of an infinite geometric progression

$$\sum_{i=1}^{\infty} \varphi^i = \frac{\varphi}{1-\varphi} \tag{3.111}$$

and the numerator sum can be expressed also in the same way as

$$\sum_{i=1}^{\infty} i\varphi^i = \frac{\varphi}{(1-\varphi)^2} \tag{3.112}$$

It follows therefore that

$$\frac{V_G}{V_{G,mon}} = \frac{c\varphi}{(1-\varphi)(1-\varphi+c\varphi)} \tag{3.113}$$

With

$$\varphi = \frac{p}{p^0} \tag{3.114}$$

equation (3.2) for the determination of the solid surface S_{BET} is obtained.

3.4.4. *Toth* isotherm

One of the assumptions of *Langmuir* is the energetic homogeneity of the adsorbent surface. This assumption is not always valid. *Toth* also tried to take into account the energetic heterogeneity in his adsorption equilibrium modell [83]. The basis of his theory is the dividing of the surface in a huge number of homogeneous fields with very small areas. With the partial loading

$$N = \frac{n}{n_{mon}} \tag{3.115}$$

he wrote in a first step the *Langmuir* equation (3.106) in the differential form

$$\frac{N}{p}\frac{dp}{dN} - 1 = K_L\, p \tag{3.116}$$

Toth introduced a differential function $\Psi(p)$ which describes the whole energetic heterogeneous loading interval:

$$\psi(p) = K_T\, p^m \tag{3.117}$$

where $0 < m < 1$ and K_T is the *Toth* constant in $(1/Pa)^m$. The backwards integration of equation (3.116) with equation (3.117) yields the *Toth* isotherm

$$N = \frac{n}{n_{\max}} = \frac{p}{\left(\frac{1}{K_T} + p^m\right)^{\frac{1}{m}}} \tag{3.118}$$

The *Henry* coefficient follows at very small pressures. It is

$$He = \lim_{p \to 0}\left(\frac{n}{p}\right) = n_{\max}\left(K_T\right)^{\frac{1}{m}} \tag{3.119}$$

The qualitative difference of *Henry* coefficient derivations via the *Langmuir* and *Toth* isotherms is discussed in Chapter 7.

3.4.5. Potential theories

The isotherms of *Langmuir, Brunauer* et al. and *Toth* are derived from equilibrium or kinetic considerations. Another possibility is the inclusion of adsorption forces or potentials in the models. In this Section classic and modern concepts of potential theories are presented.

3.4.5.1. *Polanyi* and *Dubinin*

Polanyi developed his potential theory in 1916 [84]. The assumptions made are:

- The solid concentrates the adsorbed material on its surface by means of attraction forces.
- The attraction forces are dependent on system properties and the distance of the interacting molecules.
- The attraction forces are independent of temperature.
- There is no dissolution of the adsorbed molecules in the adsorbent.
- The adsorption volume is filled by liquid adsorbate only.
- Gas phase exhibits ideal gas behaviour.
- The liquid adsorbed phase is incompressible.
- Creating a liquid surface involves negligible work.

The adsorption potential is defined by *Polanyi* as the isothermal compression work of a molecule with partial pressure p which transfers from the gas phase to a point in the adsorbed phase with saturation pressure p^0 with

$$\varepsilon = \Re T_{ads} \ln\left(\frac{p^0}{p}\right) \tag{3.120}$$

The later studies of *Dubinin* on adsorption equilibria are based on the potential theory of *Polanyi*. The adsorption in microporous adsorbents is understood as successive filling of the pore volume. The principle task in his theory consists of finding the distribution of the volume adsorption space, v, as a function of *Polanyi* adsorption potential ε with

$$v = f\left(\frac{\varepsilon}{\beta}\right) \tag{3.121}$$

where β is called the affinity coefficient. The forces of attraction of the molecules to the surface of the adsorbent are related to the ratio of polarisability of the vapourous molecules, therefore

$$\beta = \frac{\varepsilon}{\varepsilon_{ref}} = \frac{\alpha}{\alpha_{ref}} \tag{3.122}$$

where α is the polarisability of the molecule and the index "ref" indicates the reference molecule. *Dubinin* assumes that the temperature does not produce any effect on this characteristic curve v, each adsorbent has its own characteristic curve that describes its adsorption-force field. For adsorbents of type I, including active carbons and zeolites with extremely small micropores, the equation of the characteristic curve assumes the form

$$v = v_{\max} \exp\left(-\kappa \frac{\varepsilon^2}{\beta^2}\right) \tag{3.123}$$

where v_{max} is the limiting volume of adsorption space that equals the volume of all micropores. The parameter κ reflects the function of distribution of volume of the pores according to sizes. This theory was tested on the basis of numerous substances. It is very successful in describing adsorption equilibria of active carbons. The advantage of this approach is that for the description of the characteristic curve only one isotherm has to be examined experimentally over a big concentration interval [82]. With equation (3.120) in equation (3.123) the isotherm of *Dubinin-Raduskevich* is given by

$$\frac{v}{v_{\max}} = \exp\left(-\kappa\left(\frac{\Re T_{ads}}{\beta} \ln \frac{p^0}{p}\right)^2\right) = \frac{n}{n_{\max}} \tag{3.124}$$

where the ratio of the volumes can be replaced by the ratio of the loading n/n_{max} for a constant density of the adsorbed phase.

A general form of equation (3.124) was derived by *Dubinin* and *Astakhov* [130] with

$$\frac{v}{v_{\max}} = \exp\left(-\kappa^{*}\left(\frac{\Re T_{ads}}{\beta}\ln\frac{p^{0}}{p}\right)^{Y}\right) = \frac{n}{n_{\max}} \qquad 1 < Y < 3 \qquad (3.125)$$

It is not possible to transfer equation (3.124) and (3.125) to *Henry*'s-law in the low partial pressure interval. The postulation for the thermodynamic consistency of a isotherm description is not fulfilled. Nevertheless, for bigger concentrations the *Dubinin* isotherms are powerful instruments.

3.4.5.2. Monte Carlo simulations

The objective of molecular modelling systems is to predict macroscopic, experimentally observable properties by simulating the molecular motion of materials [87]. One starts with a model that describes the inter- and intra-molecular interactions and then relates this through statistical mechanics to macroscopic properties. These can range from thermodynamic properties to transport properties and to molecular arrangements.

There are two major ways to solve these problems statistically. In the first one, molecular dynamics (MD), molecules move under the influence of their own molecular forces. In micro canonical molecular dynamics, one specifies the number of molecules, the energy in the system and the volume of the system. The positions of each molecule are then calculated by solving *Newton*'s equation for the force F, the mass m and the acceleration a:

$$F = m\,a \qquad (3.126)$$

From this, the desired properties can be gained as a function of position and velocity as a function of time.

Another way is the Monte Carlo simulation which is a stochastic method. In a traditional or canonical Monte Carlo simulation, the volume, the number of molecules, and the temperature of the system are specified. The Monte Carlo method uses a

random number generator to propagate molecules according to the canonical probability distribution. Translation and rotation motions are accepted or rejected according to canonical accepted rules. By examining the accepted and rejected motions, an average of them can be made in order to obtain equilibrium properties for the system of interest. The algorithm in figure 3.11 gives the steps involved in Monte Carlo simulations.

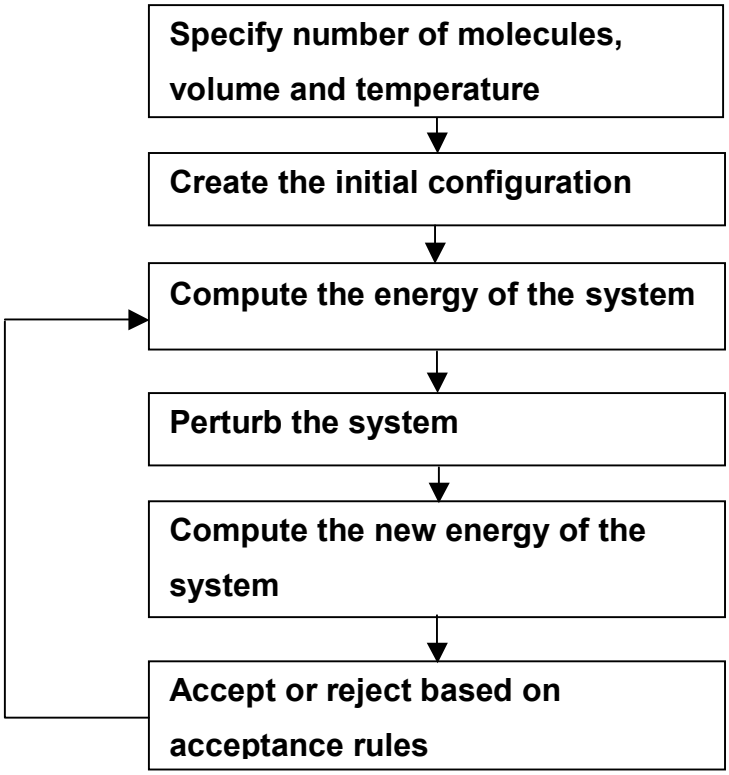

Figure 3.11: Steps involved in Monte Carlo simulations.

In the grand canonical Monte Carlo (GCMC) ensemble the number of particles fluctuates while the chemical potential is constrained. This makes GCMC a natural choice for studying phase equilibrium since the chemical potential of two phases must be equal at equilibrium. Thus, GCMC uses the chemical potential as the basis for adding and removing molecules from the system. In addition, the solid phase is in contact with a vapour phase of known fugacity, which is related to the chemical potential. In GCMC the four basic motions of a particle are as follows:

- Insertion into a random position in the system.
- Deletion
- Rotation
- Translation into a new position in the system.

In their review *Smit and Krishna* discuss the use of modern Monte Carlo simulations in the context for simulating the properties of molecules adsorbed in zeolites [88]. They show that it is possible to use Monte Carlo simulations to obtain a reasonable estimate of an adsorption isotherm of pure hydrocarbons and their mixtures in zeolites. As in all kinds of simulation methods the restrictions of Monte Carlo simulations are the limits in calculation capacity. Also the results have to be verified with experimental data because it is only a random model and not an a priori one. Nevertheless, intensive engagement with the theme of high-performance-computing is necessary to further push this auspicious methods.

3.4.6. Isotherms based on the *Hamaker* energy of the solid

Maurer [26] has demonstrated that the *Hamaker* energy Ha_j of the adsorbent and the critical data p_c and T_c of the adsorptive are basic properties in order to describe equilibrium isotherms of all gases on active carbon. *Mersmann* et al [27] introduced a diagram in which the initial or *Henry* loading is plotted versus an interaction parameter $\frac{T_C}{T_{ads}}\sqrt{\frac{2Ha_j}{\pi\sigma_j^3 p_C}}$, as can be seen in figure 3.12.

With respect to the entire isotherm in figure 3.12 the dimensionless numbers $\frac{He\,p}{n}$, $\frac{T_C}{T_{ads}}\left(\frac{Ha_j}{\sigma_j^3 p_C}\right)^{3/2}$ and $\frac{n N_A \sigma_i^2}{S_{BET}}$ have been introduced. However, all these results are restricted either to activated carbon and unpolar zeolites like silicalite-1 or to nonpolar adsorptive molecules in the case of polar zeolites.

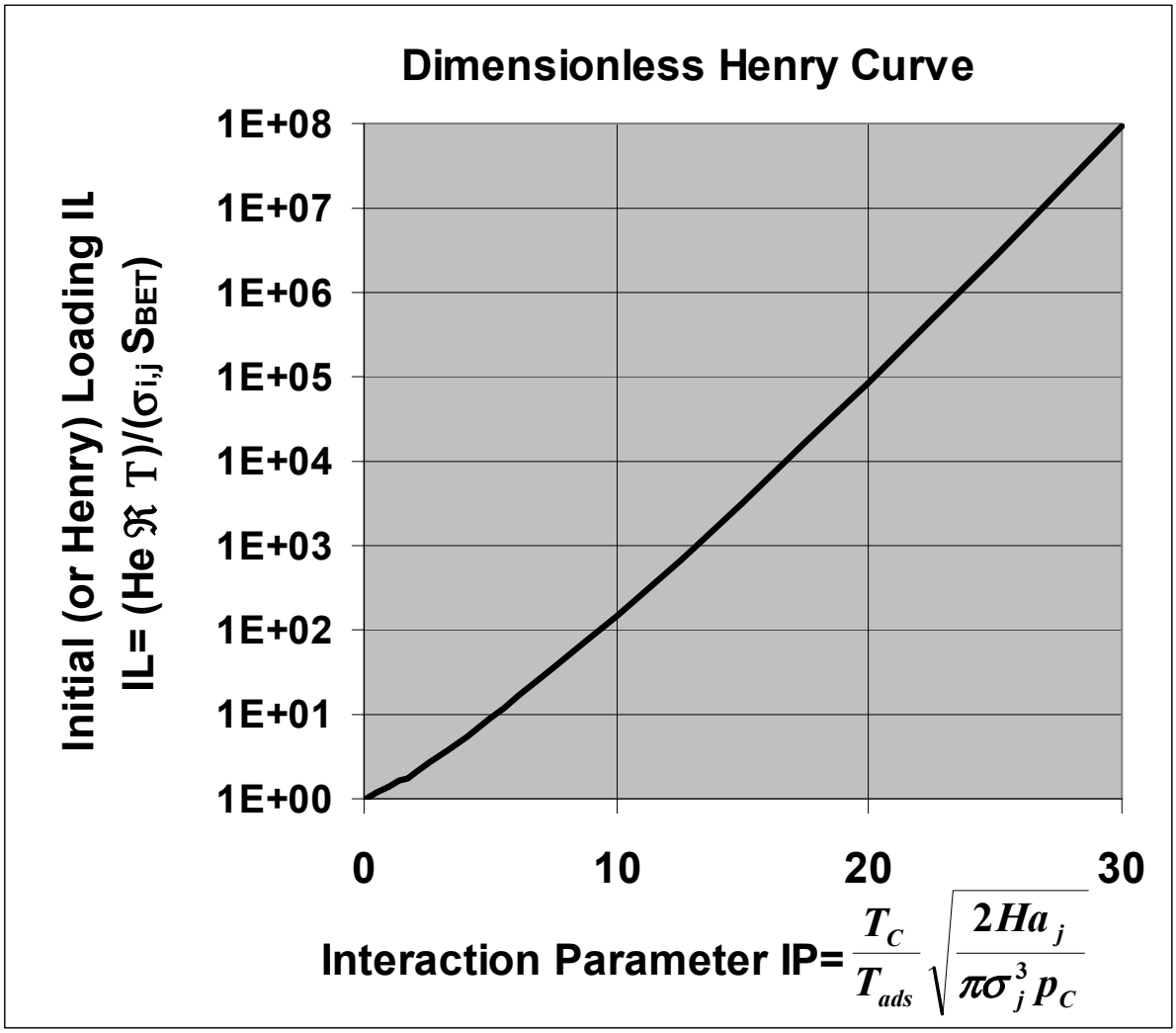

Figure 3.12: The initial or *Henry* loading plotted versus the interaction parameter [27].

4. Experimental Methods for Adsorption Measurements

There are classical and also new techniques for measuring the adsorption equilibrium of gases on microporous adsorbents. The classical procedures described in this Chapter are the volumetric [8, 37, 57] and the packing bed methods [36]. The gravimetric method is explained in Chapter 7 regarding materials and methods used in this study. Newer techniques are the zero length column [89, 90] and the concentration pulse chromatography methods [91, 92].

4.1. Volumetric method

This method is widely used in literature. The adsorption equilibrium time is shortened when a gas pump is used for forced circulation of the adsorptive. *Sievers* [37] utilized a circulation pump with an electro-magnetic clutch between motor and rotary slide valve to ensure the required sealing. Figure 4.1 shows a feasible scheme of the volumetric method.

First, carrier gas (H_2) is dosed to a defined mixing volume V_{mix}, next a small amount of adsorptive is fed. The pressure p_{bef}, the temperature T_{bef} and the molar fraction of the adsorptive y_{bef} are measured, y_{bef} with a gas chromatograph. With this data the moles of adsorptive in the mixing volume can be measured and calculated:

$$n_{bef} = \frac{y_{bef}\, p_{bef}\, V_{mix}}{Z_{bef}\, \Re\, T_{ads}} \tag{4.1}$$

The compressibility factor Z_{bef} can be calculated via the method of *Redlich-Kwong-Soave* which needs only critical data of pure substances. For adsorption the volume and also the adsorbent is switched on. The overall volume is V_{ads}. The pressure p_{aft}, the temperature T_{aft} and the molar fraction y_{aft} are measured. It follows:

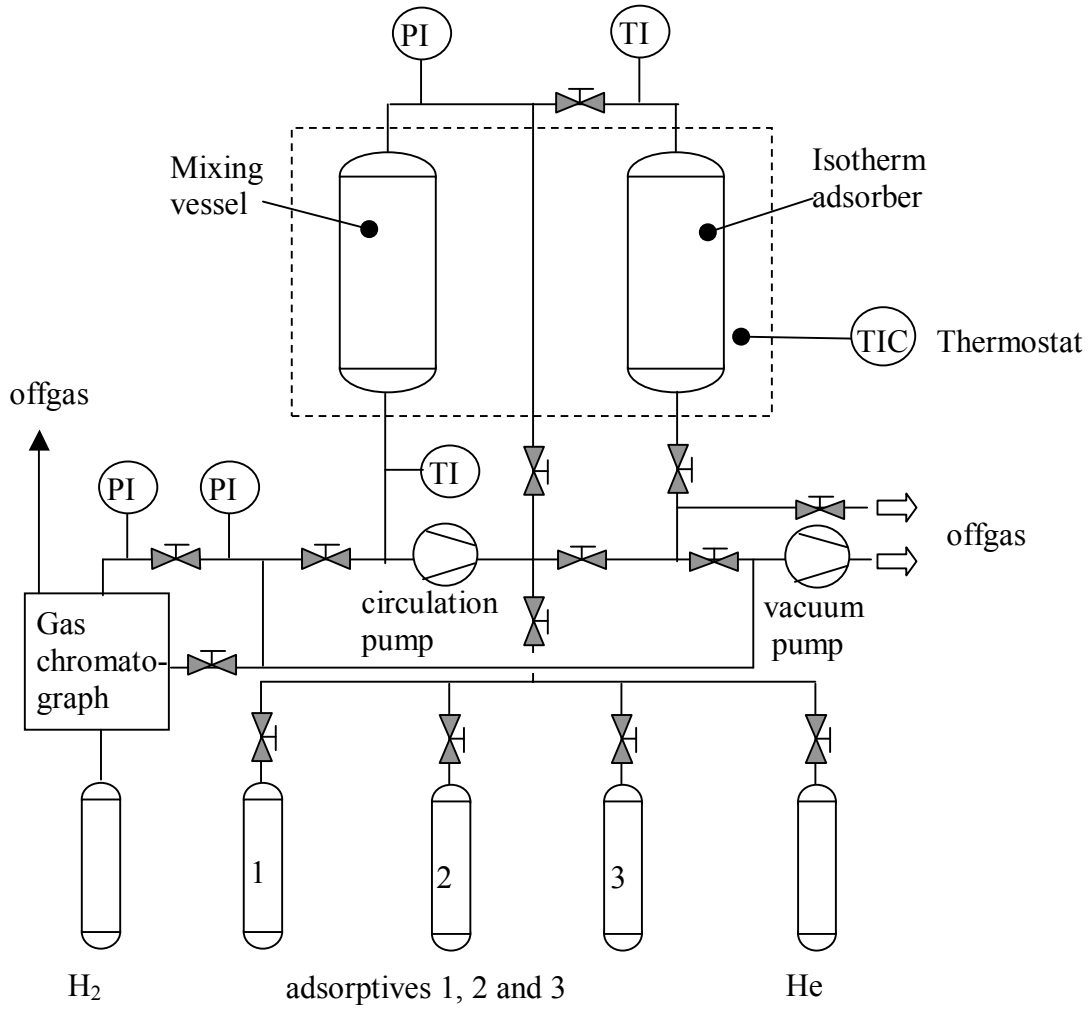

Figure 4.1: Scheme of the volumetric method.

$$n_{aft} = \frac{y_{aft}\, p_{aft}\, V_{ads}}{Z_{aft}\, \Re\, T_{ads}} \tag{4.2}$$

The adsorbed molar quantity can be calculated as the difference of moles in the vapour before and after adsorption:

$$n_{ads} = n_{bef} - n_{aft} = \frac{y_{bef}\, p_{bef}\, V_{mix}}{Z_{bef}\, \Re\, T_{ads}} - \frac{y_{aft}\, p_{aft}\, V_{ads}}{Z_{aft}\, \Re\, T_{ads}} \tag{4.3}$$

The loading n of the adsorbent is the ratio of the adsorbed moles to the mass of the adsorbent:

$$n = \frac{n_{ads}}{m_{ads}} \tag{4.4}$$

The equilibrium pressure $p_{equilibrium}$ for the adsorption isotherm is the partial pressure of the adsorptive in the carrier gas which is assumed not to be adsorbed. It is

$$p_{equilibrium} = y_{aft}\ p_{aft} \tag{4.5}$$

4.2. Packed bed method

In the packed bed method the calculation of the equilibrium is managed by examining the breakthrough curve of the adsorber. A mass balance is drawn around the packed bed. The adsorbed molar amount N of an adsorptive related to the adsorbent mass in the packed bed m_{bed} after a time t can be calculated by

$$n = \frac{N_{in} - N_{out}}{m_{bed}} \tag{4.6}$$

With

$$N_{in} = \frac{\rho_{in} V_{in}}{M_{in}} \quad \text{and} \tag{4.7a}$$

$$N_{out} = \frac{\rho_{out} V_{out}}{M_{out}}$$

it follows

$$n = \frac{\rho_{in} V_{in} - \rho_{out} V_{out}}{M\, m_{bed}} \tag{4.8}$$

where ρ is the partial density of the adsorptive in kg/ m^3, V the gas volume in m^3 and M the molecular mass of the adsorptive in kg/mol. The law of ideal gases delivers the following relationship

$$\rho = \frac{\rho_{stand}\, T_{stand}\, p}{T_{ads}\, p_{stand}} \tag{4.9}$$

The index stand means standard state (T_{stand} = 273.15 K, p_{stand} = 1.01325*10^5 Pa) and ρ_{stand} is the standard density of the adsorptive.

The gas volumes which have passed through the packed bed from t = 0 to breakthrough can be determined via integration over the time. This calculation is demonstrated exemplarily for the outlet stream. The outlet volume stream $\dot{V}_{out}(t)$ is composed of the carrier gas stream $\dot{V}_C(t)$ and the adsorptive flow $\dot{V}_{out,ads}(t)$ with the molar fraction $y_{out,ads}$, so

$$\dot{V}_{out}(t) = \dot{V}_C + \dot{V}_{out,ads}(t) = \dot{V}_C + y_{out,ads}(t)\dot{V}_{out} = \frac{\dot{V}_C}{1 - y_{out,ads}(t)} \tag{4.10}$$

The adsorptive flow is then

$$\dot{V}_{out,ads}(t) = \dot{V}_{out} - \dot{V}_C = \frac{\dot{V}_C}{1 - y_{out,ads}(t)} - \dot{V}_C = \frac{\dot{V}_C\, y_{out,ads}(t)}{1 - y_{out,ads}(t)} \tag{4.11}$$

An analogous equation for the inlet adsorptive flow can be written where the inlet molar fraction of the adsorptive $y_{in,ads}$ is constant:

$$\dot{V}_{in,ads}(t) = \frac{\dot{V}_C\, y_{in,ads}}{1 - y_{in,ads}} \tag{4.12}$$

From equation (4.10) it follows for the carrier gas stream

$$\dot{V}_C = w_G \frac{d^2 \pi}{4}\left(1 - y_{in,ads}\right) \tag{4.13}$$

with w_G as the gas velocity in the inlet which is flow controlled and d as the inner diameter of the inlet pipe. By a combination of equations it follows for the equilibrium loading

$$n = \frac{\rho_{s\tan d}\ p T_{s\tan d}\ w_g\ d^2\ \pi\ y_{in,ads}}{p_{s\tan d}\ T_{ads}\ M\ m_{bed}\ 4} \int_0^t \left(1 - \frac{y_{out,ads}(t)\left(1 - y_{in,ads}\right)}{y_{in,ads}\left(1 - y_{out,ads}(t)\right)}\right) dt \tag{4.15}$$

By continuous measuring of the mole fraction by a gas chromatograph the loading can be calculated from the partial pressure. *Schweighart* [36] could reach low pressure limits of 1.2 Pa with this method in adsorption systems like CO_2-MS5A, C_2H_4-MS5A, C_2H_6-MS5A and C_3H_8-MS5A.

4.3. Zero length column (ZLC) method

The zero length column technique was introduced in the beginning as a simple and rapid approach for the study of sorption kinetics. If the same kind of experiment is performed at a sufficiently low flow rate, the desorption rate will be determined by convection under equilibrium conditions rather than by the desorption kinetics. The effluent concentration history directly yields the equilibrium isotherm. The possibility of using this approach to measure *Henry* constants was suggested by *Ruthven* et al. [89,90].

In a ZLC experiment a couple of layers of zeolite is equilibrated in a short adsorber with an adsorptive of known partial pressure. At time t = 0 the feed (carrier gas with adsorptive) is switched to the pure carrier at constant flow rate. The concentration of the desorbed adsorbate in the outlet stream of the ZLC is continuously measured. The adsorber is so short that in can be treated as an ideal stirred tank reactor. The justification for this is as follows: The two border cases for the residence time behaviour of fluids in a pipe stream are the plug flow reactor without axial dispersion and the ideal stirred tank reactor with a very large axial mixing. Characteristic for this is the *Bodenstein* number Bo [93] with

$$Bo = \frac{w L}{D_{ax}} \tag{4.16}$$

where D_{ax} is the axial dispersion coefficient in the pipe, w the velocity of the fluid and L the length of the pipe. With $L \rightarrow 0$, as it occurs in a ZLC, the Bodenstein number goes towards zero. This corresponds to the case of the ideal stirred tank reactor. With this assumption it can be derived that the concentration of the outlet stream of the ZLC after t = 0 is equal to the inner concentration of the adsorber. The differential mass balance of the adsorptive is

$$m_{ads} \frac{dn}{dt} + V_G \frac{dc}{dt} + \dot{V}_G \, c(t) = 0 \tag{4.17}$$

where V_G is the gas volume in the adsorber, c the concentration of adsorptive in the gas phase in mol/m^3, $\dot{V}_G$ the gas stream in and t the time. Generally, the outlet stream is not the same as the carrier gas stream and equation (4.10) is valid. The adsorptive stream is equal to the third summand in equation (4.17):

$$\dot{N}_{ads} = \dot{V}_G \, c(t) \tag{4.18}$$

With the mole fraction $y_{out,ads}(t)$ and the overall number C of moles per m^3 it is

$$c = C \, y_{out,ads}(t) \tag{4.19}$$

Equation (4.10) can be rewritten in

$$\dot{N}_{ads} = \dot{V}_C \frac{C \, y_{out,ads}(t)}{(1 - y_{out,ads}(t))} \tag{4.20}$$

The term dc/dt in equation (4.17) can be rewritten to

$$\frac{dc}{dt} = \frac{d\left(C\, y_{out,ads}(t)\right)}{dt} = y_{out,ads}(t)\frac{dC}{dt} + C\frac{dy_{out,ads}(t)}{dt} = C\frac{dy_{out,ads}(t)}{dt} \tag{4.20}$$

because in an isothermal system the overall number of moles per volume, C, does not change which means that dC/dt = 0.

Equation (4.17) can be rewritten into the general form

$$m_{ads}\frac{dn}{dt} + V_G C\frac{dy_{out,ads}(t)}{dt} + \dot{V}_C\frac{C\, y_{out,ads}(t)}{\left(1 - y_{out,ads}(t)\right)} = 0 \tag{4.21}$$

or

$$dn = -\dot{V}_C\frac{C\, y_{out,ads}(t)}{\left(1 - y_{out,ads}(t)\right)}\frac{dt}{m_{ads}} - V_G\, C\frac{dy_{out,ads}(t)}{m_{ads}} \tag{4.22}$$

At t = ∞ it is $y_{out,ads}$ = 0 and n = 0. Now the start loading $n_{t=0}$ can be calculated:

$$\int_{n_{t=0}}^{0} dn = -\int_{0}^{t=\infty}\frac{\dot{V}_C\, C}{m_{ads}}\frac{y_{out,ads}(t)}{\left(1 - y_{out,ads}(t)\right)}dt - \frac{V_G\, C}{m_{ads}}\int_{y_{out,ads,t=0}}^{0} dy_{out,ads}(t) \tag{4.23}$$

Therefore, it is

$$n_{t=0} = \int_{0}^{t=\infty}\frac{\dot{V}_C\, C}{m_{ads}}\frac{y_{out,ads}(t)}{\left(1 - y_{out,ads}(t)\right)}dt - \frac{V_G\, C}{m_{ads}}\, y_{out,ads,t=0} \tag{4.24}$$

The loading n at time t can be calculated via equation (4.22) with

$$n = n_{t=0} - \int_{0}^{t}\frac{\dot{V}_C\, C}{m_{ads}}\frac{y_{out,ads}(t)}{\left(1 - y_{out,ads}(t)\right)}dt - \frac{V_G\, C}{m_{ads}}\left(y_{out,ads}(t) - y_{out,ads,t=0}\right) \tag{4.25}$$

With equation (4.24) we get for the loading n:

$$n = \int_0^{t=\infty} \frac{\dot{V}_C\, C}{m_{ads}} \frac{y_{out,ads}(t)}{\left(1 - y_{out,ads}(t)\right)} dt - \int_0^{t} \frac{\dot{V}_C\, C}{m_{ads}} \frac{y_{out,ads}(t)}{\left(1 - y_{out,ads}(t)\right)} dt - \frac{V_G\, C}{m_{ads}} y_{out,ads}(t) \qquad (4.26)$$

By integrating the adsorption isotherm in dependence of the measured concentration c the loading n is obtained. This can be converted into partial pressure by means of the law of ideal gases.

4.4. Concentration pulse chromatography method

The use of the concentration pulse chromatography for adsorbent screening is very attractive since it is relatively inexpensive to set-up [91,92]. Further, this method is capable of characterising adsorbents faster than other methods.

With the concentration pulse method, a pulse of sample is injected into the carrier gas stream and passes through an adsorbent packed column. The response of the column is measured as concentration vs. time at the exit of the column. From this response peak a mean retention time of the sample, τ, is determined experimentally with

$$\tau = \frac{\int_0^{\infty} c(t - \tau_D) dt}{\int_0^{\infty} c dt} \qquad (4.27)$$

The term τ_D is the mean dead time of the system. This dead time is the time required for a sample pulse to pass the empty volume of the interconnecting tubing from injection point to the detector and void space in the packed column.

With the that carrier gas composition the mean retention time is related to the effective isotherm slope, K, by

$$\tau = \frac{L}{w}\left(1 + \frac{(1 - \varepsilon_{bed})}{\varepsilon_{bed}} K\right) \qquad (4.28)$$

where ε_{bed} is the bed porosity. The dimensionless K factor can be transformed to the dimensional *Henry* coefficient in mol/(kg*Pa) by

$$He = \frac{K}{\Re T \rho_{pellet}} \tag{4.29}$$

where ρ_{pellet} is the apparent density of the adsorbent. With the former equations (4.27) and (4.28) inserted in equation (4.29) it follows

$$He = \left[\left(\frac{\int_0^\infty c(t-\tau_D)dt}{\int_0^\infty c dt} \right) \frac{w}{L} - 1 \right] \cdot \frac{\varepsilon_{bed}}{1-\varepsilon_{bed}} \cdot \frac{1}{\Re T_{ads} \rho_{pellet}} \tag{4.30}$$

The concentration pulse method is also applicable for determining binary adsorption isotherms [91,92].

5. Prediction of Isotherms for p $\rightarrow$ 0 (*Henry*)

The *Henry* coefficient is the first step in developing a pure component adsorption isotherm that allows for overall prediction of the adsorption equilibrium. It is characteristic for the region of diluted concentrations. In this work it is shown that the Henry coefficient is not only dependent on the adsorption temperature but also on the properties of the adsorptive and adsorbent themselves. It is a picture of the prevailing interaction forces between the gas and solid molecules and ions. Understanding the basic mechanisms of adsorption opens the door to an a priori approach of calculating adsorption isotherms in a wide concentration range.

An adsorption isotherm in the diluted concentrations region is described by the *Henry* law

$$n = He\, p \tag{5.1}$$

where n is the loading in mol/kg, He the *Henry* coefficient in mol/(kg*Pa) and p the equilibrium pressure in Pa. For graphical purposes this means that the loading n is directly proportional to p with the slope He. All adsorption isotherms intersect with the origin of the coordinate system. Logarithmising both sides of equation (5.1) leads to equation

$$\log(n) = \log(He) + \log(p) \tag{5.2}$$

with slope 1 in a graph with double logarithmic axes. The intercept of the curve with the log(n)-axes is equal to log(He) if the log(p)-axes begins at 1 Pa. Figure 5.1 shows two different plots, one with linear and one with double logarithmic axes.

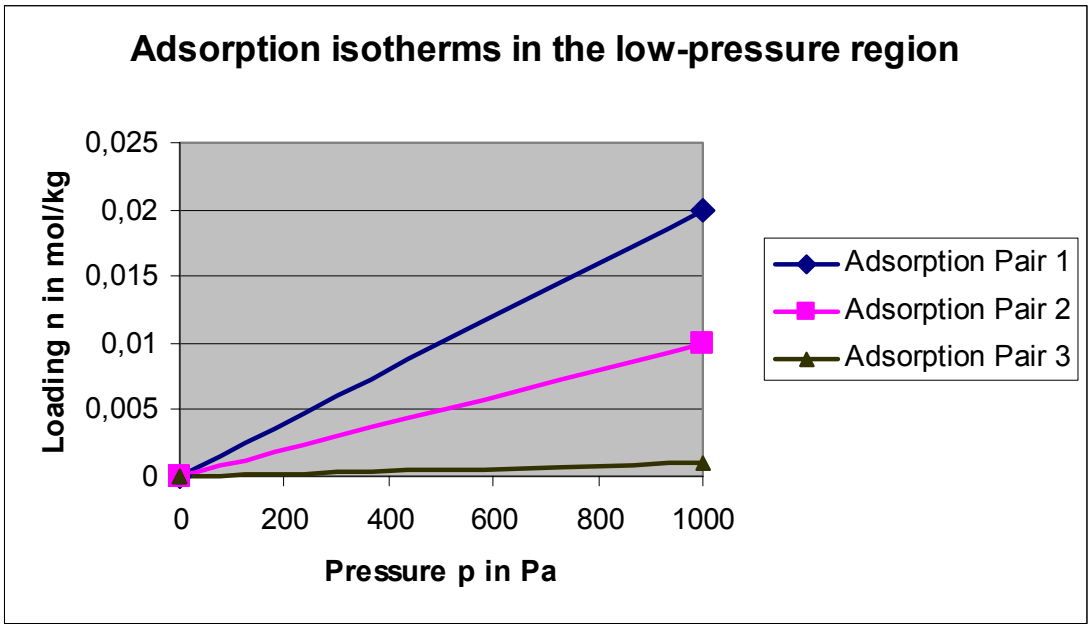

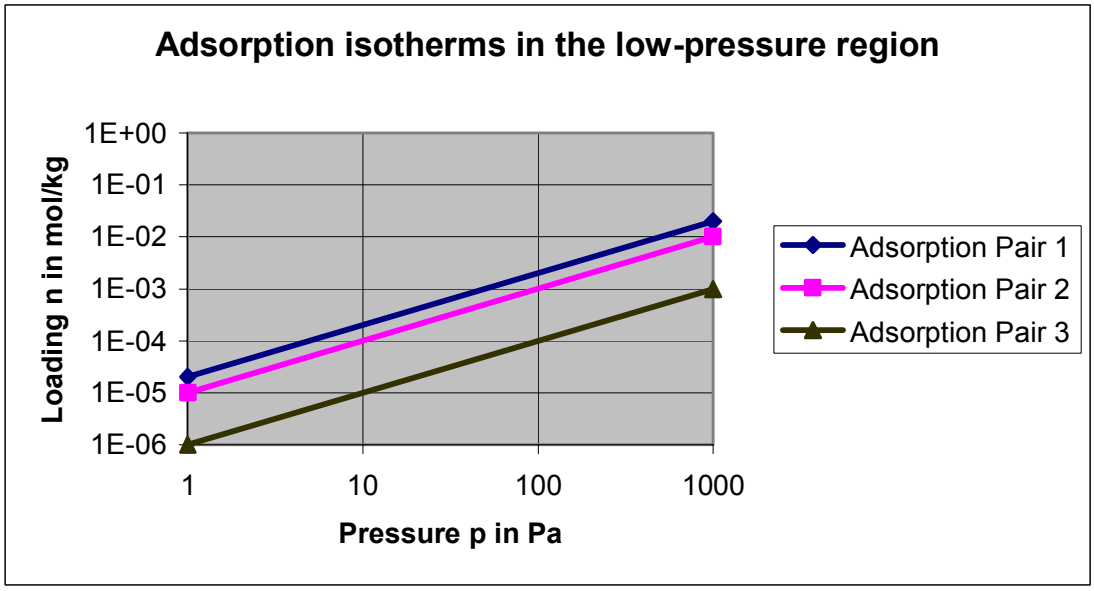

Figure 5.1: Two different views of adsorption isotherms in the low-pressure region.

Besides dimensionally correctness another important principle in chemical engineering is the thermodynamic consistency of derivations. This goal is retained in this work when the *Henry* coefficient is deduced from chemical potential equilibria. As next step in this Chapter the *Henry* coefficient is calculated in the case of energetically homogeneous adsorbents. An analytical function is derived from theoretical considerations which is a powerful instrument for process engineers. The last step introduces the general case of energetically heterogeneous adsorbents.

5.1. Thermodynamic consistency

In Chapter 3 several descriptions of adsorption equilibria were introduced of which some could be derived from thermodynamic consistent considerations. The *Langmuir* isotherm is the most famous one. This work follows that principle.

Besides disperse forces mainly electrostatic forces influence the adsorptive during exposion to an electrical field, e.g. the field of an ionic crystal lattice of a zeolite [8]. In general these electrostatic forces contribute in a non negligible degree to the adsorption equilibrium of an adsorptive with a solid surface. The overall adsorption potential Φ can therefore be written as

$$\Phi = \sum \Phi_{gas-solid} = \Phi_{indind} + \Phi_{indcha} + \Phi_{dipind} + \Phi_{dipcha} + \Phi_{quadind} + \Phi_{quadcha} + \sum_{j} \Phi_{adsads} \qquad (5.3)$$

The partial potentials are the integrated interaction energies of the adsorbate molecule with the solid continuum structure or with other adsorbate molecules. They describe the following interactions:

- The interaction of the induced dipole of the gas molecule with the induced dipole of the solid molecule (Φ_{indind}),
- the interaction of the induced dipole of the gas molecule with the electrical charge of the solid molecule (Φ_{indcha}),
- the interaction of the permanent dipole of the gas molecule with the induced dipole of the solid molecule (Φ_{dipind})
- the interaction of the permanent dipole of the gas molecule with the electrical charge of the solid molecule (Φ_{dipcha}),
- the interaction of the permanent quadrupole moment of the gas molecule with the induced dipole of the solid molecule ($\Phi_{quadind}$) and
- the interaction of the permanent quadrupole of the gas molecule with the electrical charge of the solid molecule ($\Phi_{quadcha}$).

In the following study for determining the *Henry* coefficient one important assumptions is that the interactions between the adsorbate molecules are negligible. The physical cause for this is the low concentration or partial pressure of the adsorbate molecules in the *Henry* region, so that they do not interact with each other but only with the solid surface. It is

$$\sum_j \Phi_{adsads} = 0 \tag{5.4}$$

A second assumption is that the solid elements do not have a permanent dipole or quadrupole moment.

When two phases coexist in a system equilibrium is reached between them after a certain time. In equilibrium state the chemical potentials μ of the two phases are equal. For the adsorptive and adsorbate phases it follows that

$$\mu_{adsorptive} = \mu_{adsorbate} \tag{5.5}$$

The chemical potential is a function of pressure p and temperature T with

$$\mu = f(T, p) \tag{5.6}$$

In the Henry region with its low pressure the adsorptive behaves like an ideal gas. Its chemical potential is defined as

$$\mu_{adsorptive}(T, p) = \mu_{adsorptive}(T_{ads}, p_{ref}) + kT_{ads} \ln\left(\frac{p_{ads}}{p_{ref}}\right) \tag{5.7}$$

where p_{ref} is the reference pressure in Pa, $\mu_{adsorptive}(T_{ads}, p_{ref})$ the reference chemical potential of the adsorptive and k the *Boltzman*'s constant. The second term is the correction from pressure p_{ref} to the adsorption equilibrium pressure of the gas p_{ads}. The chemical potential of the adsorbate can be expressed as

$$\mu_{adsorbate}(T,p) = \mu_{adsorbate}(T_{ads}, p_{ref}) + kT_{ads} \ln\left(\frac{p_{ads} + dp_{adsorbate}}{p_{ref}}\right) + \sum \Phi_{gas-solid} \qquad (5.8)$$

where $\mu_{adsorbate}(T_{ads}, p_{ref})$ is the reference chemical potential of the adsorbate and $dp_{adsorbate}$ is the difference pressure which acts additionally to the adsorbate layer. The second term is therefore also a correction from the reference pressure to the overall pressure of the adsorbate. The third term takes into account the sum of interactions between the adsorbate and the solid. With the assumption

$$\mu_{adsorptive}(T_{ads}, p_{ref}) = \mu_{adsorbate}(T_{ads}, p_{ref}) \qquad (5.9)$$

and that the adsorbate behaves like an ideal gas and according to

$$dp_{adsorbate} = \frac{\Re T_{ads} dn}{dv_{solid}} \qquad (5.10)$$

it follows with equations (5.7) and (5.8) that

$$kT_{ads} \ln\left(\frac{p_{ads}}{p_{ref}}\right) = kT_{ads} \ln\left(\frac{p_{ads} + \frac{\Re T_{ads} dn}{dv_{solid}}}{p_{ref}}\right) + \sum \Phi_{gas-solid} \qquad (5.11)$$

where dv_{solid} is the specific volume element of the solid. With algebraic conversions and equation (5.1) it follows that

$$He = \frac{n}{p} = \frac{1}{\Re T_{ads}} \int_{v_{solid}=0}^{v_{solid}} \left[\exp\left(\frac{-\sum \Phi_{gas-solid}}{kT_{ads}}\right) - 1\right] dv_{solid} \qquad (5.12)$$

The specific volume element of the solid can be expressed with its specific surface and the perpendicular distance z of the gas molecules from the surface:

$$dv_{solid} = S_{BET}\, dz \qquad (5.13)$$

With equation (5.12) it follows the well known equation for the *Henry* coefficient expanded with the overall interaction terms:

$$He = \frac{S_{BET}}{\Re T_{ads}} \int_0^{z_{max}} \left[\exp\left(\frac{-\sum \Phi_{gas-solid}}{kT_{ads}} \right) - 1 \right] dz \qquad (5.14)$$

The integration constant z_{max} depends on the structure of the solid. For massive solids z_{max} is infinity, for porous solids it depends on the pore volume [47]. With equations (5.3) and (5.4) the thermodynamic consistent equation for the *Henry* coefficient becomes

$$He = \frac{S_{BET}}{\Re T_{ads}} \int_0^{z_{max}} \left[\exp\left(\frac{-\left(\Phi_{indind} + \Phi_{indcha} + \Phi_{dipind} + \Phi_{dipcha} + \Phi_{quadind} + \Phi_{quadcha} \right)}{kT_{ads}} \right) - 1 \right] dz \qquad (5.15)$$

5.2. Energetic homogeneous adsorbents

A special case of equation (5.15) is the adsorption of arbitrary gases on energetic homogeneous adsorbents like active carbon or silicalite-1. For this case *Maurer* [26] derived the potential function for the interaction energy $\Phi_{indind}(z)$ which depends on the critical properties of the adsorptive and the solid properties of the adsorbent. The *Henry* coefficient reduces in this case to:

$$He = \frac{S_{BET}}{\Re T_{ads}} \int_0^{z_{max}} \left[\exp\left(\frac{-\Phi_{indind}(z)}{kT_{ads}} \right) - 1 \right] dz \qquad (5.16)$$

It is referred to the literature for the derivation of the interaction energy $\Phi_{indind}(z)$ [26]. For consistency the main formulas shall be mentioned in this work with

$$\phi_{indind}(z) = -\frac{4\pi C_{i,j} \rho_j}{3(\sigma_{i,j} + z)^3} \qquad (5.17)$$

where $C_{i,j}$ is an interaction constant between the adsorbate molecule and the solid atoms, $\sigma_{i,j}$ the minimum contact distance between the adsorption participants and ρ_j the density of the solid. Figure 5.2 shows a principle scheme for the distance of the adsorbate from the solid.

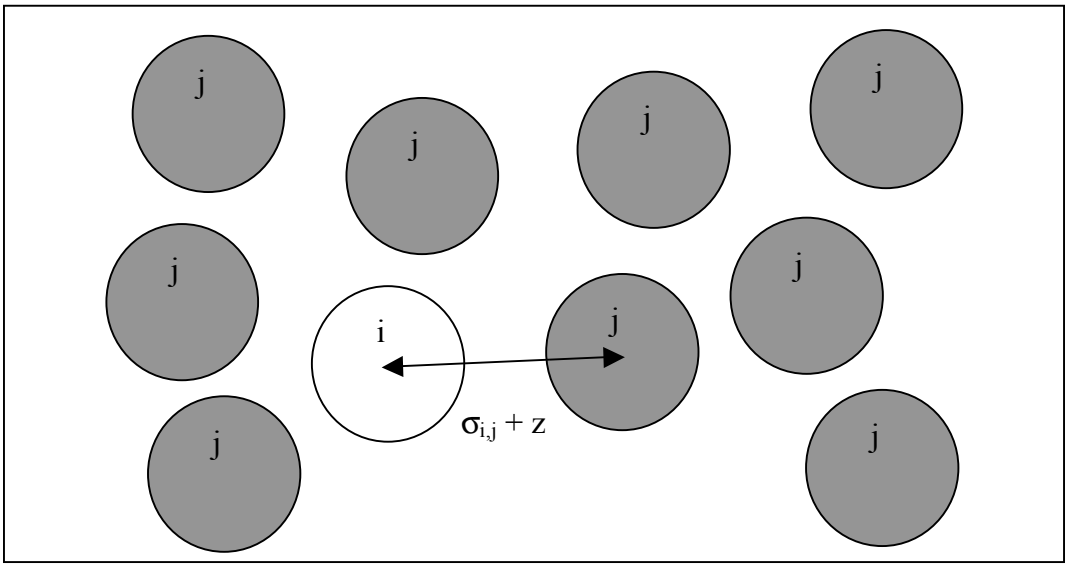

Figure 5.2: Principle scheme for the distance of the adsorbate from the solid [26].

The distance between the adsorbate sphere centre and the centre of the closest solid atom in its vicinity is ($\sigma_{i,j} + z$). The minimum distance $\sigma_{i,j}$ is calculated by the arithmetic mean of the *van-der-Waals* diameters of the adsorbate and the solid molecules with

$$\sigma_{i,j} = \frac{1}{2}\left(\sigma_{i,i} + \sigma_{j,j}\right) \tag{5.18}$$

Maurer [26] derived the *van-der-Waals* diameter of the adsorptive from its critical properties. It is

$$\sigma_{i,i} = \sqrt[3]{\frac{3\,k\,T_c}{16\,\pi\,p_c}} \tag{5.19}$$

where T_c and p_c are the critical temperature and critical pressure, respectively. The *van-der-Waals* diameter of the solid can be found in the literature. If not it is referred to Section 5.2.2 for the derivation of the parameter $\sigma_{j,j}$.

The interaction constant itself can be formulated as

$$C_{i,j} = \frac{9\Re\sigma_{i,j}^3}{16\rho_i N_A}\sqrt{\frac{2Ha_j}{\pi^3\sigma_{j,j}^3}}\frac{T_c}{\sqrt{p_c}} \tag{5.20}$$

where Ha_j is the *Hamaker* constant of the solid.

5.2.1. The dimensionless *Henry* curve

The interaction energy Φ_{indind} of two induced dipoles is also called the *London* dispersion energy [5]. This dispersion energy can also be understood by the following argument. Although the time-averaged dipole moment is zero for molecules without a dipole, there exists at any time a finite value. An electromagnetic field emanates from this dipole moment and induces a dipole in a nearby molecule. These dispersion forces are omnipresent, they are always attractive.

The scope of this Section is to formulate a dimensionless function for the *Henry* curve considering only *London* dispersion forces (*Hamaker* dominant). It is based on the advancement of the *Henry* function formulated by equation (5.16) in the case of energetic homogenous adsorbents. With equations (5.17) and (5.20) the interaction energy $\Phi_{indind}(z)$ can be rewritten by dividing by the energy unit ($k{\cdot}T_{ads}$)

$$\frac{\phi_{indind}(z)}{kT_{ads}} = -\frac{4\pi\rho_j}{3(\sigma_{i,j}+z)^3 kT_{ads}}\frac{9\Re\sigma_{i,j}^3}{16\rho_j N_A}\sqrt{\frac{2Ha_j}{\pi^3\sigma_{j,j}^3}}\frac{T_c}{\sqrt{p_c}} \tag{5.21}$$

With

$$\Re = k N_A \tag{5.22}$$

and the binomial formula

$$(a+b)^3 = a^3 + 3a^2 b + 3ab^2 + b^3 \tag{5.23}$$

equation (5.21) can be simplified:

$$\frac{\phi_{indind}(z)}{kT_{ads}} = -\frac{3\sigma_{i,j}^3}{4\left(\sigma_{i,j}^3 + 3\sigma_{i,j}^2 z + 3\sigma_{i,j} z^2 + z^3\right)}\sqrt{\frac{2Ha_j}{\pi\sigma_{j,j}^3 p_c}}\frac{T_c}{T_{ads}} \tag{5.24}$$

Therefore the Henry coefficient can then be expressed as

$$He = \frac{S_{BET}}{\Re T_{ads}}\int_0^{z_{\max}}\left[\exp\left(\frac{3\sigma_{i,j}^3}{4\left(\sigma_{i,j}^3 + 3\sigma_{i,j}^2 z + 3\sigma_{i,j} z^2 + z^3\right)}\sqrt{\frac{2Ha_j}{\pi\sigma_{j,j}^3 p_c}}\frac{T_c}{T_{ads}}\right) - 1\right]dz \tag{5.25}$$

By dividing both sides by the minimum contact distance of the adsorbate molecule and the solid atom $\sigma_{i,j}$ equation (5.25) can be rearranged to

$$\frac{He\Re T_{ads}}{S_{BET}\sigma_{i,j}} = \int_0^{\frac{z_{\max}}{\sigma_{i,j}}}\left[\exp\left(\frac{3}{4\left(1 + 3\frac{z}{\sigma_{i,j}} + 3\left(\frac{z}{\sigma_{i,j}}\right)^2 + \left(\frac{z}{\sigma_{i,j}}\right)^3\right)}\sqrt{\frac{2Ha_j}{\pi\sigma_{j,j}^3 p_c}}\frac{T_c}{T_{ads}}\right) - 1\right]d\left(\frac{z}{\sigma_{i,j}}\right) \tag{5.26}$$

Both sides of equation (5.25) are now dimensionless. The left side is defined by *Mersmann et.al*. [27] as the dimensionless Initial or *Henry* Loading IL with

$$IL \equiv \frac{He\Re T_{ads}}{S_{BET}\sigma_{i,j}} \tag{5.27}$$

which is mainly a function of the Interaction Parameter IP with

$$IP \equiv \frac{T_c}{T_{ads}}\sqrt{\frac{2Ha_j}{\pi\sigma_{j,j}^3 p_c}} \tag{5.28}$$

and the integration variable

$$x_{\max} \equiv \frac{z_{\max}}{\sigma_{i,j}} \tag{5.29}$$

With the reduced distance

$$x \equiv \frac{z}{\sigma_{i,j}} \tag{5.30}$$

and the definitions

$$y \equiv IL \tag{5.31}$$

and

$$a = \frac{4}{3\,IP} \tag{5.32}$$

the dimensionless Henry function can be expressed as

$$y(a,x) = IL = \int_0^{x_{\max}} \left[\exp\left(\frac{3}{4\left(1 + 3x + 3x^2 + x^3\right)} IP \right) - 1 \right] dx = \int_0^{x_{\max}} \left[\exp\left(\frac{1}{a + 3ax + 3ax^2 + ax^3} \right) - 1 \right] dx \tag{5.33}$$

This integral cannot be solved analytically. It was numerically analysed with commercially available mathematical programs. Nevertheless for given values of a and x_{max} the integral can be calculated on a numerical basis for example with MathCAD. In this context it is important to mention that the integration parameter a is not a function of x. The constant a only depends on the solid and adsorptive properties (the Hamaker constant Ha_j and the *van-der-Waals* diameter σ_j of the solid, the critical temperature T_c and the critical pressure p_c of the adsorptive) and also on the adsorption conditions (the adsorption temperature T_{ads}).

As next step the interval [0.1;30] of the dimensionless interaction parameter IP was examined. This interval can be recalculated via equation (5.32) to an interval [13.33;0.0444] of the integration parameter a. Through physical examinations a minimum and maximum value for the reduced distance x_{max} was derived. For this the following assumptions were made:

- The helium atom He has the smallest van-der-Waals diameter of gases which is $\sigma_{He} = 2.66*10^{-10}$ m.
- The maximum pore diameter d of microporous solids is 2 nm = $20*10^{-10}$ m and limits the distance of an adsorptive molecule from the solid surface.
- The *van-der-Waals* diameter of a solid atom is approximately $4.0*10^{-10}$ m.
- Large adsorptive molecules have a maximum van-der-Waals-diameter of $5.5*10^{-10}$ m.
- x_{max} is calculated via equation (5.34) to

$$x_{\max} = \frac{z_{\max}}{\sigma_{i,j}} = \frac{\frac{d}{2} - \sigma_{i,i}}{\frac{1}{2}\left(\sigma_{i,i} + \sigma_{j,j}\right)} \tag{5.34}$$

The values for x_{max} are then calculated as a minimum value of approximately 0.9 and a maximum value of 2. With these values and by numerical calculations of the integral (5.33) the table 5.1 was generated. Practically the integration values for the dimensionless *Henry* loading IL do no longer differ above a value of 2 for the interaction parameter IP. Both limits for the dimensionless *Henry* curve are shown in figure 5.3. It can be seen that the Henry curve only depends on the interaction parameter IP. It has to be mentioned that the curve does not cross the value pair (0/1) which is shown by *Mersmann* et al. [27] as the thermodynamic consistent point to be crossed.

For engineering purposes it would be easier to have an analytical function for determining the *Henry* coefficient in the case of energetic homogenous adsorbents. Therefore, in the next step an analytical function is introduced which is a powerful and easy instrument for calculating the *Henry* coefficient.

Table 5.1: Value table for integral equation (5.33).

Dimensionless parameter IP	Integration parameter a	Integration value IL for x_{max} = 0.9	Integration value IL for x_{max} = 2	Integration value IL for x_{max} = ∞
0.1	13.3333333	0.028	0.034	0.038
1	1.33333333	0.335	0.399	0.441
2	0.66666667	0.953	0.986	1.07
5	0.26666667	5.383	5.752	5.966
10	0.13333333	101.933	102.822	103.264
15	0.08888889	2632	2633	2634
20	0.06666667	80440	80440	80440
25	0.05333333	2.67E+06	2.67E+06	2.67E+06
30	0.04444444	9.34E+07	9.34E+07	9.34E+07

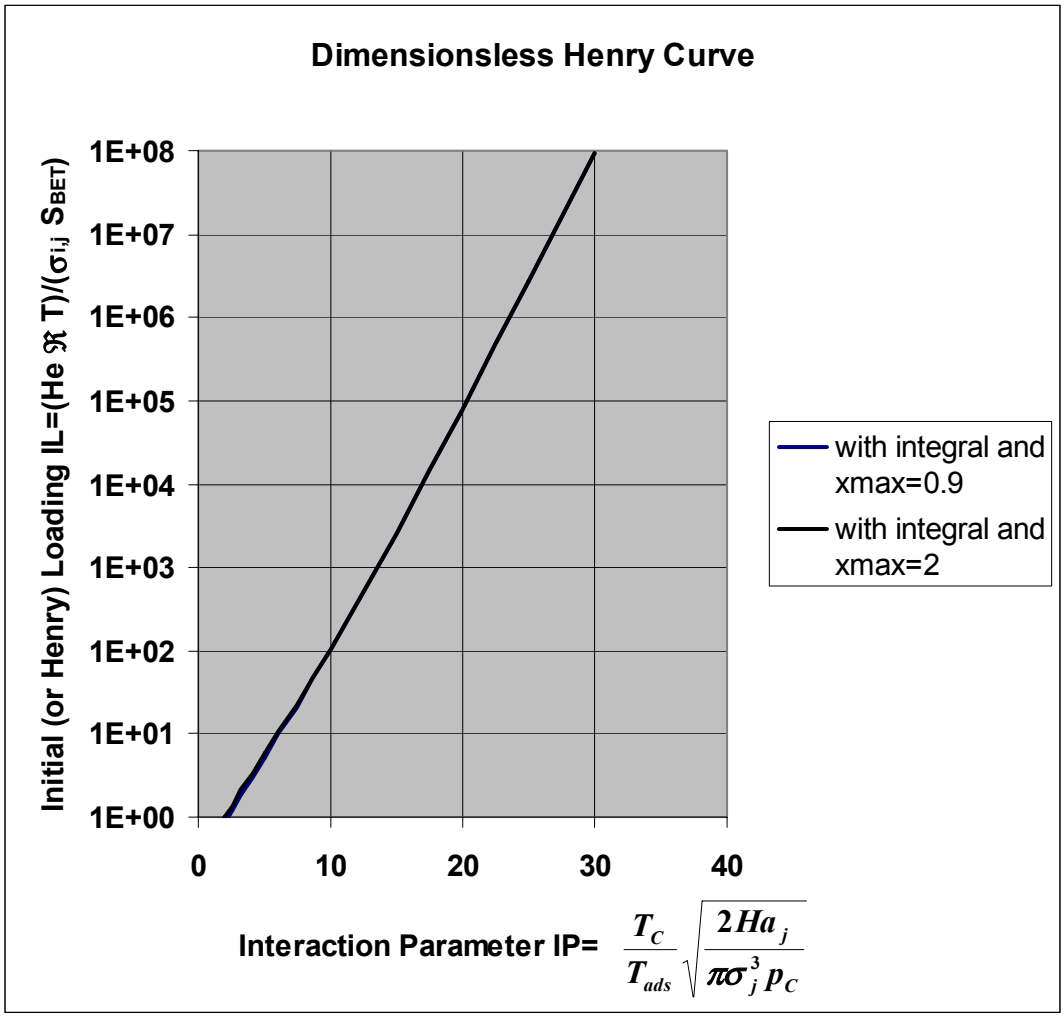

Figure 5.3: The dimensionless Henry curve – numerical values (equation (5.33)).

The numerical values of figure 5.3 are approximated by the function

$$IL = \exp\left(p_1 IP^{p_2}\right) \tag{5.35}$$

where p_1 and p_2 are parameters adjusted to the real numerical values of the integral (5.33). The adjustment was performed by the numerical software Maple. For the two cases of x_{max} = 0.9 and x_{max} = 2 the parameter values p_1 = 0.3312917 and p_2 = 1.1803227 for x_{max} = 0.9 and p_1 = 0.3312936 and p_2 = 1.1803211 for x_{max} = 2.0 were obtained. The two parameter sets do not differ significantly. For this work the second set was chosen. The exponential function (5.35) with the second set is shown and compared with the numerical values in figure 5.4.

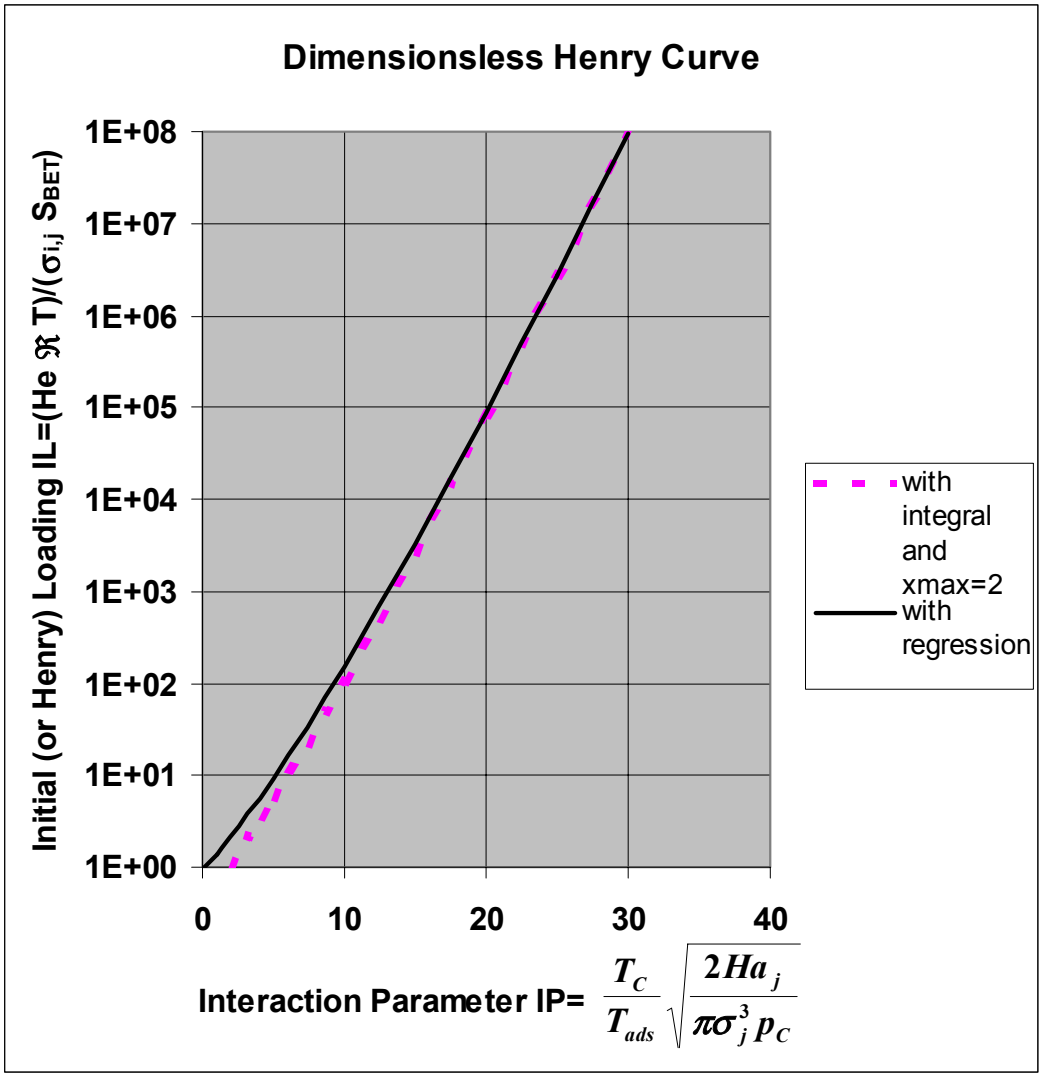

Figure 5.4: The dimensionless Henry curve – analytical regression.

The regression curve goes through the thermodynamic consistent point (0/1) [27]. The quality of the analytical form of the *Henry* curve is discussed in Chapter 7. It is shown there also that this function does not cover only the adsorption behaviour of energetic homogenous adsorbents like active carbon and silicalite-1 but also the case of non-polar adsorbents paired with energetic heterogeneous adsorbents like zeolites. This is a very new aspect derived for the first time in this work.

One of the assumptions in this Section was the value of the *van-der-Waals* diameter of solids. The diameter for active carbon coal was chosen to be that of the carbon atom [26], so $\sigma_{\text{active carbon}} = 3.40*10^{-10}$ m. In most cases there are no literature data for this parameter. So in the next Section a way for determining this solid property is derived.

5.2.2. The *van-der-Waals* diameter of solids

Because of the very strong dependency of the *Henry* curve on the interaction parameter IP the *van-der-Waals* diameter of the solid has also a great significance. It goes down as the third power in the calculation of the interaction parameter. With the assumption that the *Henry* curve is thermodynamic consistent and characterised accurately by equation (5.35) the following approach for the derivation of the diameter σ_j of the solid can be made:

$$f(\sigma_j) = \frac{2\,He\,\Re\,T_{ads}}{(\sigma_i + \sigma_j)S_{BET}} = g(\sigma_j) = \exp\left(p_1 \left(\frac{T_c}{T_{ads}} \sqrt{\frac{2\,Ha_j}{\pi\,\sigma_j^3\,p_c}} \right)^{p_2} \right) \tag{5.36}$$

It is:

$$f(\sigma_j) - g(\sigma_j) = 0 \tag{5.37}$$

where f and g are functions of the diameter σ_j as defined in equation (5.36). There is only one unknown variable in equation (5.37), the diameter σ_j, if at least one adsorption isotherm of the solid is known. For energetic homogenous adsorbents the choice of the adsorptive is not critical. For energetic heterogeneous adsorbents the

adsorptive should have no dipole or quadrupole moment. Most of the solid's surface is examined by the BET-isotherm of nitrogen at 77 K as adsorption temperature. So there is at least one experiment set of parameters (*Henry* coefficient, adsorption temperature, critical properties and *van-der-Waals* diameter of the adsorptive, specific surface and *Hamaker* constant of the solid) for each solid available without further experimental work. In this study propane adsorption isotherms were taken to calculate the *van-der-Waals* diameter of the examined solids. In the case of NaY methane was taken. The zero point search as derived in equations (5.36) and (5.37) was conducted with the program MathCAD. Table 5.2 shows the results.

Table 5.2: *Van-der-Waals* diameter of examined solids calculated with the adsorptives propane and methane.

Solid, adsorptive	S_{BET} (m^2/kg)	Ha_j (J)	T_C (K)	p_C (Pa)	T_{ads} (K)	He (mol/kgPa)	σ_i (m)	σ_j (m)
Active carbon, propane	1000000	6.0E-20	369.8	4.2E6	423	7.1E-5	4.15E-10	3.5E-10
Silicalite-1, propane	372000	7.94E-20	369.8	4.25E6	303	1.06E-3	4.15E-10	3.8E-10
MS5A, propane	727000	7.71E-20	369.8	4.25E6	343	5.36E-5	4.15E-10	3.8E-10
MS4A, propane	650000	6.5E-20	369.8	4.25E6	423	4.22E-5	4.15E-10	3.8E-10
NaX, propane	445000	8.25E-20	369.8	4.25E6	293	2.37E-3	4.15E-10	3.8E-10
NaY, methane	500000	8.40E-20	190.4	4.60E6	343	1.16E-6	3,24E-10	4.2E-10

The results show that the *van-der-Waals* diameters of zeolites are in the same magnitude as that of active carbon. Furthermore the chosen diameter for active carbon of $\sigma_{active\ carbon}$ = 3.40 E-10 m is approved by this calculation by an accuracy of +- 2.9 %.

5.3. Energetic heterogeneous adsorbents

In order to calculate the *Henry* coefficient for the adsorption of polar gases on energetic heterogeneous adsorbents like zeolites it is necessary to take into account all the possible interaction potentials between the adsorbate and the solid atoms. In this Section analytical functions for these potentials are derived. Consequently the *Henry* function of equation (5.15) can then be extended to an integral which is finally numerically solvable. Later it will be shown that the interaction energy $\frac{\Phi_{indind}}{kT_{ads}}$ is only approximately 50 % of the sum of all interaction energies in the case of polar gases.

5.3.1. The range of polarities

In the following potential calculations the polarity properties of the adsorptives are important factors. Their possible value intervals can be

- between 2.2*10^{-41} (C^2*m^2)/J (helium) and 2.13*10^{-39} (C^2*m^2)/J (n-decane) for the polarisability α_i of the gas molecule.
- The dipole moment μ_i can be between 0 (methane) and 1.0*10^{-29} C*m (acetone).
- The quadrupole moment Q_i can be between 0 (methane) and 6.21*10^{-39} C*m^2 (anthracene).

5.3.2. Induced dipole gas – electrical charge solid interaction (indcha)

The assumption for the derivation of the interaction between an induced dipole of a gas molecule and an electrical charge of a solid atom is that the solid is composed of so-

called average atoms with equal properties. In reality this is not true but it is effective for the characterisation of the interaction energy.

The proposed route of *van der Hoeven* [41] for the calculation of the Hamaker constant is based upon a subdivision of the solid molecules into atoms, which all have an average composition and polarisability identical to that of the solid molecule. The constants (*London* constant, polarisability, number density) are then calculated from these average atomic properties. In this approach it is further supposed that the atoms are all bonded by semi-polar bonds and that only the bond-forming valence electrons contribute to the disperse energetic waves with respect to the Hamaker constant.

According to *Münstermann* [131] the adsorption of polar or polarisable molecules is preferred by molecular sieves. These adsorbents are attracted by the positive charged cations of the zeolite cages. This effect has to be taken into account when dealing with charge interactions for calculating the Henry coefficient of arbitrary gases.

The potential energy E_{indcha} between two molecules or atoms, of which one is polarisible and the other one possesses an electrical charge, can be described by *Hirschfelder* [19]

$$E_{indcha}(r) = -\frac{1}{2}\frac{\alpha_i q_j^2}{r^4\left(4\pi\varepsilon_0\varepsilon_r\right)^2} \qquad (5.38a)$$

where α_i is the polarisability of the gas molecule in (C^2*m^2)/J, q_j the effective charge of the average atom of the solid in C, ε_0 the permittivity of free space = $8.854*10^{-12}$ C/(V*m), ε_r the relative permittivity of the adsorbent and r the distance between the centre of the molecules in m. For calculation of the relative permittivity of microporous adsorbents the porosity of the solid has to be taken into account. It is assumed that

$$\varepsilon_r = \varphi\cdot 1 + (1-\varphi)\cdot n^2 \qquad (5.38b)$$

where φ is the porosity and n the refractive index of the solid. For MS5A the relative permittivity is 1.73 with φ = 0.5 [24] and n = 1.57.

From a summation of all pair potentials it follows the interaction potential of the gas molecule with the whole solid continuum. In general it is [21]

$$\Phi = \int_{\sigma}^{\infty} E(r)\rho_{j,at}\, 4\pi r^2 dr \qquad (5.39)$$

where $\rho_{j,at}$ is the number density of solid atoms in $1/m^3$ calculated with equation (3.92).

In this work the following general description of the interaction potentials was chosen:

$$\Phi = \int_{\sigma_{i,j}+z}^{\infty} E(r)\rho_{j,at}\, 4\pi r^2 dr \qquad (5.40)$$

The lower integration limit of equation (5.39) was substituted by ($\sigma_{i,j}$ + z) because the minimum distance between the molecules is $\sigma_{i,j}$, also known as the minimum *van-der-Waals* contact distance. The effective mean charge of the average solid atom $q_{j,at}$ depends on the average number of positive charged cations $s_{cations}$ per solid atom. This property is introduced here for the first time as

$$s_{cations} = \frac{n_c}{n_a} \qquad (5.41a)$$

where n_c are the number of positive charges and n_a the number of atoms in the solid molecule. For example for MS5A n_c = 12, n_a = 79 and $s_{cations}$ = 0.152.

It follows for the effective mean charge that

$$q_j = s_{cations}\, e \qquad (5.41b)$$

where e is the charge of one electron (e = 1,60*10^{-19} C). The interaction energy $\Phi_{indcha}(z)$ is then due to equations (5.41b) and (5.38a)

$$\Phi_{indcha}(z) = \int_{\sigma_{i,j}+z}^{\infty} -\frac{1}{2}\frac{\alpha_i q_j^2}{r^4\left(4\pi\varepsilon_0\varepsilon_r\right)^2}\rho_{j,at}\, 4\pi r^2 dr = -\frac{1}{2}\frac{\alpha_i s_{cations}^2 e^2 \rho_{j,at}}{4\pi\varepsilon_0^2\varepsilon_r^2}\frac{1}{\left(z+\sigma_{i,j}\right)} \qquad (5.42a)$$

With the same substitution as in equation (5.30) and after dividing both sides of equation (5.42a) by the energy unit (k*T_{ads}) one gets the reduced interaction energy

$$\frac{\Phi_{indcha}(x)}{kT_{ads}} = -\frac{1}{8}\frac{\alpha_i s_{cations}^2 e^2 \rho_{j,at}}{\pi\varepsilon_0^2 \varepsilon_r^2 (k T_{ads})}\frac{1}{\sigma_{i,j}}\frac{1}{(x+1)} \tag{5.42b}$$

The dimensionless interaction parameter for the actual case is then defined as

$$A_{indcha} = \frac{\alpha_i s_{cations}^2 e^2 \rho_{j,at}}{8\pi\varepsilon_0^2 \varepsilon_r^2 (k T_{ads})\sigma_{i,j}} \tag{5.43}$$

5.3.3. Permanent dipole gas – induced dipole solid interaction (dipind)

Gas molecules can have a permanent dipole when the atoms of different charge of the molecule compound are not arranged symmetrically to each other. For example, trifluormethane CHF_3 has a dipole moment of 1.6 debye or $5.344*10^{-30}$ C*m. Permanent dipoles induce a dipole in the attraction partner if this partner is polarisible. The potential attraction energy between two molecules is according to *Debye* [4]

$$E_{dipind}(r) = -\frac{\mu_i^2 \overline{\alpha}_j}{r^6 (4\pi\varepsilon_0\varepsilon_r)^2} \tag{5.44}$$

where μ_i is the dipole moment of the gas molecule in Cm and $\overline{\alpha}_j$ the polarisability of a solid atom according to equation (4.49) in (C^2*m^2)/J. In the following it is assumed that the solid atoms are induced from the polar gas molecules but do not have a permanent dipole themselves. The interaction energy of one polar gas molecule with the whole solid continuum is with equation (5.40)

$$\Phi_{dipind}(z) = \int_{\sigma_{i,j}+z}^{\infty} E_{dipind}(r)\rho_{j,at}\, 4\pi r^2 dr \tag{5.45}$$

Therefore it is

$$\Phi_{dipind}(z) = -\frac{\mu_i^2 \overline{\alpha_j} \rho_{j,at}}{12 \cdot \pi \varepsilon_0^2 \varepsilon_r^2} \frac{1}{(\sigma_{i,j} + z)^3} \tag{5.46}$$

After introduction of the reduced location variable x the reduced interaction energy permanent dipole gas – induced dipole solid is

$$\frac{\Phi_{dipind}(x)}{kT_{ads}} = -\frac{\mu_i^2 \overline{\alpha_j} \rho_{j,at}}{12 \cdot \pi \varepsilon_0^2 \varepsilon_r^2 kT_{ads}} \frac{1}{\sigma_{i,j}^3} \frac{1}{(1+x)^3} \tag{5.47}$$

The dimensionless interaction parameter A_{dipind} is therefore

$$A_{dipind} = \frac{\mu_i^2 \overline{\alpha_j} \rho_{j,at}}{12 \cdot \pi \varepsilon_0^2 \varepsilon_r^2 (kT_{ads}) \sigma_{i,j}^3} \tag{5.48}$$

5.3.4. Permanent dipole gas – electrical charge solid interaction (dipcha)

This interaction type is dominant for highly polar adsorptives like trifluormethane (CHF_3), ammonia (NH_3) and methanol (CH_3OH). The potential attractive energy of a permanent dipole with a charged atom is quantified [19] with

$$E_{dipcha}(r) = -\frac{1}{3kT_{ads}} \frac{\mu_i^2 q_j^2}{r^4 (4\pi \varepsilon_0 \varepsilon_r)^2} \tag{5.49}$$

with already known parameters. The summation of the potential energy over the whole solid yields

$$\Phi_{dipcha}(z) = \int_{z+\sigma_{ij}}^{\infty} E_{dipcha}(r) \rho_{j,at} 4\pi r^2 dr \tag{5.50}$$

After integration and deviding by the energy unit (kT_{ads}) and introducing the dimensionless variable x it follows for this interaction energy

$$\frac{\Phi_{dipcha}(x)}{kT_{ads}} = -\frac{\mu_i^2 s_{cations}^2 e^2 \rho_{j,at}}{12 \cdot \pi \varepsilon_0^2 \varepsilon_r^2 (kT_{ads})^2} \frac{1}{\sigma_{i,j}} \frac{1}{(1+x)} \tag{5.51}$$

Then the dimensionless interaction parameter A_{dipcha} can be defined as

$$A_{dipcha} = \frac{\mu_i^2 s_{cations}^2 e^2 \rho_{j,at}}{12 \cdot \pi \varepsilon_0^2 \varepsilon_r^2 (kT_{ads})^2 \sigma_{i,j}} \tag{5.52}$$

5.3.5. Quadrupole moment gas - induced dipole solid interaction (quadind)

The quadrupole moment is a fundamental property for the description of the molecular charge distribution [103]. In the theory of electricity there are two signs of electric charge. The net total charge is the monopole moment. If there are charges of two signs separated, then there exists a dipole moment along the line connecting the charges. If there are charges of both signs, but separated in a more complicated way, an electric quadrupole may be present. The quadrupole moment gives an indication of the derivation of the charge distribution of the adsorptive from spherical symmetry.

For gases with strong quadrupole moments like CO_2 the previous potential phenomena are not sufficient to describe their great adsorption effect in the Henry region particularly because their permanent dipole is small or even zero in the case of benzene. The cause is that the quadrupole moment can also induce a dipole moment on the solid atoms or can interact with electrical charges of the adsorbent. For two molecules of which one has a quadrupole moment and the other is polarisible the potential energy is [19]

$$E_{quadind}(r) = -\frac{3}{2} \frac{Q_i^{\,2} \overline{\alpha_j}}{(4\pi\varepsilon_0\varepsilon_r)^2 r^8} \tag{5.53}$$

where Q_i is the quadrupole moment of the adsorptive in C*m^2. It follows for the reduced interaction potential with the usual procedure as in the previous chapters that

$$\frac{\Phi_{quadind}(x)}{kT_{ads}} = -\frac{3}{40} \frac{Q_i^{\,2} \overline{\alpha_j} \rho_{j,at}}{\pi \varepsilon_0^2 \varepsilon_r^2 \, k \, T_{ads}} \frac{1}{\sigma_{i,j}^5} \frac{1}{(1+x)^5} \tag{5.54}$$

Now the dimensionless interaction parameter $A_{quadind}$ can be directly specified as

$$A_{quadind} = \frac{3}{40} \frac{Q_i^{\,2} \overline{\alpha_j} \rho_{j,at}}{\pi \varepsilon_0^2 \varepsilon_r^2 \left(k T_{ads}\right) \sigma_{i,j}^5} \tag{5.55}$$

5.3.6. Quadrupole moment gas – electrical charge solid interaction (quadcha)

This potential is in the same order of magnitude as the permanent dipole – electrical charge interaction. The potential energy between two molecules with a quadrupole moment and an electrical charge is according to *Israelachvili* [21]

$$E_{quadcha}(r) = -\frac{1}{20 k T_{ads}} \frac{Q_i^{\,2} q_j^{\,2}}{\left(4\pi\varepsilon_0\varepsilon_r\right)^2 r^6} \tag{5.56}$$

It follows for the reduced interaction potential:

$$\frac{\Phi_{quadcha}(x)}{k T_{ads}} = -\frac{1}{240} \frac{Q_i^{\,2} s_{cations}^2 e^2 \rho_{j,at}}{\pi \varepsilon_0^2 \varepsilon_r^2 \left(k T_{ads}\right)^2} \frac{1}{\sigma_{i,j}^3} \frac{1}{(1+x)^3} \tag{5.57}$$

with the well known parameters of the adsorptive and the adsorbent. The dimensionless interaction parameter $A_{quadcha}$ is then

$$A_{quadcha} = \frac{Q_i^{\,2} s_{cations}^2 e^2 \rho_{j,at}}{240 \pi \varepsilon_0^2 \varepsilon_r^2 \left(k T_{ads}\right)^2 \sigma_{i,j}^3} \tag{5.58}$$

Later in chapter 7.2 the validity of this theoretical model according to the equations (5.24), (5.42b), (5.47), (5.51), (5.54) and (5.57) will be discussed.

5.3.7. Overall adsorption potential

The overall adsorption potential between a gas molecule and the solid continuum can be expressed as the sum of the partial potentials as shown in equation (5.3). Because

the *Henry* coefficient depends on the reduced overall potential $\frac{-\sum \Phi_{Gas-Solid}}{kT_{ads}}$ as shown in equation (5.14) also the partial potentials will be expressed by reduced equations relative to the energetic unit kT_{ads}. Therefore, the induced dipole – induced dipole interaction can be rewritten as:

$$\frac{\Phi_{indind}(z)}{kT_{ads}} = -\frac{3\sigma_{i,j}^3}{4(\sigma_{i,j}+z)^3}\sqrt{\frac{2Ha_j}{\pi\sigma_{j,j}^3\, p_c}}\frac{T_c}{T_{ads}} \tag{5.59}$$

It is assumed that this potential is the *London* potential expressed by a function of the *Hamaker* constant of the solid and the critical parameters of the adsorptive. This item will be discussed in Chapter 7. With the additional equations (5.41b), (5.46), (5.50), (5.54) and (5.57) for the other partial potentials the reduced overall potential can be formulated in detail as shown in equation (5.60).

$$\frac{-\Phi(z)}{kT_{ads}} = \frac{-\sum \Phi_{gas-solid}(z)}{kT_{ads}} =$$

$$= \frac{-\Phi_{indind}(z)-\Phi_{indcha}(z)-\Phi_{dipind}(z)-\Phi_{dipcha}(z)-\Phi_{quadind}(z)-\Phi_{quadcha}(z)}{kT_{ads}} =$$

$$= \frac{3\sigma_{i,j}^3}{4(\sigma_{i,j}+z)^3}\sqrt{\frac{2Ha_j}{\pi\sigma_{j,j}^3\, p_c}}\frac{T_c}{T_{ads}} + \frac{\alpha_i s_{cations}^2 e^2 \rho_{j,at}}{8kT_{ads}\,\pi\varepsilon_0^2\varepsilon_r^2}\frac{1}{(\sigma_{i,j}+z)} +$$

$$+ \frac{\mu_i^2\overline{\alpha_j}\rho_{j,at}}{12\cdot\pi\varepsilon_0^2\varepsilon_r^2 kT_{ads}}\frac{1}{(\sigma_{i,j}+z)^3} + \frac{\mu_i^2 s_{cations}^2 e^2\rho_{j,at}}{12\cdot\pi\varepsilon_0^2\varepsilon_r^2(kT_{ads})^2}\frac{1}{(\sigma_{i,j}+z)} +$$

$$+ \frac{3Q_i^{\,2}\overline{\alpha_j}\rho_{j,at}}{40\pi\,\varepsilon_0^2\varepsilon_r^2\,k\,T_{ads}}\frac{1}{(\sigma_{i,j}+z)^5} + \frac{Q_i^{\,2} s_{cations}^2 e^2\rho_{j,at}}{240\pi\varepsilon_0^2\varepsilon_r^2(kT_{ads})^2}\frac{1}{(\sigma_{i,j}+z)^3} \tag{5.60}$$

In figure 5.5 the interactions of the adsorptive molecule with the solid continuum are presented graphically. The arrows are numbered respectively to the partial potential energies which occur between adsorptive and adsorbent. It has to be mentioned that the polarisability α_i is the electronic polarisability of the molecule according to

Israelachvili [21] for further theoretic considerations. (Most important in figure 5.5 are the potentials indind, dipcha and quadcha, compare Section 7.3.5).

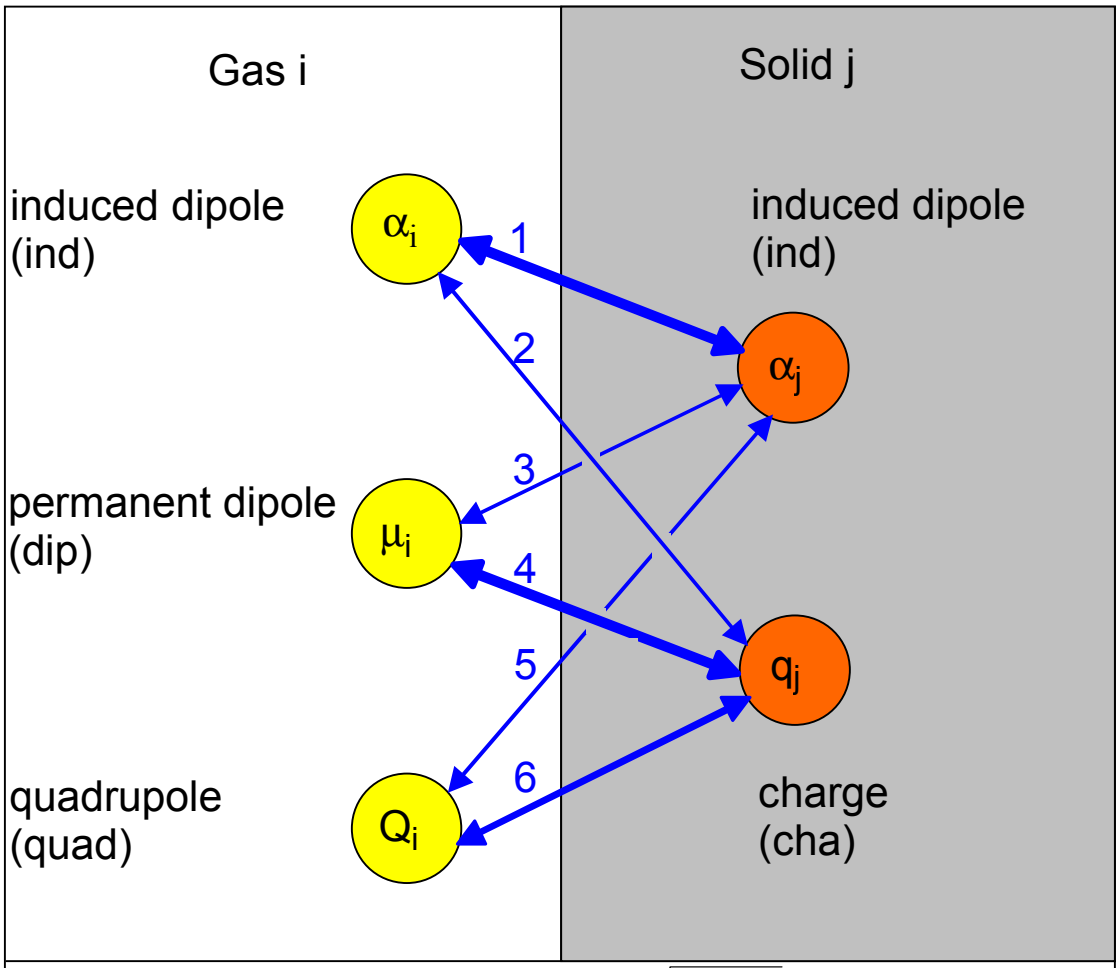

(1)	indind	$\frac{-\Phi_{indind}(z)}{kT_{ads}} = \frac{3}{4}\sqrt{\frac{2\,Ha_j}{\pi\,\sigma_{j,j}^3\,p_c}}\frac{T_c}{T_{ads}}\frac{\sigma_{i,j}^3}{(\sigma_{i,j}+z)^3}$	(5.59)
(2)	indcha	$\frac{-\Phi_{indcha}(z)}{kT_{ads}} = \frac{\alpha_i s_{cations}^2 e^2 \rho_{j,at}}{8\pi\varepsilon_0^2\varepsilon_r^2 kT_{ads}}\frac{1}{(\sigma_{i,j}+z)}$	(5.42b)
(3)	dipind	$\frac{-\Phi_{dipind}(z)}{kT_{ads}} = \frac{\mu_i^2\overline{\alpha}_j\rho_{j,at}}{12\pi\varepsilon_0^2\varepsilon_r^2 kT_{ads}}\frac{1}{(\sigma_{i,j}+z)^3}$	(5.47)
(4)	dipcha	$\frac{-\Phi_{dipcha}(z)}{kT_{ads}} = \frac{\mu_i^2 s_{cations}^2 e^2 \rho_{j,at}}{12\pi\varepsilon_0^2\varepsilon_r^2 (kT_{ads})^2}\frac{1}{(\sigma_{i,j}+z)}$	(5.51)
(5)	quadind	$\frac{-\Phi_{quadind}(z)}{kT_{ads}} = \frac{3Q_i^2\overline{\alpha}_j\rho_{j,at}}{40\pi\,\varepsilon_0^2\varepsilon_r^2\,k\,T_{ads}}\frac{1}{(\sigma_{i,j}+z)^5}$	(5.54)
(6)	quadcha	$\frac{-\Phi_{quadcha}(z)}{kT_{ads}} = \frac{Q_i^2 s_{cations}^2 e^2 \rho_{j,at}}{240\pi\varepsilon_0^2\varepsilon_r^2 (kT_{ads})^2}\frac{1}{(\sigma_{i,j}+z)^3}$	(5.57)

Figure 5.5: The partial potentials between adsorptive and adsorbent.

5.3.8. *Henry* coefficient for energetic heterogeneous adsorbents

By inserting the interaction parameters into equation (5.15) the dimensionless *Henry* coefficient becomes

$$IL = \int_0^{x_{\max}} \left(\exp\left(\frac{A_{dipcha} + A_{indcha}}{(1+x)} + \frac{A_{indind} + A_{dipind} + A_{quadcha}}{(1+x)^3} + \frac{A_{quadind}}{(1+x)^5} \right) - 1 \right) dx \qquad (5.61)$$

where A_{indind} is defined as the interaction parameter for induced dipole – induced dipole interaction

$$A_{indind} = \frac{3}{4} \sqrt{\frac{2Ha_j}{\pi \sigma_j^3 pc}} \frac{T_C}{T_{Ads}} \qquad (5.62)$$

The integral increases very strongly with increasing distance x, for small values of x it reaches a limit. In this work it is recommended to use a limiting value of 2 for x. The integral itself is not analytically solvable. It is not possible to introduce a regression function because it is a three-dimensional problem. Nevertheless, with commercial software like MathCAD numerical values for the *Henry* Loading IL can be evaluated. This value can be transformed to the *Henry* coefficient due to

$$He = \frac{IL \cdot \sigma_{i,j} \cdot S_{BET}}{\Re \cdot T_{ads}} \qquad (5.63)$$

Therefore, it is possible to compare the theoretical a priori calculated *Henry* coefficient with experimental data. The value pairs should lie on a diagonal in a coordinate system with the experimental *Henry* values as the x-axes and the calculated ones as the y-axes. The quality of the model will be discussed in Chapter 7.

5.4. Calculation methods for the *Henry* coefficient

5.4.1. *Henry* coefficients from experiments and literature

The *Henry* coefficients from experiments were derived in this work by applying the *Langmuir* and *Toth* formulae for adsorption, in this study the equations (3.109) and (3.119).

The proposed *Langmuir* method is a graphical method from which the Henry coefficient can be obtained by regressing the transformed data by a linear curve. The intercept of this linear curve with the y-axis is indirectly proportional to the *Henry* coefficient. In this plot the y-axis shows the ratio of the equilibrium pressure p to the equilibrium loading n in Pa/(mol*kg) whereas the x-axis shows the equilibrium pressure p itself in Pa. The data were analysed by using commercial programs.

The same experimental data have also been analysed by the *Toth* equation (3.119) due to an analytical fitting method because a three parameter isotherm cannot be represented by a two dimensional graph. Model parameters are obtained using the non-linear least square method of *Margules*. The parameters are optimised based on the minimum sum of square error given by

$$ss = \sum_{i=1}^{NP}\left(\frac{n_{\text{model}}}{n_{\text{experiment}}}\right)^2 + \sum_{i=1}^{NP}\left(n_{\text{model}} - n_{\text{experiment}}\right)^2 \qquad (5.64)$$

where ss is the sum of square errors and NP the number of data points from the experiment.

In many literature essays *Henry* coefficients are tabulated or given as a function of temperature and heat of adsorption. If not, adsorption isotherms were analysed by the two mentioned methods of *Langmuir* and *Toth*. In some of the essays the authors did not tabulate the data points of equilibrium pressure and loading. In such cases the adsorption graphs were scanned and the data points were quantified by the graphical program Origin®.

5.4.2. Theoretical *Henry* coefficients

Theoretical Henry coefficients have been calculated by using the derived equations (5.59) and (5.61) in the commercially available mathematic program MathCAD® (Version 13, Mathsoft Engineering & Education, Inc.). This program has a Maple kernel to calculate mathematical equations. Equation (5.65) was used in MathCAD® to calculate the dimensionless *Henry* coefficient of Z different adsorption pairs with

$$\begin{aligned}&IL := \left\| \begin{array}{l} \text{for } i \in 0..Z \\ v_i \leftarrow \displaystyle\int_0^2 \left[\exp\left[\frac{\frac{A\_QUADIND_i}{f\_quadind}}{(1+x)^5} + \frac{0.75\cdot\frac{A\_INDIND_i}{f\_indind} + \frac{A\_DIPIND_i}{f\_dipind} + \frac{A\_QUADCHA_i}{f\_quadcha}}{(1+x)^3} + \frac{\frac{A\_DIPCHA_i}{f\_dipcha} + \frac{A\_INDCHA_i}{f\_indcha}}{1+x} \right] - 1 \right] dx \\ \text{return } v \end{array} \right. \\ &\end{aligned} \tag{5.65}$$

where the interaction parameters $A_{i,j}$ are one-dimensional vectors with length of Z and x is the reduced distance as in equation (5.30). The result IL, also a vector with length of Z, is written back to a calculation sheet. The unknown coefficients $f_{i,,j}$ have been determined by theoretical and experimental considerations and will be discussed in Chapter 7. They can be interpreted as potential factors of the interaction parameters $A_{i,j}$. At a first approach it is expected that these potential factors should be close to unity or even $f_{i,j} = 1$. However, experimental results show that in the case for interactions which refer to the electrical charge q derived in the Sectionss 5.3.2, 5.3.4 and 5.3.6 the factors are only close to unity. All other factors are equal to 1. The reasons for this behaviour may be the fact that the distance of the different atoms and their angles with respect to the dipole axis of the adsorptive molecule differs from atom to atom. Therefore all average values depend on these distances and angles. For instance, equation (5.49) is valid for freely rotating molecules. This may not be true for molecules adsorbed in the cage of a zeolite. *Israelachvili* [21] has shown that calculations with the objective to average distances and angles are problematic. It is assumed that these average values can be calculated by complex integrals. In Chapter 7 the $f_{i,,j}$ are derived from theoretical considerations and experimental results. They will be discussed later in more detail.

6. Prediction of Isotherms for p $\rightarrow\infty$ (Saturation)

The a priori prediction of adsorption isotherms based only on the properties of the adsorptive and the adsorbent molecules is a challenging goal. In this Chapter a new model will be introduced which enables the prediction of the isotherm from the *Henry* to the saturation region for *Hamaker* dominant adsorption pairs and for systems where the adsorptive is polar and the adsorbent is heterogeneous with respect to energy.

Examples for the *Hamaker* dominant case are the adsorption of an unpolar gas like an alkane on active carbon or any molecular sieve or the adsorption of polar adsorptives on any energetic homogenous adsorbent. Furthermore the fourth case is the adsorption of any polar molecule like methanol on energetically heterogeneous microporous solids like zeolite NaY.

The idea of the presented new model is that any isotherm of type I has two boundary conditions for the two variables loading n and partial pressure p. The first boundary condition is that in the *Henry* region the loading and the equilibrium pressure have a constant ratio, equal to the *Henry* coefficient. The second boundary condition is that in the saturation region the slope of the curve n=f(p) becomes zero. With a differential equation for the variables the intermediate range it is possible to calculate the whole adsorption isotherm mathematically.

In this model it is assumed that a narrow relationship between the relevant interaction energies and the *Henry* coefficient exists. The saturation is calculated only in dependence on the properties of the adsorptive and the adsorbent.

In Chapter 7 the quality of this new model will be validated by comparing the predicted isotherms with data from the literature and also with data from own adsorption experiments.

6.1. Differential form

The maximum loading n_∞ for $p \rightarrow \infty$ is given when the micropore volume is completely filled with adsorbate which has the molar volume $\beta(T)$:

$$n_\infty = \frac{v_{micro}\rho_{adsorb}}{M_i} = \frac{v_{mciro}}{\beta(T)} \tag{6.1}$$

The relationship between

- the pore filling degree $n_s^* = \frac{n}{n_\infty}$
- the number N of molecule layers
- the microporosity parameter $\frac{S_{BET}\sigma_j}{v_{micro}}$ and
- the adsorbate parameter $\frac{N_A\sigma_i^3}{\beta(T)}$

can be described by

$$n_s^* \equiv \frac{n}{n_\infty} = N \cdot \frac{S_{BET}\sigma_j}{v_{micro}} \cdot \frac{\beta(T)}{N_A\sigma_i^3} \tag{6.2}$$

The microporosity parameters of the adsorbents investigated in this work are in the range 0.60 < $\frac{S_{BET}\sigma_j}{v_{micro}}$ < 1, see as examples tables 7.4, 7.5 and 7.6. Nearly all adsorptives with molar masses above M = 16 kg/kmol valid for methane have adsorbate parameters in the range 0.5 < $\frac{N_A\sigma_i^3}{\beta(T)}$ < 0,75 at a temperature of 300 K, see as examples tables 7.4, 7.5 and 7.6. This means that the maximum number N_{max} of

molecular layers is between N_{max} = 0.3 up to N_{max} = 1 for the pore filling $n_s^* \equiv \frac{n}{n_\infty} = 1$ which corresponds for a complete filling of all micropores.

According to Mersmann [122] the Henry range of an adsorption isotherm is finished when the number of layers, N_{He}, assumes approximately the value 0.1. This means that the borderline between the Henry range and the transition range can be expected between $\left(\frac{n}{n_\infty}\right)_{He}$ = 0.1 and $\left(\frac{n}{n_\infty}\right)_{He}$ = 0.2. In the loading range $\left(\frac{n}{n_\infty}\right) < \left(\frac{n}{n_\infty}\right)_{He}$ the adsorption places with the highest energies will be occupied. Therefore, the interaction energy is smaller than the overall energy $-\frac{\Phi(z)}{kT_{ads}}$ in equation (5.60) in the case $\left(\frac{n}{n_\infty}\right) > \left(\frac{n}{n_\infty}\right)_{He}$. It can be shown that the energy $-\frac{\Phi_{indind}}{kT_{ads}}$ is at least 50 % up to 93 % of the overall energy.

It is further assumed that in the transition range between the *Henry* and the saturation region the *Hamaker* energy is dominant in comparison to other possible potentials. According to *Braun* [4] and *Hirschfelder et. al.* [19] *Hamaker* potentials are long-range interactions. For the first layer of adsorbate molecules on the solid surface the electrostatic potentials have to be taken into account as done for the calculating of the *Henry* coefficient. In the second layer the *Hamaker* energy is dominant because of its long-range attraction compared to the electrostatic forces.

Furthermore, the reduction of the interaction energy is caused by the presence of adsorbate molecules and by their distance from the surface molecules of the adsorbent. According to equation (5.24) the energy is reduced by a factor $\left(\frac{1}{2}\right)^3$ = 0.125 for adsorptive molecules in the second layer. Therefore, the slope $\frac{d(\ln n)}{d(\ln p)}$ of an isotherm decreases with an increasing pore filling $\left(\frac{n}{n_\infty}\right)$ and increasing interaction energy. This is demonstrated in figure 6.1 where the pore filling of some adsorptives

is plotted against the pressure. The higher the interaction energy the smaller is the pressure valid for leaving the *Henry* range and entering the transition range.

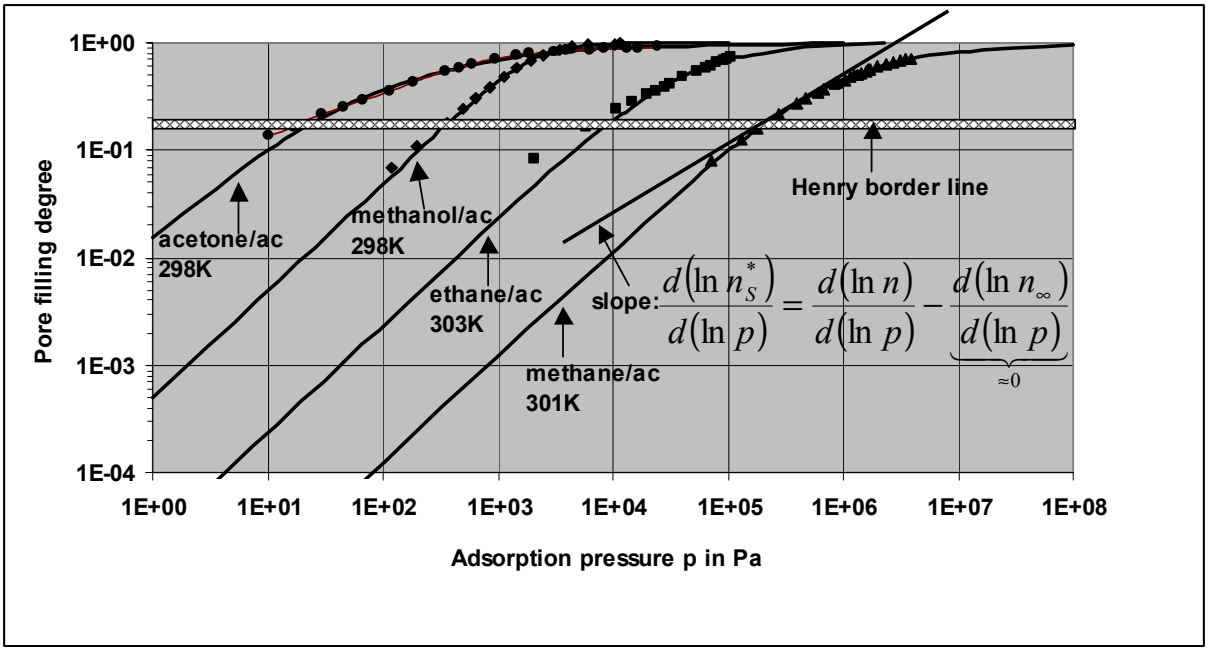

Figure 6.1: Adsorption isotherms on active carbon coal, fitted with Langmuir (methane/ac and ethane/ac) and Toth (acetone/ac and methanol/ac).

Consequently, adsorptives with high $\frac{T_c}{T_{ads}}\left(\frac{Ha_j}{\sigma_j^3 p_c}\right)^{3/2}$ data lead to a wide transition range over several orders of magnitude of the pressure and their mean slope $\frac{d(\ln n)}{d(\ln p)}$ in the transition range is small. This slope assumes zero for $n_s^* \to 1$ (saturation). All this ideas lead to the following differential equation which fulfils these requirements [122]:

$$\frac{d(\ln n)}{d(\ln p)} = \frac{dn}{dp}\frac{p}{n} = \frac{1}{1 + C\, T_{r\_ads}\left(E_{Ha}^*\right)^{3/2}\left(\frac{n/n_\infty}{1 - n/n_\infty}\right)} \qquad (6.3)$$

with $\frac{d(\ln n)}{d(\ln p)} = 1$ for n $\to$ 0 and $\frac{d(\ln n)}{d(\ln p)} = 0$ for n $\to$ n_∞.

It is assumed that C is a constant, and its order of magnitude can be evaluated from the condition that the expression $C\,T_{r\_ads}\left(E_{Ha}^{*}\right)^{3/2}\left(\frac{n/n_{\infty}}{1-n/n_{\infty}}\right)$ must be noticeable compared to 1 (say 0.1) when leaving the *Henry* range. In this work C = 0.55 * 10^{-3}.

Some parameters in equation (6.3) are dimensionless numbers and can be defined as

$$T_{r\_ads} = \frac{T_{ads}}{T_c} \tag{6.4a}$$

$$E_{Ha}^{*} = \frac{Ha_j}{\sigma_j^3 p_c} \tag{6.4b}$$

where T_{r_ads} is the reduced adsorption temperature and E_{Ha}^{*} the reduced *Hamaker* energy. The loading n_∞ is equal to the saturation loading when the micropore volume v_{micro} is completely filled with adsorbate of the density ρ_{adsorb} and can be calculated by equation (6.1) where v_{micro} is in $m^3/kg_{adsorbent}$, the density ρ_{adsorb} in $kg_{adsorbate}/m^3$ and the molar mass M_i in $kg_{adsorbate}/mol_{adsorbate}$.

The calculation of the adsorbate density, especially in the supercritical region, is afflicted with uncertainties because the physical state of an adsorbed molecule cannot be described definitely. In this work, if no data for the density of the liquid was available, the ratio of molar mass of the adsorbate and adsorbate density is calculated by the molar volume of the adsorbate β [36] which depends on the adsorption temperature T_{ads}. The molar volume is inter- and extrapolated between the molar volume of the adsorptive molecule at the normal boiling point v_b and the *van-der-Waals* volume v_{vdW} [36]. It is

$$\frac{M_i}{\rho_{adsorb}} = \beta\left(T_{ads}\right) = v_b + \left(\frac{T_{ads}-T_b}{T_c-T_b}\right)\left(v_{vdW}-v_b\right) \tag{6.5}$$

where T_b is the normal boiling temperature of the adsorptive. T_b and the normal molar volume of the adsorptive v_b are tabulated for many cases in the literature [106]. For any other case the normal molar volume in m^3/mol can be calculated by the method of *Tyn* and *Calus* [106] with

$$v_b = 0.285 * 10^{-6} * v_c^{1.048} \tag{6.6}$$

where v_c is the critical volume of the adsorptive in cm^3/mol, see figure 6.2.

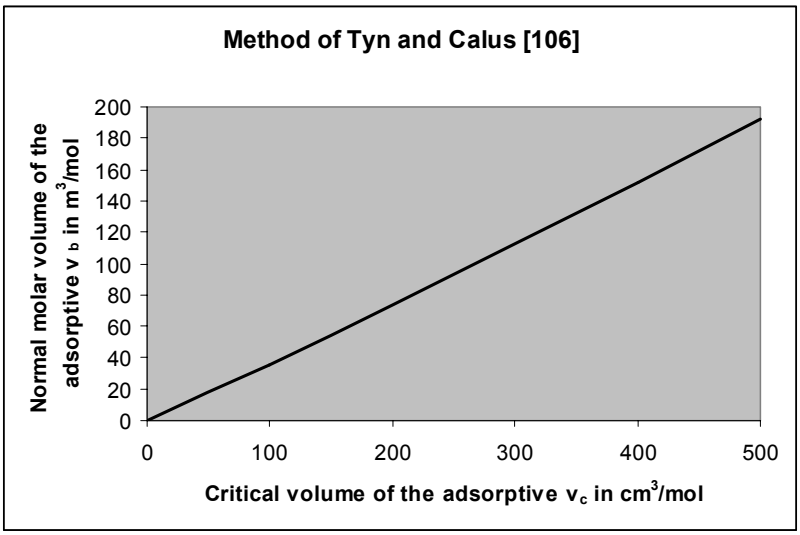

Figure 6.2: Normal molar volume of the adsorptive in dependence of the critical volume [106].

The van-der-Waals volume v_{vdW} can be expressed by equation (3.29). The saturation loading n_∞ is now

$$n_\infty = \frac{v_{micro}}{\beta(T_{ads})} \tag{6.7}$$

The ratio of the loading n to the saturation loading n_∞ is defined as the saturation degree n_s^* with

$$n_s^* = \frac{n}{n_\infty} = \frac{n M_i}{v_{micro}\, \rho_{adsorb}} \qquad \text{or} \tag{6.8}$$

$$n_s^* = \frac{n}{n_\infty} = \frac{n\,\beta(T)}{v_{micro}} \tag{6.9}$$

Equation (6.3) can be rewritten with the definition

$$B = C\frac{T_c}{T_{ads}}\left(\frac{Ha_j}{\sigma_j^3 p_c}\right)^{3/2} \tag{6.10}$$

which is independent of the loading n and the pressure p to

$$d(\ln n)\left(1 + B\left(\frac{n/n_\infty}{1 - n/n_\infty}\right)\right) = d(\ln p) \tag{6.11}$$

6.2. Integrated form with boundary conditions

Generally, three cases can be distinguished with respect to the slope $\frac{d(\ln n)}{d(\ln p)}$ of an adsorption isotherm:

- $\frac{d(\ln n)}{d(\ln p)} = 1$ (dilute or Henry range) (6.12)
- $\frac{d(\ln n)}{d(\ln p)} = 0$ (saturation range) and (6.13)
- $\frac{d(\ln n)}{d(\ln p)} = g\left(f\left(n_s^*\right), T_{r\_ads}, E_{Ha}^*, n_S^*\right)$ (6.14)

6.2.1. The dilute region

The first case is the region where the loading n is much smaller than the saturation loading n_∞, so

$$n << n_\infty \tag{6.15}$$

The differential equation (6.11) reduces to equation (6.12). The integration of the differential equation (6.12) leads to

$$\int d(\ln n) = \int d(\ln p) \quad \text{or} \tag{6.16}$$

$$\ln n = \ln p + \ln Const. \tag{6.17}$$

The integration constant Const. can be interpreted as the Henry coefficient:

$$\ln Const. = \ln He \tag{6.18}$$

It follows that

$$\ln\left(\frac{n}{He\,p}\right) = 0 \qquad \text{or} \tag{6.19}$$

$$n = He\,p \tag{6.20}$$

which is known as *Henry*'s law. Some authors doubt that a real Henry region exists with respect to the more or less degree of heterogeneity of the adsorbent surface. However, dealing with chemical engineering predictions the assumption of a Henry range is reasonable and helpful.

6.2.2. The saturation region

In the saturation region the slope of the loading n relative to the equilibrium pressure does not change significantly. The limit of the differential equation (6.3) is for $n \rightarrow n_\infty$

$$\lim_{n\to n_\infty}\frac{d(\ln n)}{d(\ln p)} = \lim_{n\to n_\infty}\frac{1}{1 + C\frac{T_c}{T_{ads}}\left(\frac{Ha_j}{\sigma_j^3 p_c}\right)^{3/2}\left(\frac{n/n_\infty}{1-n/n_\infty}\right)} = \lim_{n\to n_\infty}\frac{1}{1 + B\left(\frac{n/n_\infty}{1-n/n_\infty}\right)} = 0 \tag{6.21}$$

or

$$d(\ln n) = 0 \qquad \text{or} \tag{6.22}$$

$$n = const. = n_\infty \tag{6.23}$$

6.2.3. The general case

In the regime between the *Henry* and the saturation region the differential equation (6.11) has to be solved. It follows with

$$d(\ln n) = \frac{dn}{n} \tag{6.24}$$

the integral form

$$\int d(\ln n) + B \int \frac{n/n_\infty}{1 - n/n_\infty} \frac{dn}{n} = \int d(\ln p) \qquad \text{or} \tag{6.25}$$

$$\ln n - B \ln\left(1 - n/n_\infty\right) = \ln p + \ln He \tag{6.26}$$

Equation (6.26) can be rewritten to

$$\ln\left(\frac{He\, p}{n}\right) = -B \ln\left(1 - \frac{n}{n_\infty}\right) = \ln\left(1 - \frac{n}{n_\infty}\right)^{-B} \tag{6.27}$$

It follows the adsorption isotherm description for the general case (see figures 6.3 and 6.4) with

$$\frac{He\ p}{n} = \left(\frac{1}{1 - \frac{n}{n_\infty}} \right)^B \quad \text{or} \quad (6.28):$$

$$p = \frac{n}{He} \left(\frac{1}{1 - \frac{n}{n_\infty}} \right)^B \quad (6.29)$$

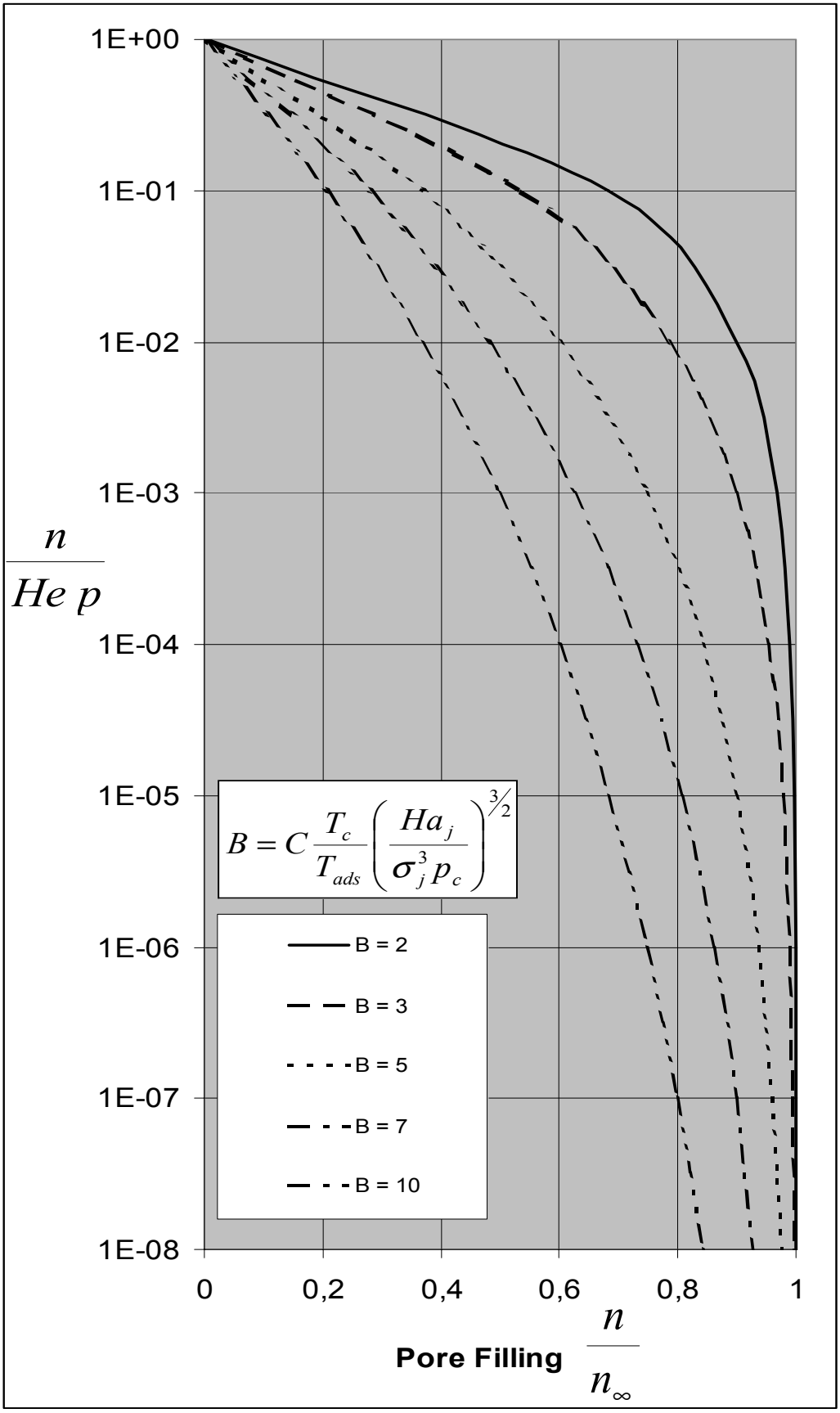

Figure 6.3: Pore filling for the general case.

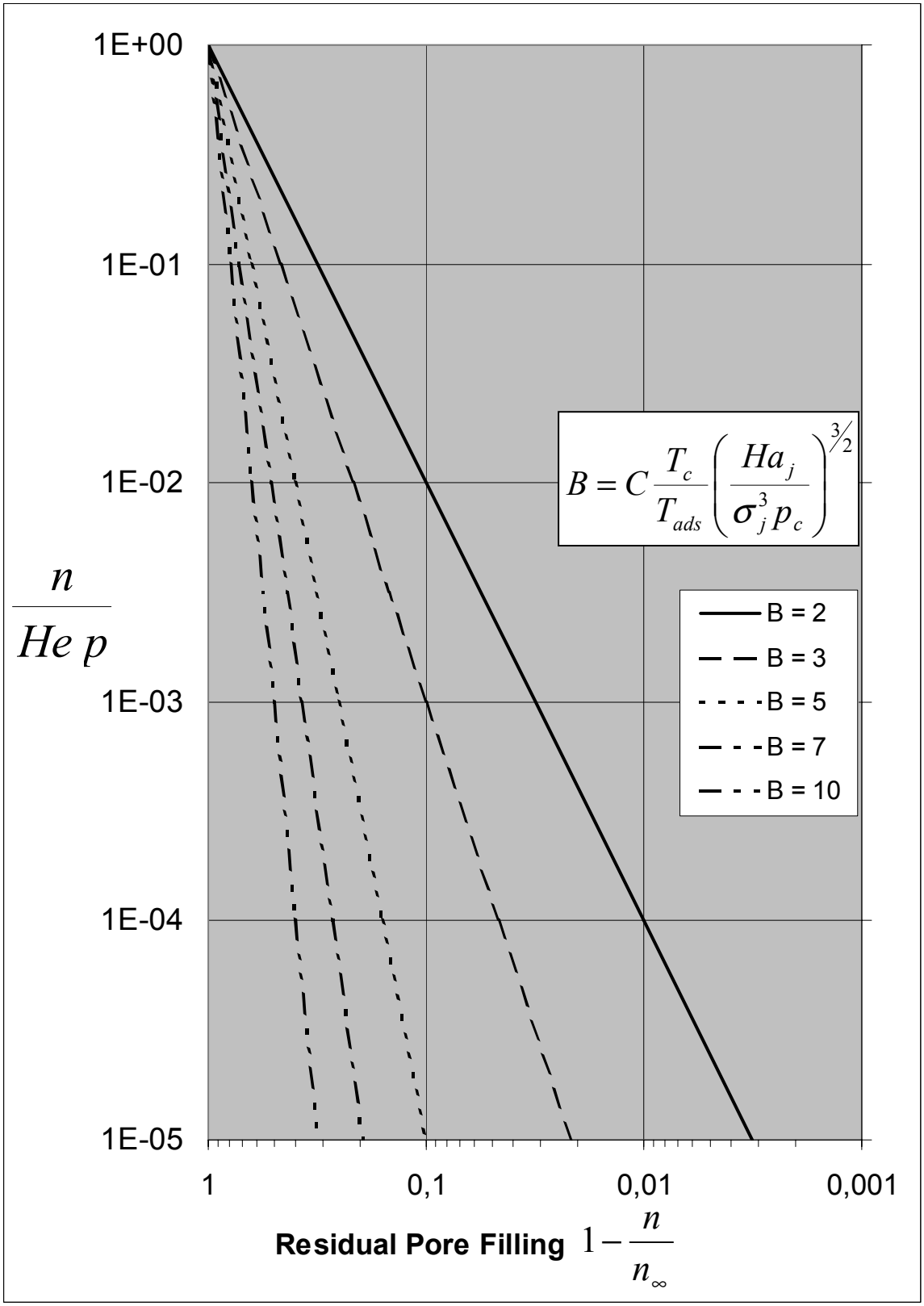

Figure 6.4: Residual pore filling for the general case

7. Results and Discussion

7.1. New experimental results

The experiments carried out for measurements are described in the appendix B2. Experiments were carried out in Garching and Leipzig.

7.1.1. Adsorption isotherms

Adsorption isotherms of methanol and dichloromethane were measured on zeolites MS5A, NaX and NaY. These systems were chosen to expand literature data with experimental data in the case of adsorption of polar molecules or such with high polarisabilities on energetic heterogeneous sorbents. The experiments were carried out in the pressure range from 0.1 Pa to saturation pressure of the adsorptive at room temperature. Figure 7.1 shows adsorption isotherms of methanol on several zeolites. Figure 7.2 shows adsorption isotherms of dichloromethane on the same zeolites. The temperatures ranged from 44°C to 47°C.

As can be seen in figure 7.1 methanol has the highest adsorption affinity with NaY followed by MS5A and NaX, which seem to have the same adsorption attraction to methanol. NaY was pure crystalline, MS5A and NaX have been used as industrial pellets with binder amount. The MS5A zeolite was grated to powder, pressed together and then broken to small pieces for the glass crucible. Adsorption was repeated for this modified molecular sieve. The experiment shows that there is some diffusion resistance when adsorbing into industrial pellets with binder amount. For the theoretical calculations only the data of the crystals and grated pellets were taken. Reliable data from the Garching experiments begin at 0.1 Pa, the reliable data from Leipzig begin at 10 to 100 Pa. The saturation loading for methanol on the examined zeolites was in the magnitude of 6 to 6.5 mol/kg. This is in good agreement with the theory of micropore filling as will be shown later. The Henry region of methanol adsorption on zeolites ends at high loadings of approximately 3 mol/kg or 10 Pa,

respectively. In the experiments the Henry region could be reached very well down to pressures of 0.1 Pa.

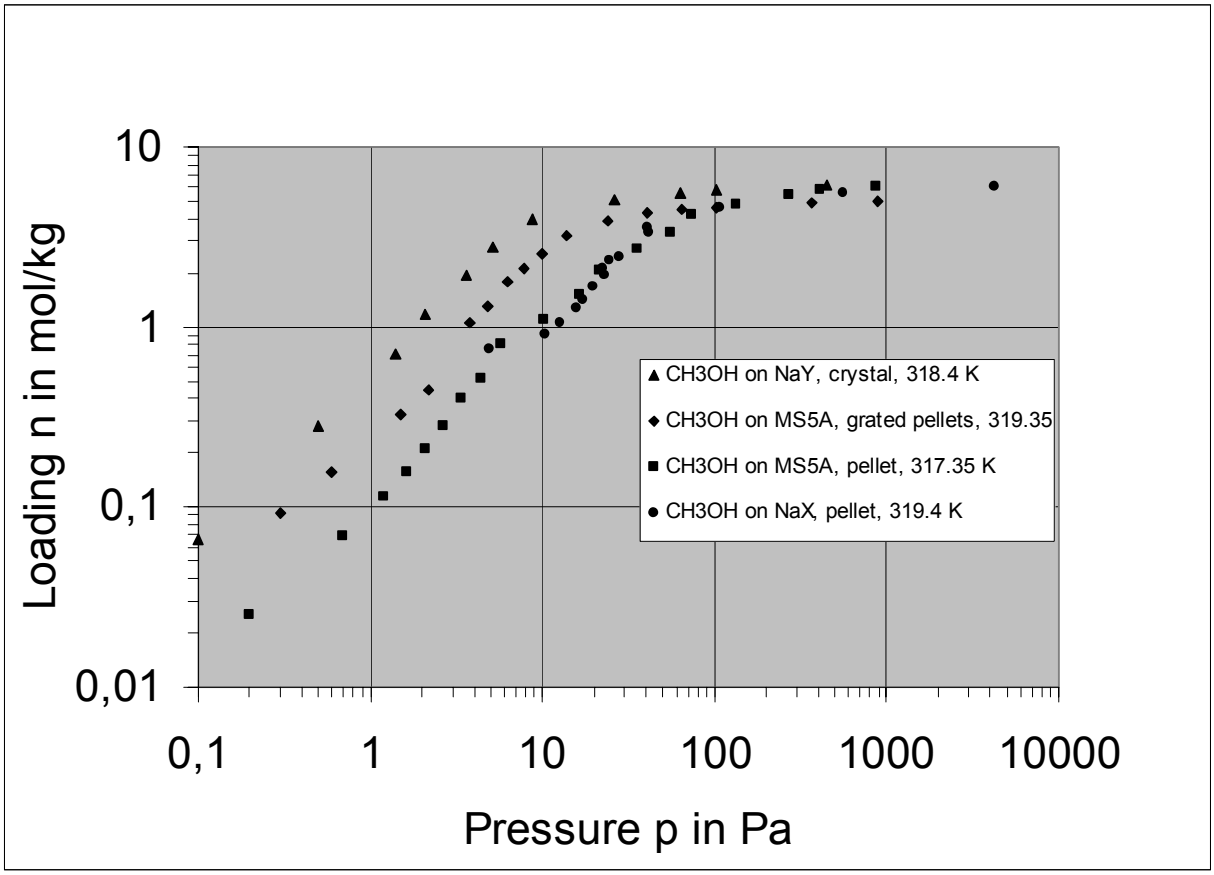

Figure 7.1: Methanol adsorption on zeolites NaY, MS5A and NaX.

Dichloromethane adsorption was conducted with crystal NaY and grated MS5A zeolite pellets and additionally with NaX zeolite. The *Henry* region ends at approximately 2 Pa for MS5A and 10 Pa for NaY. The saturation loading is in the range of approximately 3.5 mol/kg, less than methanol because of the higher molar mass of approximately 84 kg/kmol. *Henry* coefficient calculations will be compared later regarding to *Langmuir* and *Toth* regressions.

With this experiments it could be shown that the *Henry* region and the saturation region of solvents with moderate dipole moments of approximately 1.5 debye on zeolites can be measured with gravimetric adsorption methods.

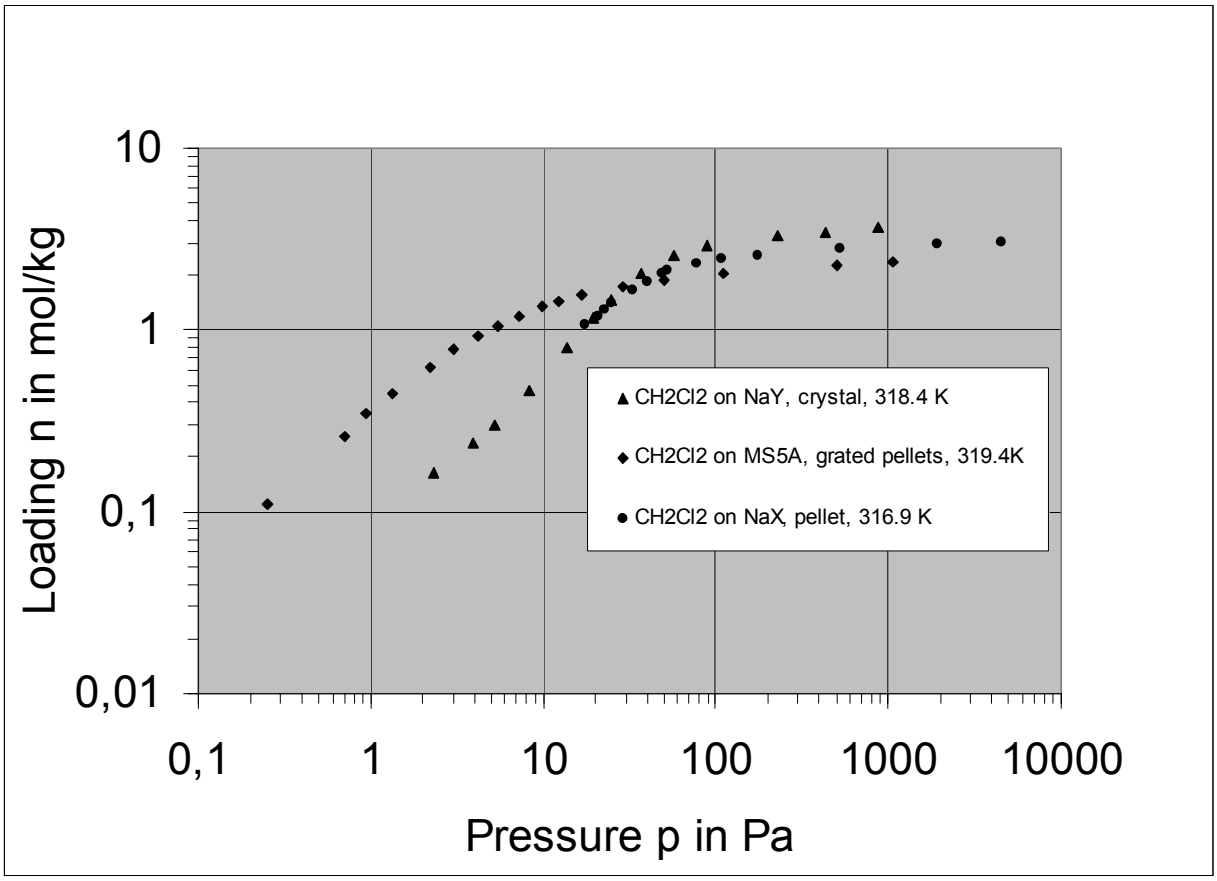

Figure 7.2: Dichloromethane adsorption on zeolites NaY, MS5A and NaX.

7.1.2. Comparison of *Langmuir* and *Toth* regression quality

In this Section the experimental data are fitted with both *Langmuir* and *Toth* adsorption isotherms. Figure 7.3 shows the adsorption of methanol on NaY and in figure 7.4 the adsorption equilibrium of dichloromethane on MS5A zeolite is shown. In both cases the *Toth* isotherm delivers better fits to the experimental data than the *Langmuir* isotherm. The standard deviation is 8.1 % for Toth and 17.3 % for Langmuir in the case of methanol adsorption on NaY. Furthermore the standard deviation is 3.8 % for *Toth* and 5.8 % for *Langmuir* in the case of dichloromethane adsorption on MS5A. In Table 7.1 the standard deviations for the experimental data are listed. On the basis of this table it was decided to calculate the *Henry* coefficient with *Toth* regression which fitted better to the data. *Toth* parameters n_{max}, K_T and m and *Langmuir* parameters n_{mon} and K_L are explained in Chapter 3.

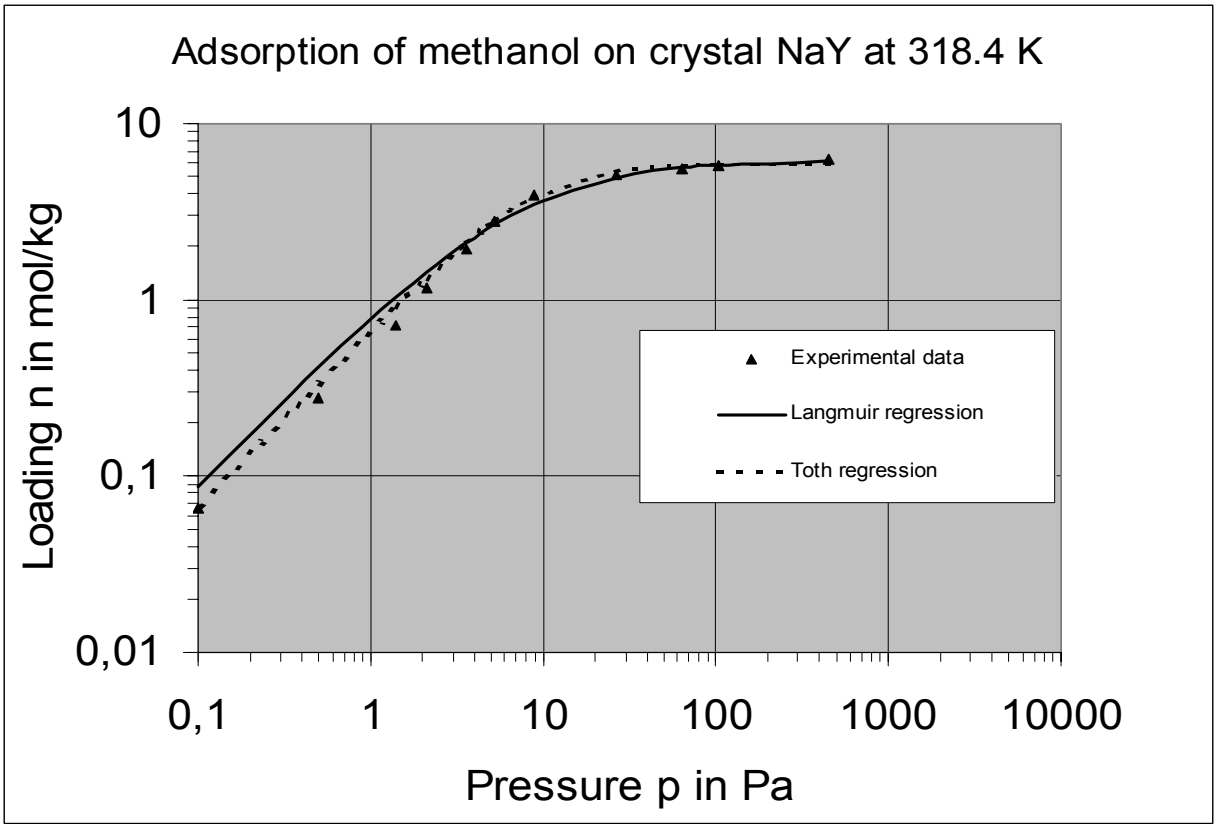

Figure 7.3: Methanol (CH_3OH) adsorption on crystal NaY at 318.4 K.

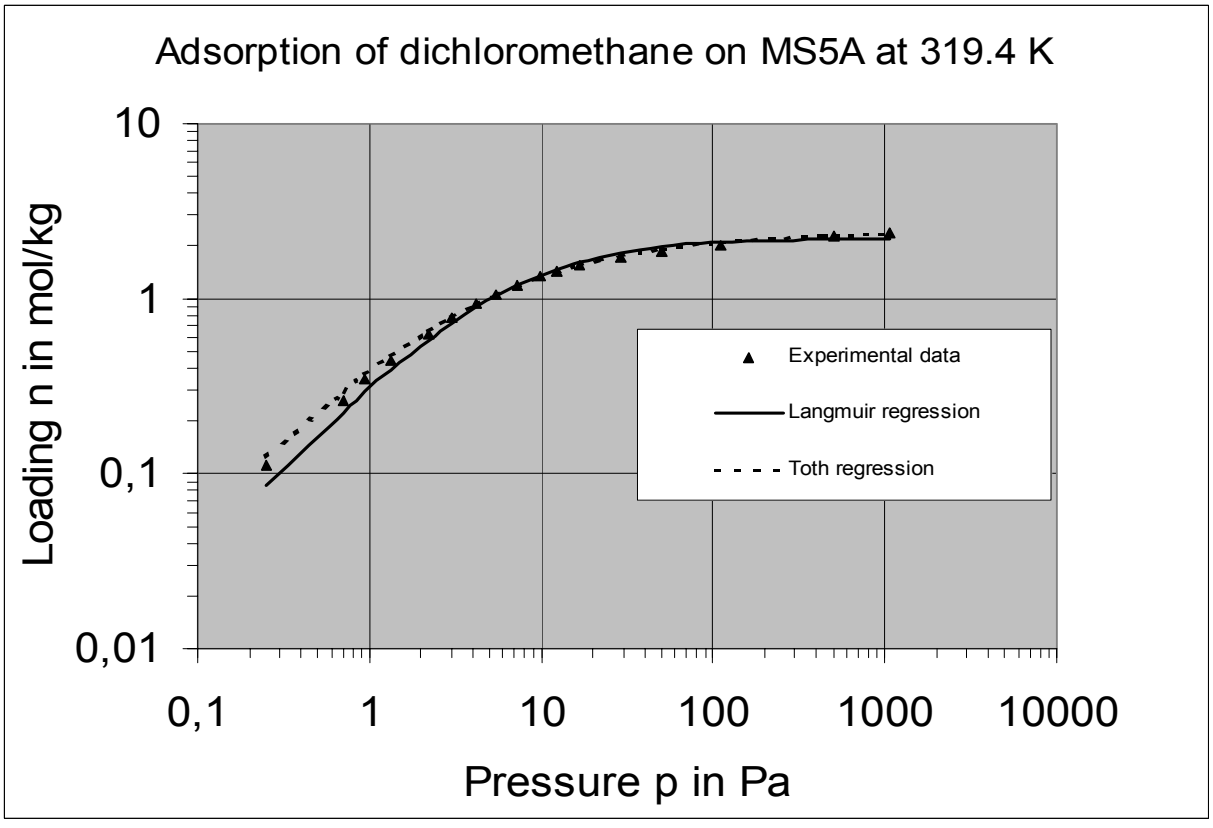

Figure 7.4: Dichloromethane (CH_2Cl_2) adsorption on MS5A, grated pellets at 319.4 K.

Table 7.1: Comparison of Langmuir and Toth regression quality.

Adsorptive	Adsorbent	Temperature in K	*Langmuir* standard deviation in %	*Toth* standard deviation in %
Methanol	MS5A, pellet	317.7	13.6	**9.8**
Methanol	MS5A, grated pellets	319.4	28.9	**13.8**
Methanol	NaY, crystal	318.4	17.3	**8.1**
Methanol	NaX, pellet	319.4	10.1	**7.9**
Dichloromethane	MS5A, grated pellets	319.4	5.8	**3.8**
Dichloromethane	NaY, crystal	318.4	17.1	**8.1**
Dichloromethane	NaX, pellet	316.9	3.1	**2.3**

7.1.3. BET surface and micropore volume

The specific surface of the solids has been measured by adsorption of nitrogen at 77 K. Figure 7.5 shows the BET isotherm for zeolite NaY in the linear form of equation (3.7) with the relative pressure interval from 0.05 to 0.30. The intercept point of the linear fit to the experimental data has the value b = - 0.00297 kg/mol and the gradient m is equal to 0.152 kg/mol. With equation (3.5) the monolayer loading of the BET isotherm n_{mon} is equal to 6.72 mol/kg. The BET constant can be calculated by equation (3.6) and it is c = -50.05. With equation (3.7) and the occupied area of one nitrogen molecule $a_{mol}(N_2) = 0.162*10^{-18}$ m^2 at 77.4 K it is S_{BET} = 655400 m^2/kg for NaY zeolite. The other solids have been measured with the same method.

The micropore volume of the adsorbents were determined by the t-plot method. The data for the evaluation of the micropore volume was taken from the same interval as for the BET method, e.g. in the relative pressure interval 0.05 to 0.30. For NaY the micropore volume has been calculated to $v_{micro} = 0.272*10^{-3}$ m^3/kg.

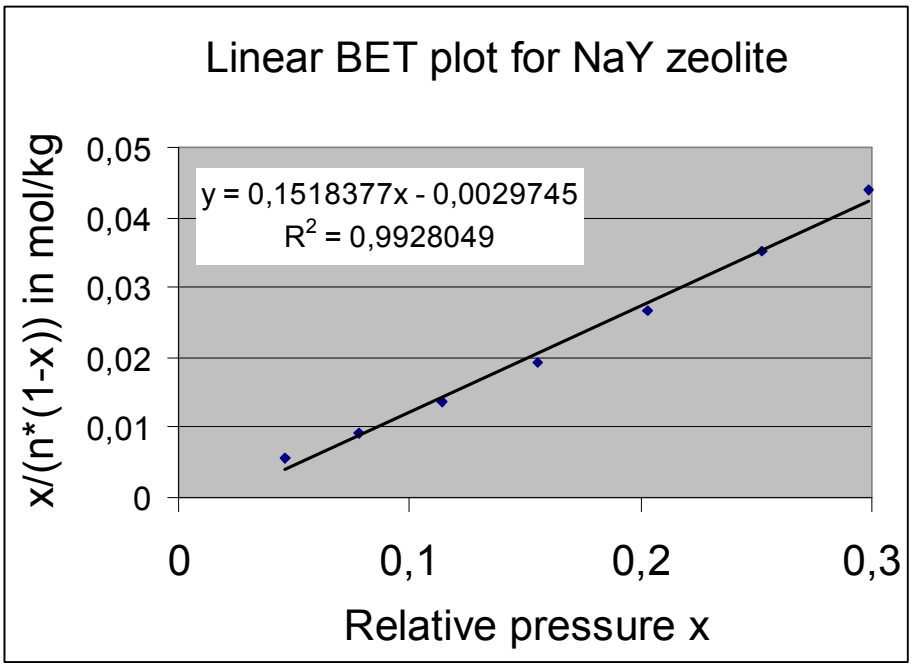

Figure 7.5: Linear BET plot for NaY zeolite.

7.2. Prediction of isotherms

7.2.1. *Henry* coefficient predictions

Henry coefficients were calculated with the new method (equations (5.15) and (5.65)) explained in Chapter 5 and compared with data from the literature and with own experimental data, respectively. The model quality is exmeplarly discussed on zeolites MS5A, MS4A, NaY and NaX.

As mentioned in Chapter 5 the potential factors for charge interactions were calculated based on theoretical assumptions and experimental results. For induced dipole interactions (indind, dipind and quadind) where no charge is involved on the solid side it is assumed that

$$f_{indind} = f_{dipind} = f_{quadind} = 1 \qquad (7.1a)$$

For charge involved interactions (indcha, dipcha, quadcha) it is assumed in first approximation that

$$f_{indcha\,j} = f_{dipcha\,j} = f_{quadcha\,j} = f_{charge} \cdot \left(\frac{Al}{Si}\right)_j \qquad (7.1b)$$

where $\left(\frac{Al}{Si}\right)_j$ is the aluminium to silicon ratio of adsorbent j and f_{charge} the potential factor for charge involved interactions. $\left(\frac{Al}{Si}\right)_j$ is different for every zeolite. The parameter f_{charge} is equal to 1.35 for every microporous adsorbent. For MS5A it is $\left(\frac{Al}{Si}\right)_j$ = 1, therefore f_{indcha} is assumed to be 1.35. It will be shown next that this first approximation is very sufficient for charge interactions. In order to test the validity and the accuracy of the new model the Henry coefficients were calculated for several adsorption cases of gases on zeolites and compared with experimental values. With this method it was possible to determine the unknown potential factors $f_{i,,j}$ in equation (5.65).

- According to the theoretical and experimental results of *Maurer* [26] the induced dipole – induced dipole potential for the zeolites also were calculated with a potential factor f_{indind} = 1.
- Methane has no dipole moment (μ_i = 0), no quadrupole moment (Q_i = 0) and a polarisability of α_i = 3.0*10^{-40} (C^2*m^2)/J. Adsorption on MS5A (S_{BET} = 600000 m^2/kg) at 293 K was examined regarding to [35]. The experimental Henry coefficient is tabulated [35] as 8.8*10^{-6} mol/(kg*Pa). With f_{indind} = 1 in equation (5.62) the calculated Henry coefficient is 7.93*10^{-6} mol/(kg*Pa) if the parameter f_{indcha} is calculated with equation (7.1b) to 1.35. It will be shown later that the factor f_{indcha} calculated by equation (7.1b) is adequate with respect to isotherms investigated in this study.
- Ethene has no dipole moment (μ_i = 0), a quadrupole moment Q_i = 1.44*10^{-39} C*m^2 and a polarisability α_i = 3.0*10^{-40} (C^2*m^2)/J. It adsorbs on NaY (S_{BET} = 500000 m^2/kg) at 305 K with a Henry coefficient of 2.56*10^{-3} mol/(kg*Pa) [117]. NaY has an aluminium to silicon ratio of $\left(\frac{Al}{Si}\right)_{NaY}$ = 0.41. With known potential factors f_{indind} = 1 and f_{indcha} = 1.35*0.41 = 0.554 and an assumed potential factor $f_{quadind}$ = 1 the calculated Henry coefficient is 7.0*10^{-4} mol/(kg*Pa).

- Carbon dioxide has a small dipole moment μ_i = 2.34*10^{-30} Cm, a strong quadrupole moment Q_i = 1.5*10^{-39} C*m^2 and a polarisability α_i = 2.9*10^{-40} (C^2*m^2)/J. It adsorbs on MS4A (S_{BET} = 350000 m^2/kg) at 298 K with a Henry coefficient of 1.36*10^{-3} mol/(kg*Pa) [22]. In adsorptive molecules with strong quadrupole moments two dipoles in counterdirection can exist [132]. Furthermore a strong quadrupole moment can induce a dipole moment μ_j in the adsorbent molecule (see chapter 5 in this thesis). The order of magnitude of the ratio $\frac{Q_i}{\mu_i \sigma_i}$ of many polar adsorptive molecules is ≈ 1 or $\mu_i \sigma_i = \mu_i \sigma_{i,j} = Q_i$. With respect to this simple relationship it may be reasonable to introduce the factor 2*(2)^2 = 8 in equation (5.57) in order to take into account the phenomena described above:

$$\frac{\Phi_{quadcha}(x)}{kT_{ads}} = -\frac{8}{240}\frac{Q_i^{\,2} s_{cations}^2 e^2 \rho_{j,at}}{\pi \varepsilon_0^2 \varepsilon_r^2 (kT_{ads})^2}\frac{1}{\sigma_{i,j}^3}\frac{1}{(1+x)^3} \qquad (7.1c)$$

  An introduction of this factor 8 leads to the result that the charge potential factor f_{charge} seems to have the value 1.35 for all zeolites. With an aluminium to silicon ratio of 1 for MS4A it follows $f_{quadcha}$ = 1.35 and a calculated Henry coefficient of 3.4*10^{-3} mol/(kg*Pa).♠
- Ammonia has a strong dipole moment μ_i = 5.0*10^{-30} Cm, a strong quadrupole moment Q_i = 8.7*10^{-40} C*m^2 and a relative small polarisability α_i = 3.1*10^{-40} (C^2*m^2)/J. It adsorbs on NaY (S_{BET} = 500000 m^2/kg) at 373 K with a Henry coefficient of 2.82*10^{-4} mol/(kg*Pa) [118]. With a potential factor f_{charge} = 1.35 and an aluminium to silicon ratio of 0.41 the Henry coefficient can be calculated to 2.14*10^{-4} mol/(kg*Pa).
- Methanol has a big dipole moment μ_i = 5.7*10^{-30} Cm, a small quadrupole moment Q_i = 4.3*10^{-40} C*m^2 and a small polarisability α_i = 3.7*10^{-40} (C^2*m^2)/J. It adsorbs on the zeolite NaY (S_{BET} = 655400 m^2/kg) at 318 K with a Henry coefficient of 6.71*10^{-1} mol/(kg*Pa). The predicted Henry coefficient is 2.5*10^{-1} mol/(kg*Pa) if a potential factor f_{dipind} = 1 is assumed.

♠ Another way for deriving the factor 8 is explained in the appendix C.

- The potential factors as shown above were taken to calculate the adsorption of arbitrary gases on any microporous solid. The results are explained in the following.

Figure 7.6 and 7.7 show *Henry* coefficients of zeolite MS4A with the adsorptives ammonia, carbon dioxide, carbon monoxide, methane, propane, hexane, helium, nitrogen, oxygen and benzene on zeolite MS4A. In figure 7.6 the theoretical *Henry*

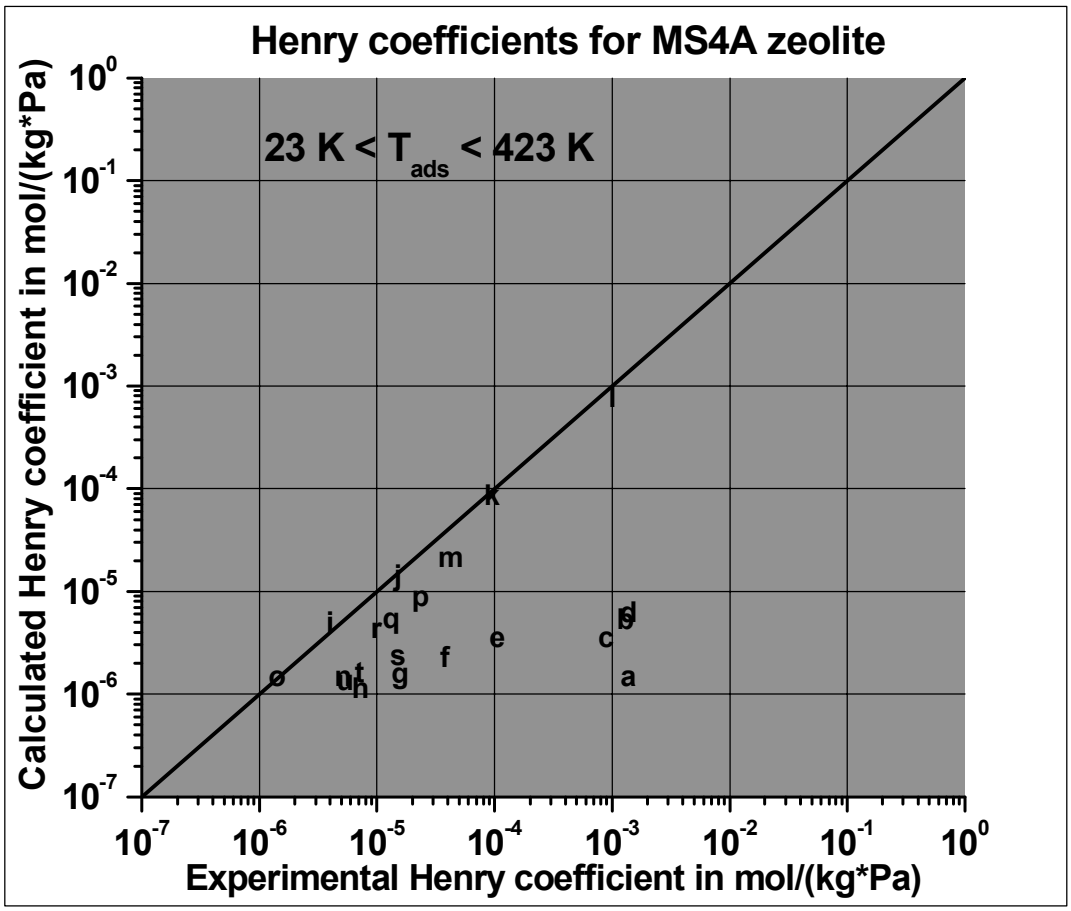

coefficients were calculated on basis of the induced dipole- induced dipole potential.

Figure 7.6: Henry coefficients for adsorption of gases on MS4A zeolite on basis of only induced dipole – induced dipole interactions (table 7.2).

The next figure 7.7 is based on all potentials taken into account as described in Chapter 5 and on the potential factors. Besides benzene and hexane the prediction works very well as can be seen in table 7.2. The *van-der-Waals* diameters of benzene and n-hexane are 4.56 E-10 m and 5.18 E-10 m, respectively. It seems that these

molecules are too big for the effective micropore opening of MS4A. The model predicts *Henry* coefficient values between 3 and 5 magnitudes larger than the experimental ones. Although sterical effects like these cannot be represented the new model works very well over 4 orders of magnitudes in the case of the MS4A adsorption examples. It is interesting to mention that in the case of NH_3 for instance the loading is by a factor 10^3 higher than calculated with induced dipole – induced dipole interactions only.

The tested adsorptives cover different types of molecules with different polar properties. Noble gases like helium have no dipole moment, no quadrupole moment and small polarisabilities. Alkanes like methane, propane and hexane have no dipole moment, small quadrupole moments and intermediate polarisabilities. Carbon monoxide and carbon dioxide have small and medium dipole moments, respectively, large quadrupole moments and small polarisabilities. NH_3 has a relative big dipole moment of 1.5 debye, a big quadrupole moment of $8.67*10^{-40}$ $C*m^2$ but only a small

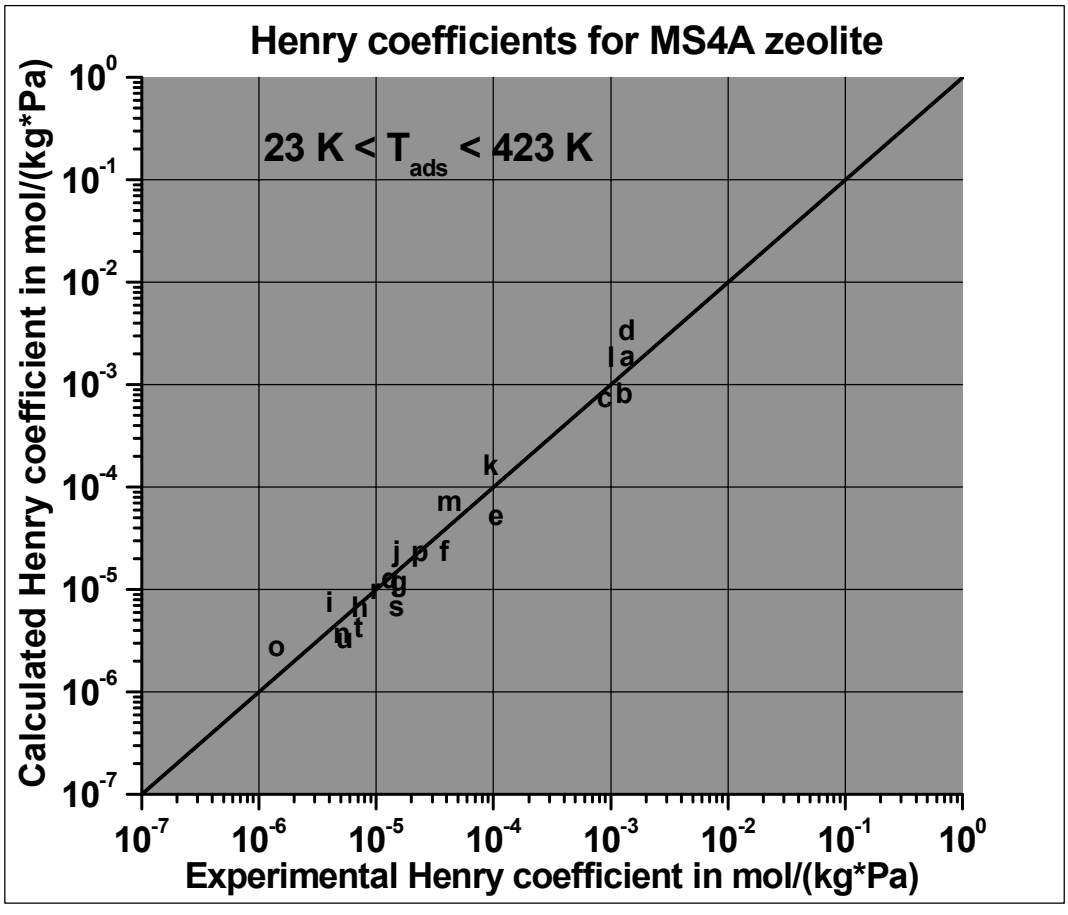

polarisability of $3.13*10^{-40}$ C^2*m^2/J.

Figure 7.7: Henry coefficients for adsorption of gases on MS4A zeolite (table 7.2).

Table 7.2: Comparison of predicted and experimental Henry coefficients of different gases on MS4A zeolite (figure 7.7).

Gas	Sym-bol	Exp. Henry coefficient in mol/(kg*Pa)	Calc. Henry coefficient in mol/(kg*Pa)	Adsorption temperature in K	S_{BET} in m^2/kg	Deviation in % $\left(\frac{He_{exp.} - He_{calc.}}{He_{exp.}}\right)$
NH_3	a	1.38E-03	1.89E-04	393	350000	-38
CO_2	b	1.29E-03	8.23E-04	333	650000	36
CO_2	c	8.87E-04	7.48E-04	323	350000	16
CO_2	d	1.36E-03	3.39E-03	298	350000	-145
CO	e	1.05E-04	5.25E-05	243	650000	50
CO	f	3.78E-05	2.32E-05	263	650000	39
CO	g	1.56E-05	1.18E-05	283	650000	24
CO	h	7.19E-06	6.71E-06	303	650000	7
He	i	4.00E-06	7.35E-06	50	650000	-84
He	j	1.50E-05	2.32E-05	40	650000	-55
He	k	9.50E-05	1.62E-04	30	650000	-70
He	l	1.00E-03	1.81E-03	23	650000	-81
C_3H_8	m	4.22E-05	7.16E-05	423	650000	-70
N_2	n	5.10E-06	3.73E-06	278	650000	27
O_2	o	1.40E-06	2.78E-06	278	650000	-98
CH_4	p	2.35E-05	2.32E-05	253	650000	1
CH_4	q	1.30E-05	1.30E-05	273	650000	-0.3
CH_4	r	9.79E-06	10.0E-06	283	650000	-2.6
N_2	s	1.50E-05	6.91E-06	253	650000	54
N_2	t	7.04E-06	4.19E-06	273	650000	40
N_2	u	5.30E-06	3.35E-06	283	650000	37

As second example for energetic heterogeneous adsorbents figures 7.8 and 7.9 show the comparison of experimental and calculated Henry coefficients for the zeolite NaX. Table 7.3 lists the deviations in percent. Besides ammonia, methanol is a molecule with a high dipole moment of 1.7 debye. The deviation of the calculated Henry coefficient from the experimental one is only 41 %, whereas its deviation is 290432 % when calculated on the basis of the induced dipole – induced dipole interaction only. A second example for polar molecules is naphthalene $C_{10}H_8$. It has a high quadrupole moment of $4.5*10^{-39}$ Cm^2 and a high polarisability of $1.94*10^{-39}$ C^2*m^2/J but no dipole moment. The deviation in figure 7.9 is 56 % whereas in figure 7.8 it is 11579 %. These data prove the efficiency of the new model very clearly. It is interesting to note that the largest deviations are observed in the case of adsorptives with strong quadrupole moments (NH_3, CO, CO_2, C_2H_4).

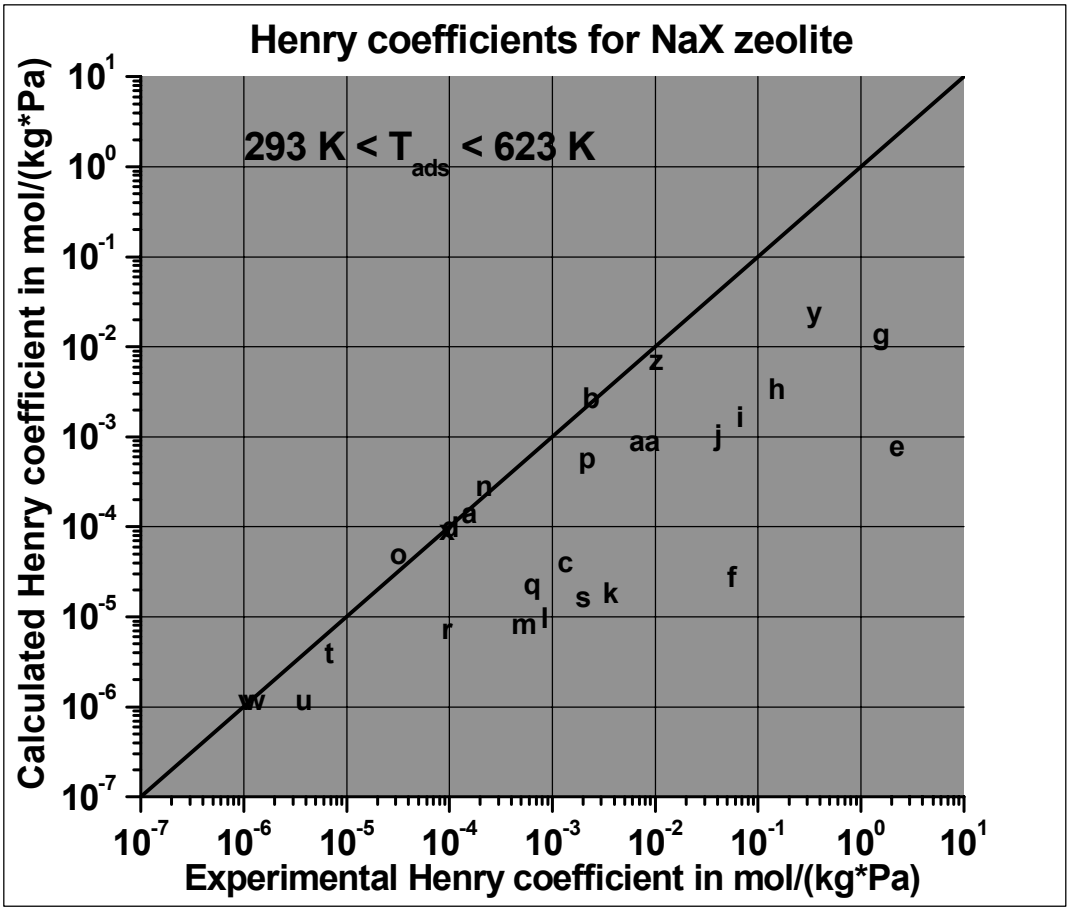

Figure 7.8: Henry coefficients for adsorption of gases on NaX zeolite on basis of induced dipole – induced dipole interactions only (table 7.3).

Table 7.3: Comparison of predicted and experimental Henry coefficients of different gases and vapours on NaX zeolite (figure 7.9).

Gas	Sym-bol	Exp. Henry coefficient in mol/(kg*Pa)	Calc. Henry coefficient in mol/(kg*Pa)	Adsorption temperature in K	S_{BET} in m^2/kg	Deviation in % $\left(\frac{He_{exp.} - He_{calc.}}{He_{exp.}}\right)$
C_2H_6	a	1.55E-04	3.10E-04	293	560000	-100
C_3H_8	b	2.37E-03	7.42E-03	293	560000	-213
C_2H_4	c	1.33E-03	3.10E-04	305,6	560000	76
C_2H_6	d	1.01E-04	2.09E-04	303,6	560000	-105
CH_3OH	e	2.25E+00	1.33E+00	323	591000	41
NH_3	f	5.57E-02	7.27E-02	298,2	462000	-31

$C_{10}H_8$	g	1.56E+00	0.69E+00	523	560000	56
$C_{10}H_8$	h	1.50E-01	9.80E-02	573	560000	35
$C_{10}H_8$	i	6.67E-02	3.59E-02	603	560000	46
$C_{10}H_8$	j	4.10E-02	1.96E-02	623	560000	52
CO_2	k	3.70E-03	6.96E-04	298,2	525000	81
CO_2	l	8.49E-04	2.15E-04	323,2	525000	75
CO_2	m	5.23E-04	1.53E-04	333	560000	70
C_2H_6	n	2.16E-04	6.65E-04	273,2	525000	-207
C_2H_6	o	3.17E-05	1.01E-04	323,2	525000	-217
C_2H_4	p	2.17E-03	5.15E-03	298,2	525000	-134
C_2H_4	q	6.31E-04	1.46E-04	323,2	525000	77
C_2H_4	r	9.30E-05	3.07E-05	373,2	525000	67
CO_2	s	1.98E-03	5.37E-04	304,6	560000	73
CH_4	t	6.78E-06	8.01E-06	304,5	560000	-18
N_2	u	3.80E-06	1.88E-06	305,7	560000	51
O_2	v	1.05E-06	1.60E-06	306,5	560000	-52
Ar	w	1.27E-06	1.55E-06	304,2	560000	-22
C_2H_6	x	9.46E-05	1.94E-04	305,6	560000	-105
i-C_4H_{10}	y	3.45E-01	8.86E-02	298,2	560000	74
i-C_4H_{10}	z	1.02E-02	2.28E-02	323,2	560000	-124
C_3H_6	aa	7.88E-03	5.29E-03	303	560000	33

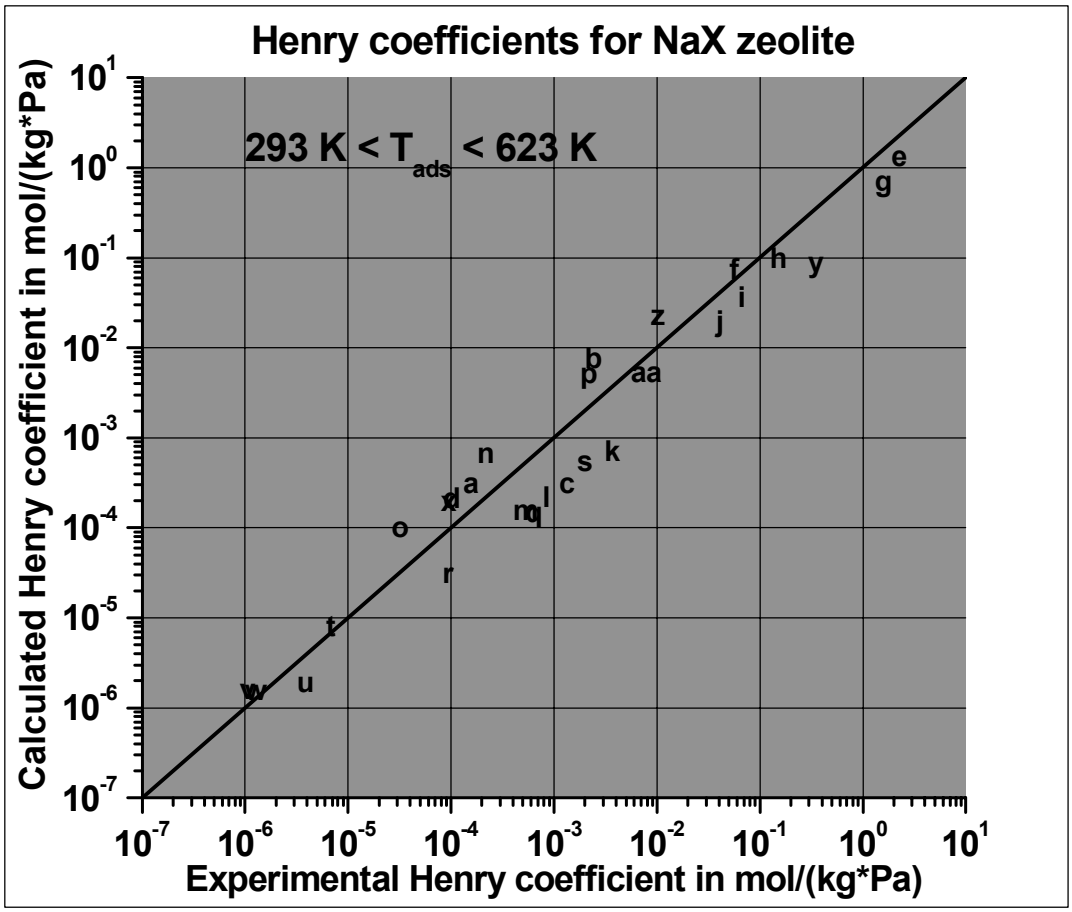

Figure 7.9: Henry coefficients for adsorption of gases on NaX zeolite (table 7.3).

7.2.2. Isotherm predictions

In Chapter 6 a new model was introduced to calculate the whole adsorption isotherm from the linear region until saturation. In this Section the model will be verified based on literature and experimental data. *Henry* coefficients of the model are calculated as shown in Chapter 6 and verified in Section 7.2.1. The saturation data which is the second main boundary condition is tabulated in tables in addition to the graphic presentation.

In figure 7.10 the prediction of isotherms for active carbon coal is shown. Active carbon coal is an energetic homogeneous adsorbent. In this case the adsorption attraction of arbitrary gases is dominated by the reduced *Hamaker* energy.

Active carbon coal can be modelled very well with the prediction theory of Chapter 6. It it assumed that the parameter C is a constant with C = $0.55*10^{-3}$. This is verified also in Section 7.3.3. The calculated *Henry* coefficients of various types of molecules differ at most 19 % (in the case of carbon dioxide) from the experimental data. Also the saturation region is modelled very well. It seems that the new model can cover any arbitrary gas if adsorbed on energetic homogenous adsorbents like active carbon.

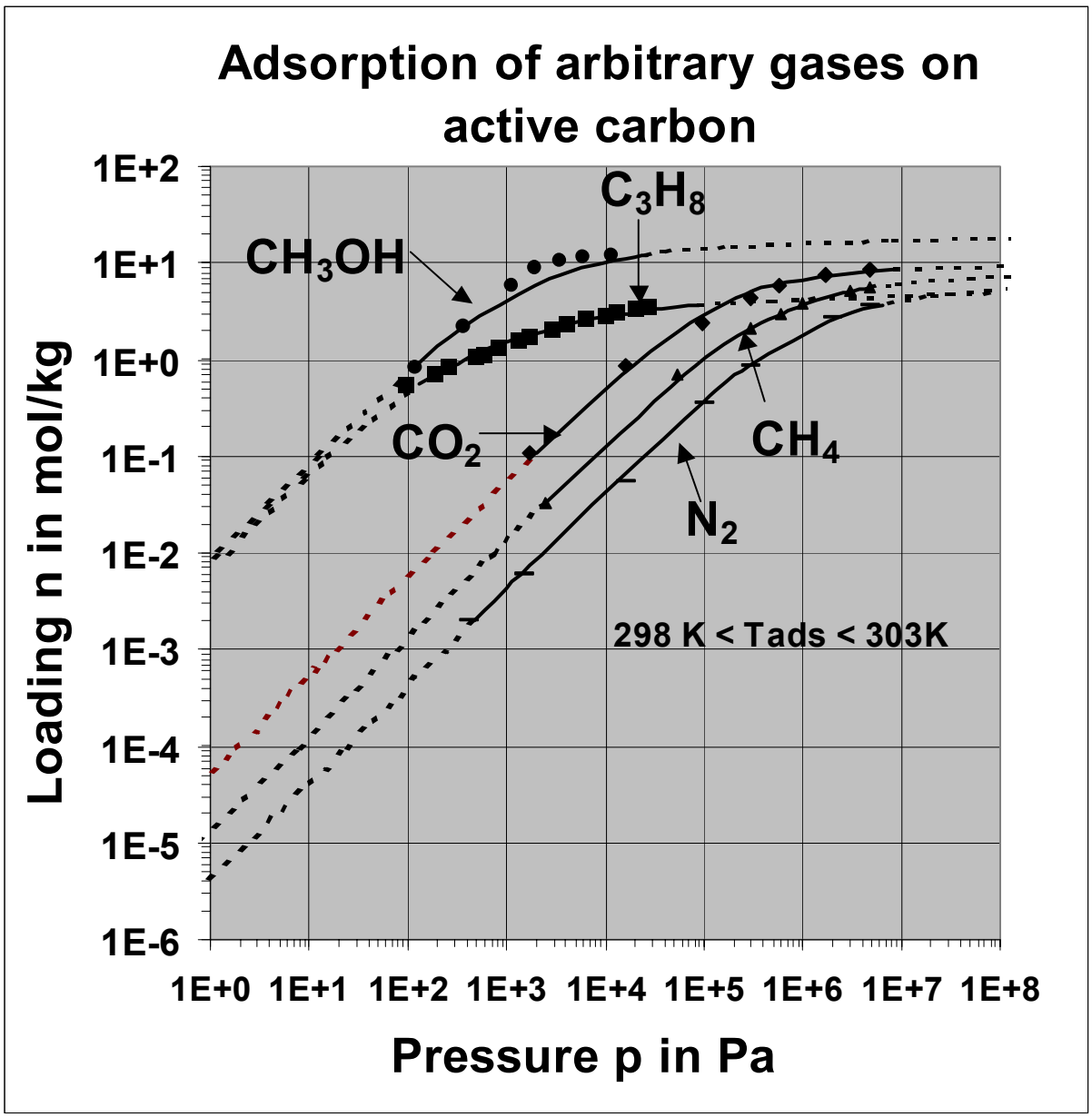

Figure 7.10: Experimental and predicted adsorption isotherms of active carbon coal. Experimental data are for nitrogen (303.15 K, –), methane (303.15 K, ▲), carbon dioxide (303.15 K, ♦), propane (298 K, ■) and methanol (298.15 K, •), –, -- calculated.

Table 7.4: Properties of adsorptives and adsorbents in figure 7.10.

Adsorptive and cited literature	He_{exp} in mol/(kg*Pa)	He_{calc} in mol/(kg*Pa)	T_{ads} in K	S_{BET} in m^2/kg	v_{micro} in m3/kg	$\frac{S_{BET}\,\sigma_j}{v_{micro}}$	$\frac{N_A \cdot \sigma_i^3}{\beta(300K)}$
Nitrogen [37]	4.12E-6	4.25E-6	303	1105000	4.0E-4 [120]	0.967	0.28
Methane [37]	1.33E-5	1.32E-5	303	1105000	4.0E-4 [120]	0.967	0.40
Carbon dioxide [37]	6.78E-5	5.47E-5	303	1105000	4.0E-4 [120]	0.967	0.48
Propane [124]	3.35E-2	6.99E-3	298	1200000	4.5E-4 [125]	0.933	0.52
Methanol [119]	8.04E-3	8.35E-3	298	1440000	6.5E-4 [121]	0.775	0.85

In order to test the validity and the accuracy of the new model adsorption isotherms over the entire range from the Henry region up to saturation have been calculated for special adsorptives on zeolites.

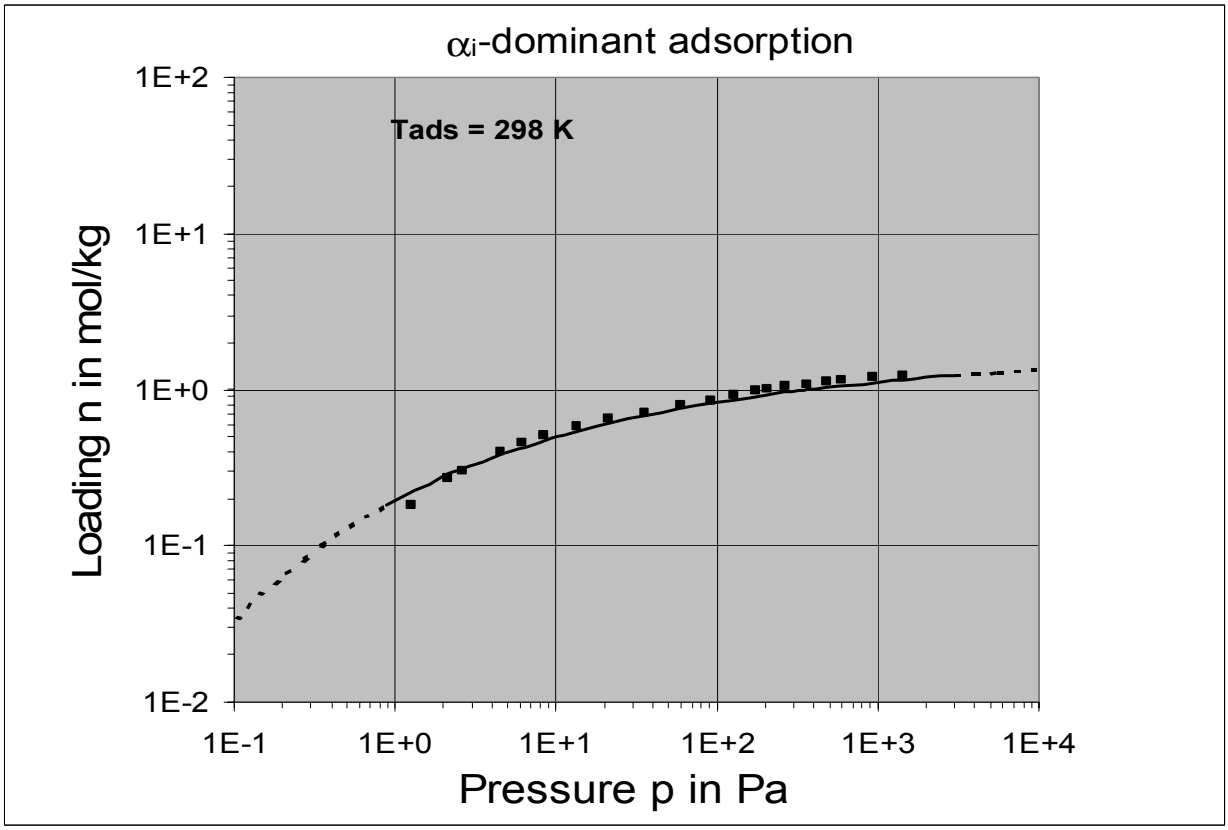

Figure 7.11: Adsorption of n-hexane on silicalite-1 at 298 K [126]. –, -- calculated.

Figure 7.11 shows an α_i-dominant adsorption case of n-hexane on silicalite-1 [126]. n-hexane possesses a high polarisability but zero polarities. Silicalite-1 has no cations in its structure, therefore it has no charge involved interactions, The example shows that the α_i-dominant adsorption case is covered very well by the model.

An additional approach for *Hamaker*-dominant systems will be presented here. In figure 7.12 the dimensionless loading n/(He*p) is plotted versus a dimensionless term which contains the loading n, the saturation loading n_∞, the critical data p_c and T_c of the adsorptive and the *Hamaker* energy Ha_j. The diagram is valid for *Hamaker*-dominant systems (for instance activated carbon as adsorbent). The plot is similar to the diagram published in [27] as figure 3.22. However, in the figure of [27] the expression of (He*p)/n is plotted versus an abscissa expression with the number of molecule layers $N = \frac{N_A \sigma_i^2}{S_{BET}} n$. In figure 7.12 the term $\left(1 - n/n_\infty\right)$ can be interpreted as the fraction of the micropore volume not occupied by the adsorbate yet. Furthermore, the expression is powered by the exponent 2/3 in order to obtain the *Hamaker* energy Ha_j with the exponent one instead of 3/2 [27]. The straight line in figure 7.12 is supported by experimental results of N_2, CH_4, C_3H_8, C_3H_6, C_6H_{14} and ethylacetate adsorbed on activated carbon in the temperature range between 25°C and 93°C and delivers the relationship

$$\ln\left(\frac{n}{He\,p}\right) = \left\{-\left[-4.36\cdot 10^{-4}\left(\frac{Ha_j}{\sigma_j^3 p_C}\right)^{3/2} \frac{T_C}{T_{ads}} \ln\left(1-\frac{n}{n_\infty}\right)\right]^{2/3}\right\} \qquad (7.1)$$

As can be seen the adsorption isotherm for T_{ads} depends on

- the *Henry* coefficient He,
- the saturation loading n_∞ and on
- the physical properties of the adsorptive and the adsorbent.

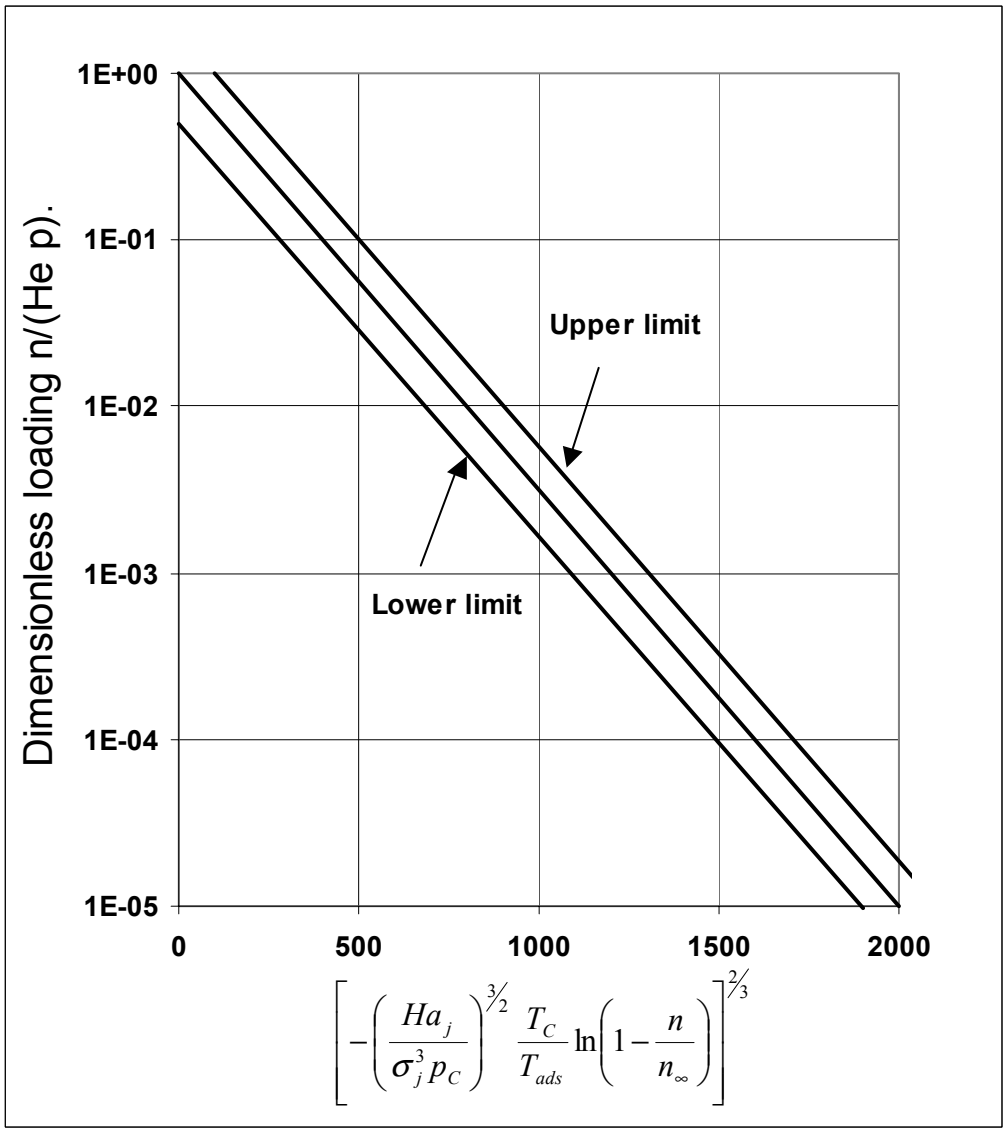

Figure 7.12: The dimensionless group $\frac{n}{He\,p}$ is plotted against the dimensionless group $\left[-\left(\frac{Ha_j}{\sigma_j^3 p_C}\right)^{3/2}\frac{T_C}{T_{ads}}\ln\left(1-\frac{n}{n_\infty}\right)\right]^{2/3}$.

According to *Mersmann et.al.* [27] the Henry coefficient He can be approximated by

$$He \approx \frac{\sigma_{i,j} S_{BET}}{\Re T_{ads}} \exp\left(0.4\frac{T_C}{T_{ads}}\left(\frac{Ha_j}{\sigma_j^3 p_C}\right)^{1/2}\right) \qquad (7.2)$$

In this equation the diameter $\sigma_{i,j}$ and the BET surface are additional parameters. A combination of the two equations (7.1) and (7.2) results in

$$\frac{n}{p} \approx \frac{\sigma_{i,j} S_{BET}}{\Re T_{ads}} \frac{\exp\left(0.4 \frac{T_C}{T_{ads}} \left(\frac{Ha_j}{\sigma_j^3 p_C} \right)^{1/2} \right)}{\exp\left\{ -\left[-4.36 \cdot 10^{-4} \left(\frac{Ha_j}{\sigma_j^3 p_C} \right)^{3/2} \frac{T_C}{T_{ads}} \ln\left(1 - \frac{n}{n_\infty} \right) \right]^{2/3} \right\}} \qquad (7.3)$$

In figure 7.12 most of the experimental data are located in between the upper and lower line. With respect to the accuracy of an adsorption isotherm calculated by equation (7.3) the *Hamaker* energy Ha_j plays the biggest role. In order to obtain an accuracy of +- 20 % with respect to the entire isotherm an accuracy of approximate +- 5% of the volumetric *Hamaker* energy $\left(\frac{Ha_j}{\sigma_j^3} \right)$ is necessary. This may explain some deviations between experimental and predicted data.

Figure 7.13 shows the adsorption of other nonpolar adsorptives on zeolites NaX, NaY and MS5A. Table 7.5 lists the properties of the adsorptives and adsorbents in figure 7.13. The new model is very successful also in predicting adsorption isotherms in the case of nonpolar gases and energetic heterogeneous adsorbents. It has to be mentioned that the success of the model depends strongly on reliable data of the *Hamaker* energy, the BET surface and the micropore volume of the adsorbent. In the case of zeolites the micropore volume was taken from *Kast* [24]. The BET surfaces for NaX and NaY in figure 7.13 are average values of literature data. For practical purposes the predicted isotherms are calculated down to the equilibrium pressure 1 Pa. Thus, it is possible to read the Henry coefficient directly from the intercept of the predicted isotherm with the y-axes. For all adsorbents, zeolites and active carbon, the saturation loading seems to be achieved at 10^{+8} Pa.

Table 7.5: Properties of adsorptives and adsorbents in figure 7.13.

Adsorptive and cited literature	He_{exp} in mol/(kg*Pa)	He_{calc} in mol/(kg*Pa)	T_{ads} in K	S_{BET} in m^2/kg	v_{micro} in m3/kg	$\frac{S_{BET}\,\sigma_j}{v_{micro}}$	$\frac{N_A \cdot \sigma_i^3}{\beta(300K)}$
Methane/NaY [115]	3.75E-6	4.42E-6	298	500000	3.0E-4 [24]	0.70	0.40
Methane/NaX [7]	6.78E-6	8.01E-6	304	560000	3.0E-4 [24]	0.72	0.40
Ethane/MS5A [36]	1.18E-4	1.09E-4	313	727000	2.5E-4 [24]	1.1	0.48
Propane/MS5A [36]	1.95E-3	1.40E-3	313	727000	2.5E-4 [24]	1.1	0.52

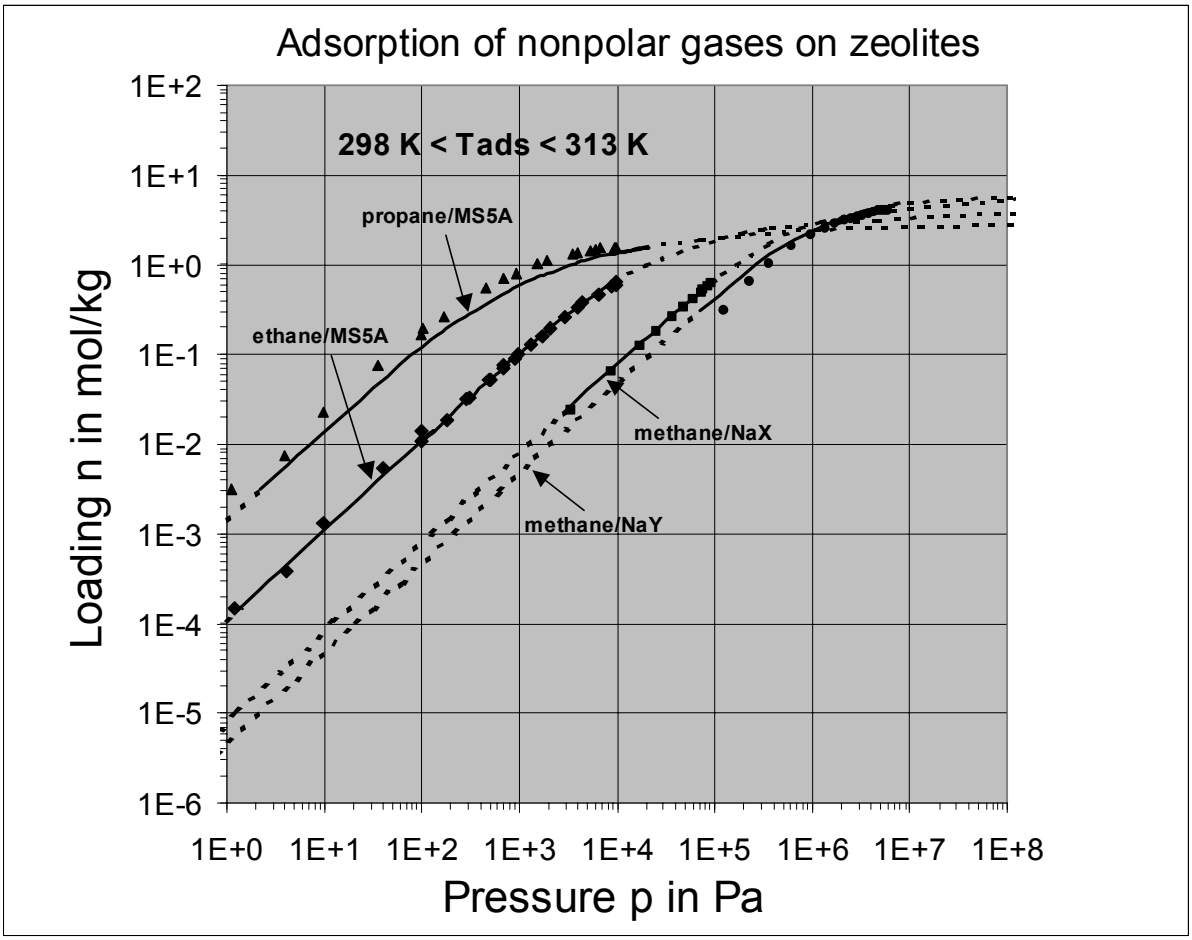

Figure 7.13: Experimental and predicted adsorption isotherms of zeolites. Experimental data are for methane/NaY (298 K, •), methane/NaX (304.5 K, ■), ethane/MS5A (313 K, ♦) and propane/MS5A (313 K, ▲). –, -- calculated.

Methanol and ammonia are adsorptives with high dipole moments but rather small polarisabilities. Furthermore the quadrupol moment of ammonia is very high. Especially methanol is an adsorptive which offers the possibility to test the validity of the equations (3) and (4) of figure 5.5. Figure 7.14 shows the adsorption of methanol and ammonia [18] on the zeolites NaY and NaX, respectively.

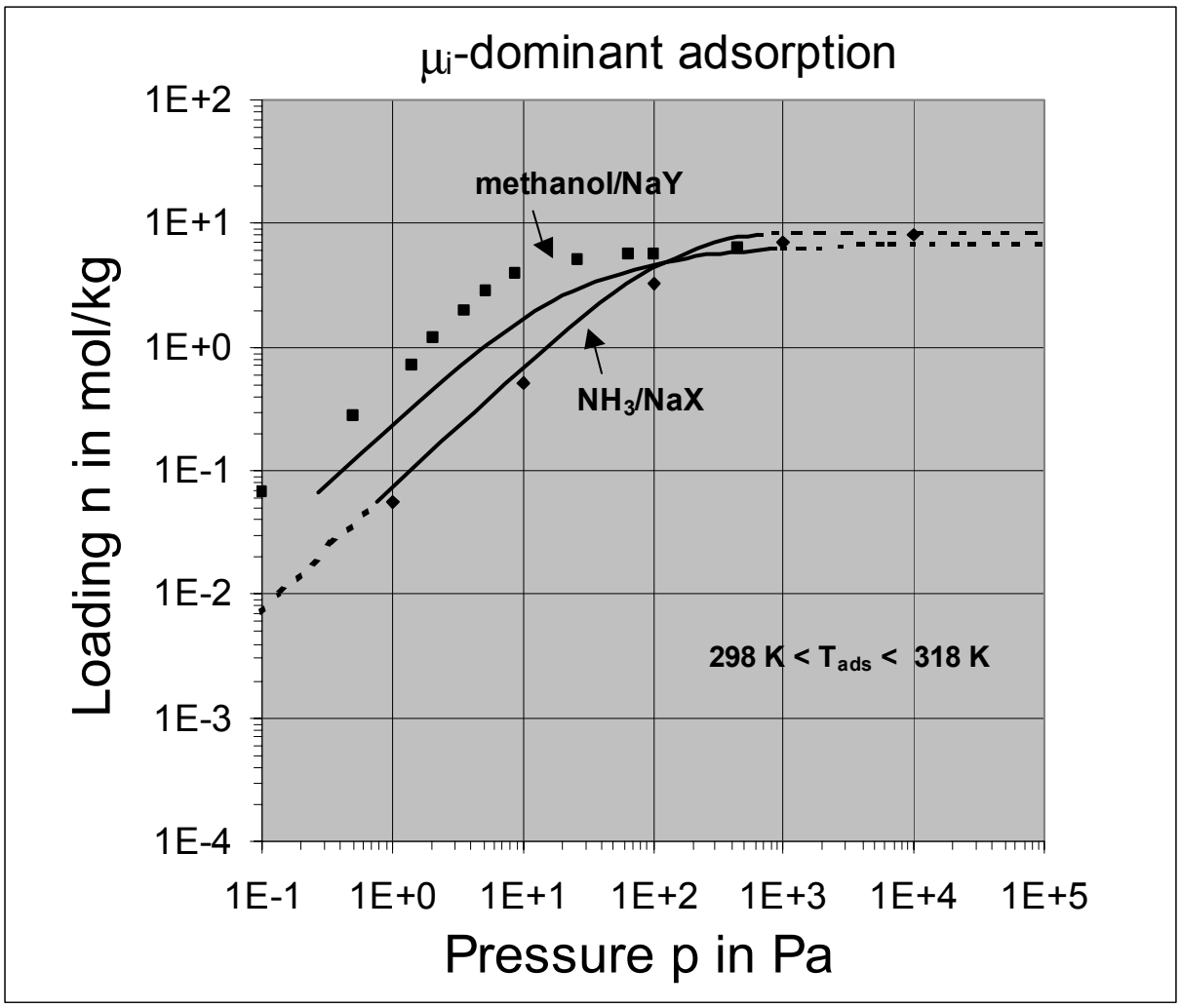

Figure 7.14: Adsorption of methanol on NaY (318 K, ■) and ammonia on NaX (298 K, ♦). –, -- calculated.

The adsorptives ethene and carbon dioxide are characterised by large quadrupole moments but zero (ethene) or moderate (carbon dioxide) dipole moments and rather moderate polarisabilites. Calculated adsorption isotherms of these adsorptives can be used for testing the validity and accuracy of equations (5) and (6) in figure 5.5. Figure 7.15 shows the adsorption of ethene on MS5A [27] at 303 K and the adsorption of carbon dioxide on NaY [117] at 305 K.

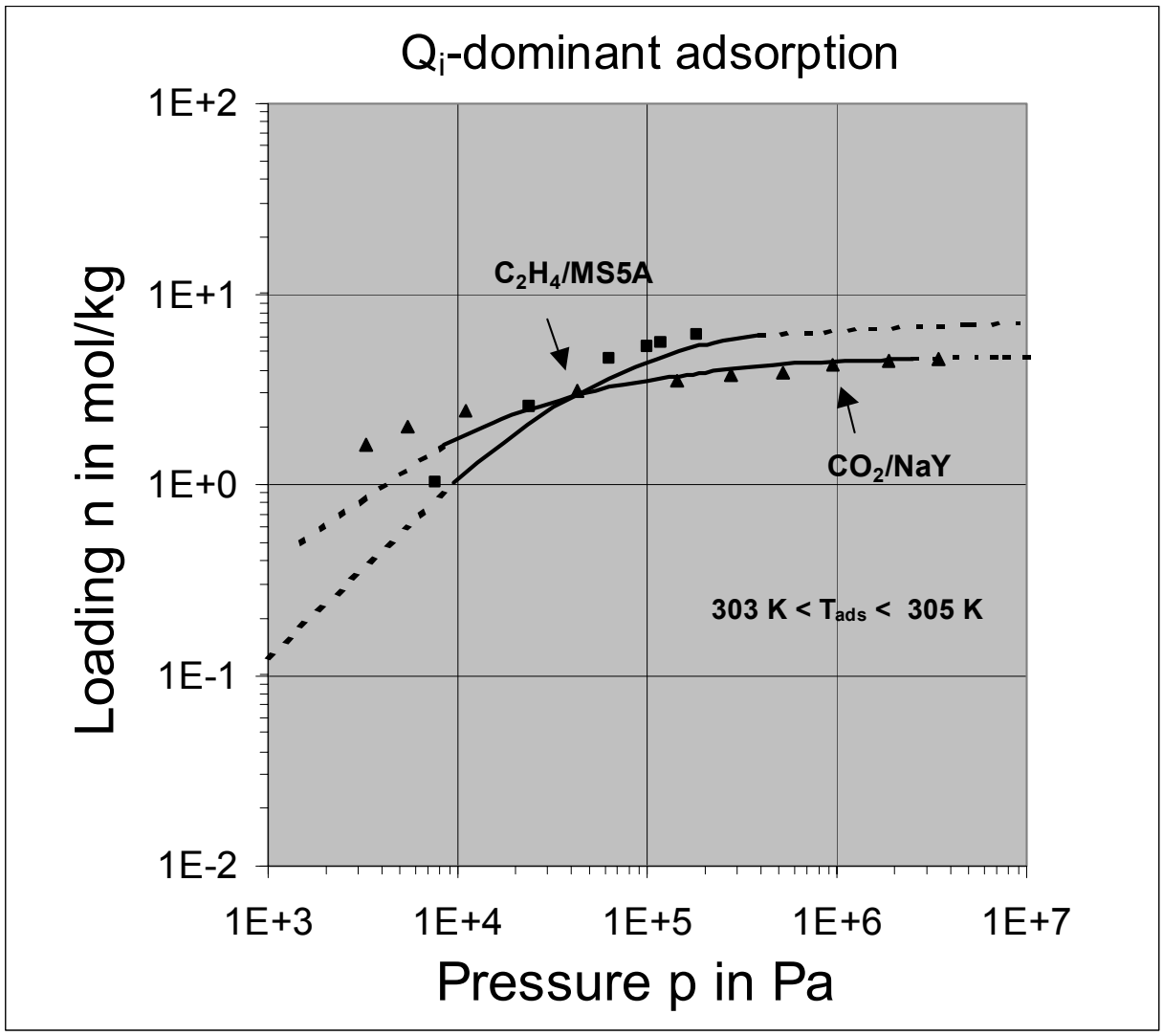

Figure 7.15: Adsorption of ethene on MS5A [27] at 303 K and the adsorption of carbon dioxide on NaY [117] at 305 K. –, -- calculated.

As overall case figure 7.16 and table 7.6 show the adsorption of any polar gases on energetic heterogeneous adsorbents.

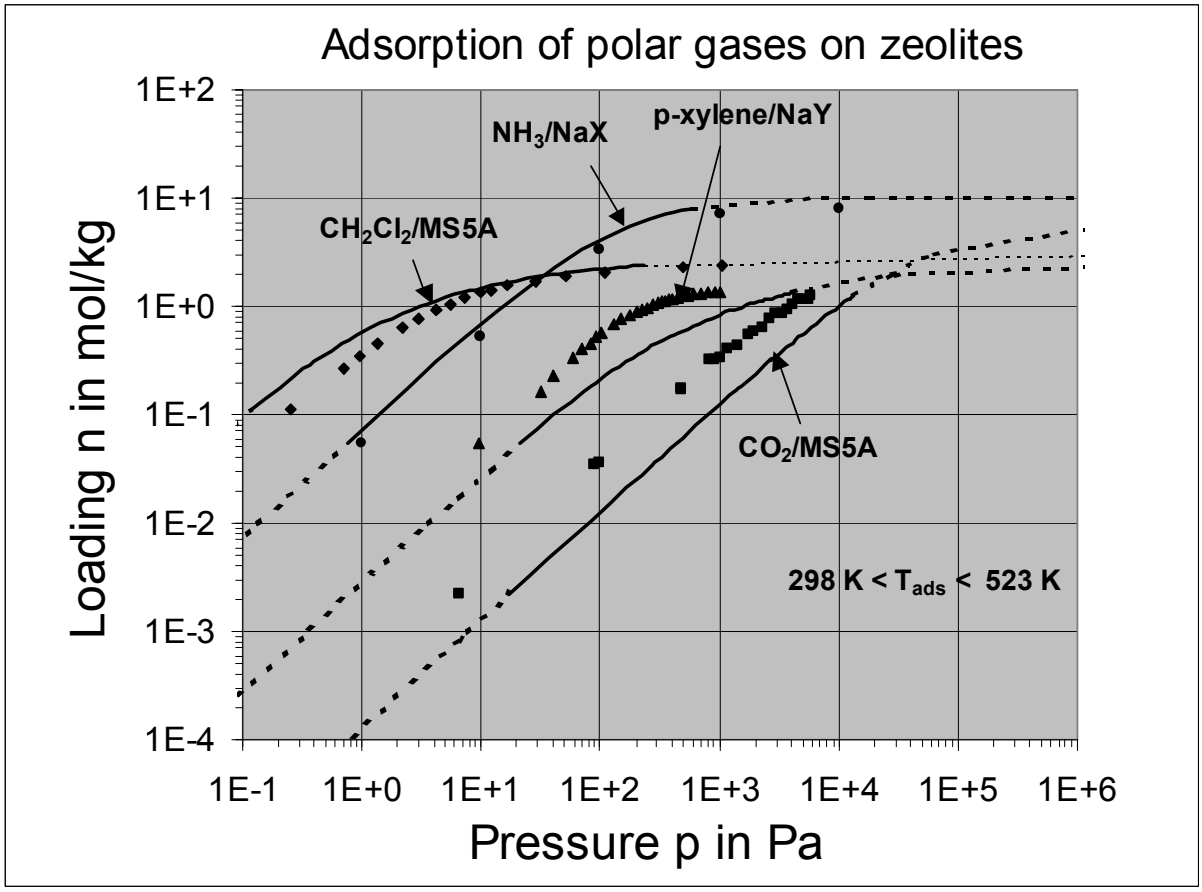

Figure 7.16: Experimental and predicted adsorption isotherms of zeolites. Experimental data are for CO_2/MS5A (343 K, ■), NH_3/NaX (298 K, •), p-xylene/NaY (523K, 7) and CH_2Cl_2/MS5A (319.35 K, ♦). –, -- calculated.

Table 7.6: Properties of adsorptives and adsorbents in figure 7.16.

Adsorptive and cited literature	He_{exp} in mol/(kg*Pa)	He_{calc} in mol/(kg*Pa)	T_{ads} in K	S_{BET} in m^2/kg	v_{micro} in m3/kg	$\frac{S_{BET}\,\sigma_j}{v_{micro}}$	$\frac{N_A \cdot \sigma_i^3}{\beta(300K)}$
CO_2/MS5A [36]	3.93E-4	2.17E-4	343.0	727000	2.5E-4 [24]	1.1	0.48
NH_3/NaX [18]	5.57E-2	7.27E-3	298	462000	3.0E-4 [24]	0.59	0.6
CH_2Cl_2/MS5A [own]	6.14E-1	1.06E-0	319.4	464000	2.3E-4	0.77	0.58
p-xylene/NaY	8.93E-3	2.78E-3	523	500000	see text		

The isotherms of figure 7.16 show a highly polar adsorptive (dichlormethane) with a dipole moment of 1.6 debye and three molecules with high polarisabilities and high quadrupole moments (NH_3, p-xylene and CO2). In the case of p-xylene the saturation loading was calculated with the adsorbate density as given in the literature, $1.08*10^{+3}$ kg/m^3 [116] and with equation 6.4.

All the predicted isotherms fit the experimental data very well in the Henry region and the saturation region. By the different systems it is verified that the new model can predict the adsorption of any kind of gas, polar or unpolar, on any kind of microporous adsorbent, energetic homogeneous or heterogeneous. However, in the figure 7.14 the system methanol/NaY show higher loadings than calculated in the transition range.

In the next Sections the parameters of the new model will be verified.

7.3. Model verifications

7.3.1. Refractive index verification

The refractive index is an important parameter for calculating the *Hamaker* constant of microporous solids like zeolites. In this work the *Clausius-Mosotti* relation was used to calculate this parameter. In Chapter 3 additional ways were introduced for calculating the refractive index that should be reviewed in comparison to the used method.

As can be seen in equation (3.34) and also as explained in Chapter 3 the *Clausius-Mosotti* formula describes a border case of the general formula of *Marler*. In this case the electrical fields of the solid ions do not overlap each other. The other case is described by the formula of *Newton-Drude*. Here, the overlapping field compensates the *Lorentz* field exactly. All other cases are between these two border cases, which can be described by the parameter b. So the refractive index can be rewritten as a function of b and the solid parameters.

By introducing a dimensionless solid parameter P^* with

$$P^* = \frac{\alpha_{solid}\, N_A\, \rho_{solid}}{\varepsilon_0\, M_{solid}} = \frac{3\, R_m\, \rho_{solid}}{M_{solid}} \tag{7.4}$$

the refractive index is

$$n = \sqrt{\frac{1 + P^* - \frac{b\, P^*}{4\pi}}{1 - \frac{b\, P^*}{4\pi}}} \tag{7.5}$$

The two border cases are for *Marler* with b = 0

$$n_{Marler} = \sqrt{1 + P^*} \tag{7.6}$$

and for *Clausius-Mosotti* with $b = \frac{4\pi}{3}$ (7.7)

$$n = \sqrt{\frac{1 + \frac{2\, P^*}{3}}{1 - \frac{P^*}{3}}} \tag{7.8}$$

For MS5A the solid parameter P^* is equal to $9{,}83 * 10^{-1}$ with the assumptions made in Chapter 3 and in table 7.7.

Table 7.7: Solid parameters of zeolite MS5A.

Parameter	Value
Chemical Structure	$Ca_5Na_2((AlO_2)_{12}(SiO_2)_{12})$
Molar refraction R_m in m^3/mol regarding to chemical structure	$4.79*10^{-4}$
Apparent density ρ_{solid} in kg/ m^3	1150
Molar mass M_{solid} in kg/mol regarding to chemical structure	1.68
Parameter P^*	0.983

The function of n in dependence of parameter b (equation 7.5) with the two border cases is plotted in figure 7.17 for zeolite MS5A.

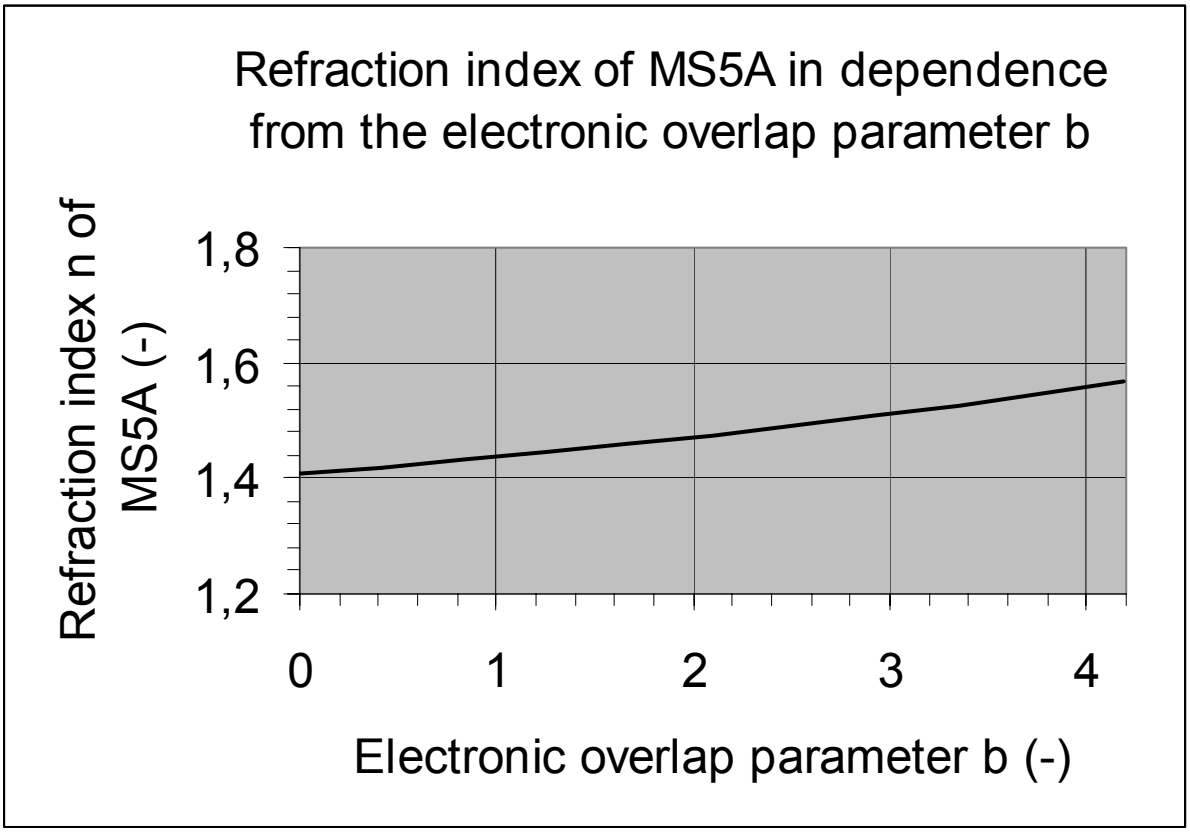

Figure 7.17: Refractive index of MS5A in dependence on the electronic overlap parameter b.

The two border cases result in a refractive index n_{min} = 1,41 and n_{max} = 1,57. Following the equations in Chapter 3 the dependence of the *Hamaker* constant Ha on the refractive index n is described by

$$\alpha_{solid} \sim \frac{n^2 - 1}{n^2 + 2} \quad \text{and} \quad \nu_0 \sim \frac{1}{\sqrt{\alpha}} \quad \text{and} \quad Ha \sim \beta \sim \nu_0 \, \alpha^2 \tag{7.9a}$$

Therefore, it follows that

$$Ha \sim \left(\frac{n^2 - 1}{n^2 + 2} \right)^{1,5} \tag{7.9b}$$

The two border cases lead to a difference of ca. 35 % of the numerical value of the Hamaker constant of MS5A. The maximum value in this work, $Ha_{MS5A,max}$ = 7.66*10^{-20} J, is calculated with *Clausius-Mosotti* whereas the minimum value is $Ha_{MS5A,min}$ = 5.0*10^{-20} J.

The *Henry* coefficient depends on the *Hamaker* constant. For further calculations propane adsorption on MS5A is taken as example. The parameters for this case are T_c = 369.8 K, T_{ads} = 343 K, p_c = 4.25*10^6 Pa and σ_{MS5A} = 3.8*10^{-10} m. It follows with

$$IP_{\min/\max} = \frac{T_c}{T_{ads}} \sqrt{\frac{2\,Ha_{\min/\max}}{\pi \sigma_j^3 \, p_c}} \tag{7.10}$$

and

$$He \sim IL \tag{7.11}$$

the percentage difference of the *Henry* coefficient with

$$\Delta He(\%) = \frac{IL_{\max} - IL_{\min}}{IL_{\min}} \cdot 100\% = \frac{\exp\left(p_1 \, IP_{\max}^{p_2}\right) - \exp\left(p_1 \, IP_{\min}^{p_2}\right)}{\exp\left(p_1 \, IP_{\min}^{p_2}\right)} \cdot 100\% \tag{7.12}$$

For the given example the percentage difference is ca. 550 %.

The discussion in the previous section has shown that the theoretical and experimental Henry coefficients differ much less. So it seems that the *Clausius-Mosotti* formula is the right choice for calculating the refractive index and also the Hamaker constant. Another reason is that the *Clausius-Mosotti* formula is described as standard equation in widely accepted literature [6].

7.3.2. Dependency on the saturation degree

In Chapter 6 the parameter C in equation (6.3) was assumed to be constant in a first approximation. In this Section a linear dependency of C on the saturation degree n_S^* is discussed with

$$C = a\frac{n}{n_\infty} + b \tag{7.13}$$

Approximating C between the border values $0.6*10^{-3}$ and $0.5*10^{-3}$ for saturation degrees 0 and 1, respectively, the parameters of equation (7.13) are equal to a = $-0.1*10^{-3}$, b = $0.6*10^{-3}$. The differential equation (6.3) turns then to

$$\frac{d(\ln n)}{d(\ln p)} = \frac{dn}{dp}\frac{p}{n} = \frac{1}{1+\left(a\frac{n}{n_\infty}+b\right)\frac{T_c}{T_{ads}}\left(\frac{Ha_j}{\sigma_j^3 p_c}\right)^{3/2}\left(\frac{n/n_\infty}{1-n/n_\infty}\right)} \tag{7.14}$$

Equation (7.14) can be rewritten with the term B' defined by

$$B' = \frac{T_c}{T_{ads}}\left(\frac{Ha_j}{\sigma_j^3 p_c}\right)^{3/2} \tag{7.15}$$

into

$$d(\ln n)\left(1+B'\left(\frac{n/n_\infty}{1-n/n_\infty}\right)\left(a\frac{n}{n_\infty}+b\right)\right)=d(\ln p) \qquad \text{or} \qquad (7.16)$$

$$\ln n+\int B'\left(\frac{n/n_\infty}{1-n/n_\infty}\right)\left(a\frac{n}{n_\infty}+b\right)\frac{dn}{n}=\ln p+\ln He \qquad (7.17)$$

This can be reduced to

$$\ln\left(\frac{pHe}{n}\right)=\int B'\left(\frac{a\frac{n}{n_\infty^2}+\frac{b}{n_\infty}}{1-n/n_\infty}\right)dn \qquad (7.18)$$

Integration of the right hand side of equation (7.18) leads to

$$\ln\left(\frac{p\,He}{n}\right)=B'\left(a\left(-\frac{n}{n_\infty}-\ln\left(1-\frac{n}{n_\infty}\right)\right)+b\left(-\ln\left(1-\frac{n}{n_\infty}\right)\right)\right) \qquad (7.19)$$

or

$$\ln\left(\frac{p\,He}{n}\right)=-B'(a+b)\ln\left(1-\frac{n}{n_\infty}\right)-B'a\frac{n}{n_\infty} \qquad (7.20)$$

or

$$\ln\left(\frac{p\,He}{n}\left(1-\frac{n}{n_\infty}\right)^{B'(a+b)}\right)=-B'a\frac{n}{n_\infty} \qquad (7.21)$$

It is therefore

$$p = \frac{n}{He} \frac{1}{\left(1 - \frac{n}{n_\infty}\right)^{B'(a+b)}} \exp\left(-B'a\frac{n}{n_\infty}\right) \tag{7.22}$$

or in dependence on the saturation degree $n_s^* = \frac{n}{n_\infty}$ it follows that

$$p = \frac{n}{He} \frac{1}{\left(1 - n_S^*\right)^{B'(a+b)}} \exp\left(-B'an_S^*\right) \tag{7.23}$$

This modified model is verified on the adsorption example carbon dioxide on active carbon, the same example as in figure 7.10. The result is shown in figure 7.18. As can be seen in figure 7.18 there is no significant difference between the two cases. So it is assumed that the parameter C in equation (6.3) is a constant being independent on the saturation degree.

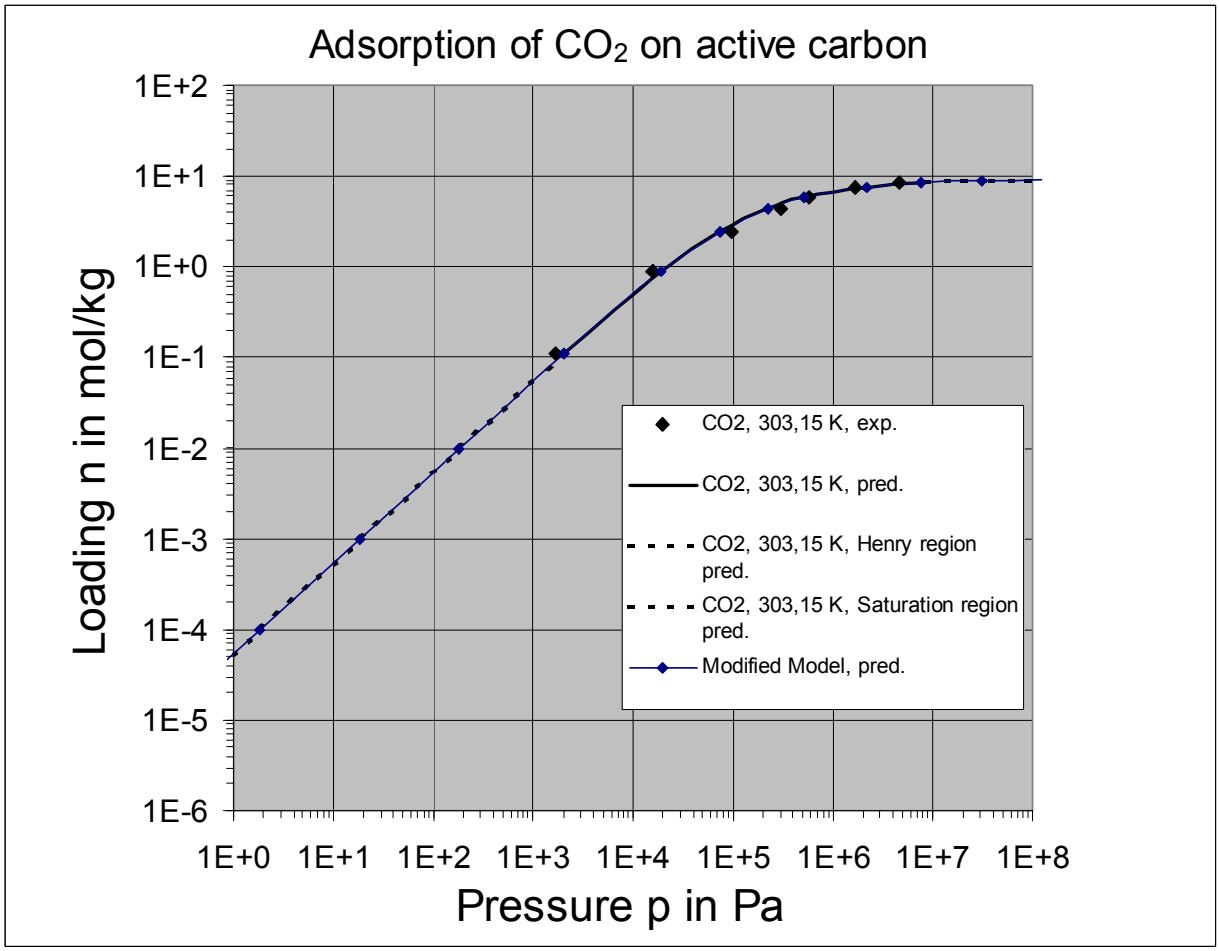

Figure 7.18: Comparison of modified model with the original prediction isotherm.

7.3.3. The *London* potential

In Chapter 5 the assumption was made that the induced dipole – induced dipole interaction energy can be derived from the *London* potential also. In [24] the London potential for two dissimilar atoms is calculated by

$$E_L(r) = -\frac{3}{2}\frac{\alpha_i \alpha_j}{(4\pi\varepsilon_0)^2 r^6}\frac{h\nu_i\nu_j}{(\nu_i+\nu_j)} \qquad (7.24)$$

where α_i is the polarisability of the gas molecule in (C^2*m^2)/J and α_j the polarisability of the solid molecule. It can be replaced by $\overline{\alpha}_{solid}$, the mean average polarisability of the solid continuum molecule calculated by equation (3.97). ν_j is assumed to be the

frequency of the solid electrons in the ground state in 1/s and can be calculated by (3.98). Furthermore it is defined that

$$I_i = h\nu_i \tag{7.25}$$

where I_i is the ionisation energy of the adsorptive molecule in J. It is tabulated in literature [6]. Inserted in equation (7.24) it is

$$E_L(r) = -\frac{3}{2}\frac{\alpha_i \overline{\alpha}_{solid}}{(4\pi\varepsilon_0)^2 r^6}\frac{I_i \nu_0}{\left(\frac{I_i}{h}+\nu_0\right)} \tag{7.26}$$

With the general interaction energy as calculated in equation (5.40) the induced dipole – induced dipole potential is

$$\Phi_{indind}(z) = \int_{z+\sigma_{ij}}^{\infty} E_L(r)\rho_{j,at} 4\pi r^2 dr \tag{7.27}$$

or

$$\frac{\Phi_{indind}(x)}{kT_{ads}} = -\rho_{j,at}\frac{\alpha_i \overline{\alpha}_{solid} I_i \nu_0}{8\cdot\pi\varepsilon_0^2 kT_{ads}\left(\frac{I_i}{h}+\nu_0\right)}\frac{1}{\sigma_{i,j}^3}\frac{1}{(1+x)^3} \tag{7.28}$$

It can be defined an alternative interaction parameter for the induced dipole – induced dipole interaction:

$$A_{indind} = -\rho_{j,at}\frac{\alpha_i \overline{\alpha}_{solid} I_i \nu_0}{8\cdot\pi\varepsilon_0^2 kT_{ads}\left(\frac{I_i}{h}+\nu_0\right)}\frac{1}{\sigma_{i,j}^3} \tag{7.29}$$

In table 7.8 the values for A_{indind} calculated by equations (5.62) and (7.29) are compared for the case of adsorption of gases on zeolite MS5A.

Table 7.8: Interaction parameter A_{indind} calculated with the two equations (5.62) and (7.29)

Molecule	Ionisation energy I_i in 10^{-18}J	T_{ads} in K	A_{indind} with equation (5.62)	A_{indind} with equation (7.29)
N_2	2.5	303	3.8	3.7
CO	2.25	303	5.2	4.0
NO	1.48	383	4.1	2.7
CH_4	2.02	343	5.8	4.5
O_2	1.93	293	5.3	3.5
Xe	1.94	195	13.7	10.8
Kr	2.24	195	10.2	7.9
C_2H_4	1.68	303	9.3	6.5
CHF_3	2.22	303	10.0	5.8
NH_3	1.62	298	9.0	5.4

The values are very similar. The assumption in Chapter 5 is proved now. In this work equation (5.62) was taken to be consistent with the literature [26, 27].

7.3.4. Potential energy comparison and formula overview

The introduced model according to equations (5.61) and (6.3) is a theoretical basis for predicting isotherms of gases on microporous solids. It is derived from the potential energies which are attractive between the adsorptive and the adsorbent. In this section the main formulae of the different cases will be tabulated for engineering purposes.

As example for the acting different attraction energies the adsorption between methanol and NaY zeolite will be examined quantitatively. Between molecules of this adsorption pair all kinds of potential energy can exist. Therefore, it is ideal for the comparison of the adsorption forces. As discussed in Chapter 5 the *Henry* coefficient of polar gases with energetic heterogeneous microporous solids is described by the integral equation (5.61). For comparing the energies of attraction the percentage of

the energies is calculated when the adsorptive is attached on the solid surface, in other words the distance z between adsorptive and adsorbent is equal to 0. Table 7.9a gives a detailed overview of the situation. With an adsorption temperature of T_{ads} = 318.4 K, the energy unit is k*T_{ads} = 4.395E^{-21} J. The other parameters are: σ_j = $4.2 \cdot 10^{-10}$ m, He = 0.671·mol/(kg·Pa), S_{BET} = 655400 m^2/kg, μ_i = $5.67 \cdot 10^{-30}$ C·m, α_i = $3.66 \cdot 10^{-40}$ $C^2 \cdot m^2/J$, Q_i = $4.34 \cdot 10^{-40}$ $C \cdot m^2$, T_c = 512.6 K, p_c = 8090000 Pa, s = 2.4, $s_{cations}$ = 0.09, $\left(\frac{Al}{Si}\right)_{NaY} = 0.41$, $\rho_{j,at} = 3.3 \cdot 10^{28}$ 1/m^3, Ha_j = $8.4 \cdot 10^{-20}$ J and α_j = $2.82 \cdot 10^{-40}$ $C^2 \cdot m^2/J$.

In the case of methanol adsorption on NaY at 318.4 K there are two potentials, which contribute 97 % of the overall attraction energy, respectively the induced dipole – induced dipole and the permanent dipole – charge interactions. From the other four the two quadrupole interactions only make up 0.42 % of the overall potential. A second calculation for CO_2 on NaX at 304.55 K (table 7.9b) shows that the quadrupole - charge interaction contributes approximately 12,3 % of Φ. These two results make it clear that three potentials are eminent for the calculation of *Henry* coefficients: Always the induced dipole – induced dipole interaction indind and dependent from the adsorptive and the adsorbent the permanent dipole – charge interaction dipcha and/or the quadrupole moment – charge interaction quadcha.

The main formulae of this work are collected in table 7.10. These are the refractive index and *Hamaker* constant of zeolites, the Henry coefficient for the adsorption of gases in the case of *Hamaker* dominant attraction energies and also for the case of polar-polar adsorption pairs and finally the new model for predicting the whole adsorption isotherm. The section in which the formula appears in a detailed description is also tabulated.

Table 7.9a: Attraction energies between methanol and NaY at a distance z = 0 of the adsorptive from the adsorbent surface.

Induced dipole – induced dipole interaction (indind)	Induced dipole – charge interaction (indcha)	Permanent dipole – induced dipole interaction (dipind)	Permanent dipole – charge interaction (dipcha)	Quadrupole moment – induced dipole interaction (quadind)	Quadrupole moment – charge interaction (quadcha)
$\left\|\Phi_{indind}(0)\right\| = k \cdot \cdot \frac{3}{4}\sqrt{\frac{2\,Ha_j}{\pi\,\sigma_{j,j}^3\,p_c}}\,T_c$	$\left\|\Phi_{indcha}(0)\right\| = \frac{1}{8} \cdot \cdot \frac{\alpha_i\, s_{cations}{}^2 e^2}{\pi\varepsilon_0^2\varepsilon_r^2} \cdot \cdot \frac{\rho_{j,at}}{f_{indcha}} \frac{1}{\sigma_{i,j}}$	$\left\|\Phi_{dipind}(0)\right\| = = \frac{\mu_i^2\,\overline{\alpha}_j}{12 \cdot \pi\varepsilon_0^2\varepsilon_r^2} \cdot \cdot \frac{\rho_{j,at}}{f_{dipind}} \frac{1}{\sigma_{i,j}}$	$\left\|\Phi_{dipcha}(0)\right\| = \frac{1}{kT_{ads}} \cdot \cdot \frac{\mu_i^2\, s_{cations}{}^2 e^2}{12 \cdot \pi\varepsilon_0^2\varepsilon_r^2} \cdot \cdot \frac{\rho_{j,at}}{f_{dipcha}} \frac{1}{\sigma_{i,j}}$	$\left\|\Phi_{quadind}(0)\right\| = \frac{1}{kT_{ads}} \cdot \cdot \frac{3}{40} \frac{\overline{\alpha}_j Q_i{}^2}{\pi\,\varepsilon_0^2\varepsilon_r^2} \frac{\rho_{j,at}}{f_{quadind}} \cdot \cdot \frac{1}{(\sigma_{i,j})^5}$	$\left\|\Phi_{quadcha}(0)\right\| = \frac{1}{kT_{ads}} \cdot \cdot \frac{s_{cations}{}^2 e^2 Q_i{}^2}{240\pi\varepsilon_0^2\varepsilon_r^2} \frac{\rho_{j,at}}{f_{quadcha}} \cdot \cdot \frac{1}{(\sigma_{i,j})^3}$
$\left\|\Phi_{indind}(0)\right\| = = 6{,}7 \cdot 10^{-20}\,J$	$\left\|\Phi_{indcha}(0)\right\| = = 2.07 \cdot 10^{-21}\,J$	$\left\|\Phi_{dipind}(0)\right\| = = 5.98 \cdot 10^{-22}\,J$	$\left\|\Phi_{dipcha}(0)\right\| = = 2.76 \cdot 10^{-20}\,J$	$\left\|\Phi_{quadind}(0)\right\| = = 2.00 \cdot 10^{-23}\,J$	$\left\|\Phi_{quadcha}(0)\right\| = = 4.10 \cdot 10^{-22}\,J$
$\left\|\Phi_{indind}(0)\right\| = = 15{,}21 \cdot kT_{ads}$	$\left\|\Phi_{indcha}(0)\right\| = = 0.47 \cdot kT_{ads}$	$\left\|\Phi_{dipind}(0)\right\| = = 0.14 \cdot kT_{ads}$	$\left\|\Phi_{dipcha}(0)\right\| = = 6.27 \cdot kT_{ads}$	$\left\|\Phi_{quadind}(0)\right\| = = 0.005 \cdot kT_{ads}$	$\left\|\Phi_{quadcha}(0)\right\| = = 0.1 \cdot kT_{ads}$
$\left\|\Phi_{indind}(0)\right\| \hat{=} = 68.5\% \cdot \left\|\Phi\right\|$	$\left\|\Phi_{indcha}(0)\right\| \hat{=} = 2.1\% \cdot \left\|\Phi\right\|$	$\left\|\Phi_{dipind}(0)\right\| \hat{=} = 0.6 \cdot \% \cdot \left\|\Phi\right\|$	$\left\|\Phi_{dipcha}(0)\right\| \hat{=} \hat{=} 28.3\% \cdot \left\|\Phi\right\|$	$\left\|\Phi_{quadind}(0)\right\| \hat{=} \hat{=} 0.02\% \cdot \left\|\Phi\right\|$	$\left\|\Phi_{quadcha}(0)\right\| \hat{=} \hat{=} 0.4\% \cdot \left\|\Phi\right\|$

Table 7.9b: Attraction energies between CO_2 and MS5A at a distance z = 0 of the adsorptive from the adsorbent surface.

Induced dipole – induced dipole interaction (indind)	Induced dipole – charge interaction (indcha)	Permanent dipole – induced dipole interaction (dipind)	Permanent dipole – charge interaction (dipcha)	Quadrupole moment – induced dipole interaction (quadind)	Quadrupole moment – charge interaction (quadcha)
$\left\|\Phi_{indind}(0)\right\| = k \cdot \cdot \frac{3}{4}\sqrt{\frac{2\,Ha_j}{\pi\,\sigma_{j,j}^3\,p_c}}T_c$	$\left\|\Phi_{indcha}(0)\right\| = \frac{1}{8} \cdot \cdot \frac{\alpha_i s_{cations}{}^2 e^2}{\pi\varepsilon_0^2\varepsilon_r^2} \cdot \cdot \frac{\rho_{j,at}}{f_{indcha}} \frac{1}{\sigma_{i,j}}$	$\left\|\Phi_{dipind}(0)\right\| = = \frac{\mu_i^2 \overline{\alpha}_j}{12 \cdot \pi\varepsilon_0^2\varepsilon_r^2} \cdot \cdot \frac{\rho_{j,at}}{f_{dipind}} \frac{1}{\sigma_{i,j}}$	$\left\|\Phi_{dipcha}(0)\right\| = \frac{1}{kT_{ads}} \cdot \cdot \frac{\mu_i^2 s_{cations}{}^2 e^2}{12 \cdot \pi\varepsilon_0^2\varepsilon_r^2} \cdot \cdot \frac{\rho_{j,at}}{f_{dipcha}} \frac{1}{\sigma_{i,j}}$	$\left\|\Phi_{quadind}(0)\right\| = \frac{1}{kT_{ads}} \cdot \cdot \frac{3}{40} \frac{\overline{\alpha}_j Q_i{}^2}{\pi\,\varepsilon_0^2\varepsilon_r^2} \frac{\rho_{j,at}}{f_{quadind}} \cdot \cdot \frac{1}{(\sigma_{i,j})^5}$	$\left\|\Phi_{quadcha}(0)\right\| = \frac{1}{kT_{ads}} \cdot \cdot \frac{s_{cations}{}^2 e^2 Q_i{}^2}{240\pi\varepsilon_0^2\varepsilon_r^2} \frac{\rho_{j,at}}{f_{quadcha}} \cdot \cdot \frac{1}{(\sigma_{i,j})^3}$
$\left\|\Phi_{indind}(0)\right\| = = 4.67 \cdot 10^{-20} J$	$\left\|\Phi_{indcha}(0)\right\| = = 1.97 \cdot 10^{-21} J$	$\left\|\Phi_{dipind}(0)\right\| = = 1.42 \cdot 10^{-22} J$	$\left\|\Phi_{dipcha}(0)\right\| = = 5.91 \cdot 10^{-21} J$	$\left\|\Phi_{quadind}(0)\right\| = = 4.18 \cdot 10^{-22} J$	$\left\|\Phi_{quadcha}(0)\right\| = = 7.75 \cdot 10^{-21} J$
$\left\|\Phi_{indind}(0)\right\| = = 11{,}11 \cdot kT_{ads}$	$\left\|\Phi_{indcha}(0)\right\| = = 0.47 \cdot kT_{ads}$	$\left\|\Phi_{dipind}(0)\right\| = = 0.03 \cdot kT_{ads}$	$\left\|\Phi_{dipcha}(0)\right\| = = 1.41 \cdot kT_{ads}$	$\left\|\Phi_{quadind}(0)\right\| = = 0.09 \cdot kT_{ads}$	$\left\|\Phi_{quadcha}(0)\right\| = = 1.84 \cdot kT_{ads}$
$\left\|\Phi_{indind}(0)\right\| \hat{=} = 74.3\% \cdot \left\|\Phi\right\|$	$\left\|\Phi_{indcha}(0)\right\| \hat{=} = 3.1\% \cdot \left\|\Phi\right\|$	$\left\|\Phi_{dipind}(0)\right\| \hat{=} = 0.2 \cdot \% \cdot \left\|\Phi\right\|$	$\left\|\Phi_{dipcha}(0)\right\| \hat{=} \hat{=} 9.4\% \cdot \left\|\Phi\right\|$	$\left\|\Phi_{quadind}(0)\right\| \hat{=} \hat{=} 0.7\% \cdot \left\|\Phi\right\|$	$\left\|\Phi_{quadcha}(0)\right\| \hat{=} \hat{=} 12.3\% \cdot \left\|\Phi\right\|$

Table 7.10: Main formulae and cases for the adsorption of gases on microporous solids.

Description of formula	Formula	Section
Clausius-Mosotti relationship	$\frac{N_A \alpha}{3\varepsilon_0} = \frac{M}{\rho}\frac{\varepsilon_r - 1}{\varepsilon_r + 2}$	3.3.5.1
Refractive index n of zeolites	$n = \sqrt{\frac{1 + 2\frac{R_m \rho}{M}}{1 - \frac{R_m \rho}{M}}}$	3.3.5.2
Hamaker constant Ha_j of solids	$Ha_j = \pi^2 \rho_{\mathrm{j,at}}{}^2 \, \overline{\beta}$, $\rho_{\mathrm{j,at}} = n_a \frac{N_A \rho}{M}$, $\nu_0 = \frac{e}{2\pi\sqrt{m_e}}\frac{1}{\sqrt{\overline{\alpha}}}$, $\overline{\alpha} = \varepsilon_0 \frac{3M}{n_a N_A \rho}\frac{n^2 - 1}{\left(n^2 + 2\right)}$, $\overline{\beta} = \frac{3}{4}\sqrt{s}\, h\nu_0 \left(\frac{\overline{\alpha}}{4\pi\varepsilon_0}\right)^2$	3.3.6.2
Henry coefficient He for *Hamaker*-dominant adsorption	$IL \equiv \frac{He \Re T_{ads}}{S_{BET}\, \sigma_{i,j}}$, $IP \equiv \frac{T_c}{T_{ads}}\sqrt{\frac{2\, Ha_j}{\pi \sigma_{j,j}^3\, p_c}}$, $IL = \exp\left(p_1 IP^{p_2}\right)$, $p_1 = 0.331$, $p_2 = 1.180$	5.2.1
Henry coefficient He for adsorption of polar adsorptives on energetic heterogeneous solids	$IL = \int_0^{x_{\max}} \left(\exp\left(\frac{A_{diplad} + A_{indlad}}{(1+x)} + \frac{A_{indind} + A_{dipind} + A_{quadlad}}{(1+x)^3} + \frac{A_{quadind}}{(1+x)^5} \right) - 1 \right) dx$, $x_{\max} = 2$	5.3.8
Adsorption isotherm for gases on microporous solids	$p = \frac{n}{He}\left(\frac{1}{1 - n/n_\infty}\right)^B$, $B = C\frac{T_c}{T_{ads}}\left(\frac{Ha_j}{\sigma_j^3 p_c}\right)^{3/2}$, $n_\infty = \frac{v_{micro}}{\beta(T_{ads})}$, $\beta(T_{ads}) = v_b + \left(\frac{T_{ads} - T_b}{T_c - T_b}\right)(v_{vdW} - v_b)$, $C = 0.55\ 10^{-3}$	6.1 and 6.2.3

8. Summary

The main objective of this thesis is the theoretical prediction of adsorption equilibria of single gaseous substances on microporous solids like active carbon or zeolites (e.g. MS4A, MS5A, NaX and NaY). A novel equilibrium model was derived from a differential equation considering two boundary conditions. These boundaries were the Henry coefficient for diluted gases and the saturation loading for highly concentrated gases.

A historical overview on adsorption is presented in Chapter 3 which also addresses some important chemical and technical aspects. An essential prerequisite for the predicition of adsorption equilibria is a detailed knowledge of the properties of the solid adsorbents. The characterisation of microporous adsorbents is treated in Section 3.3. The novel equilibrium model is compared with classical adsorption theories as the models of *Langmuir* and *Toth*. Techniques for the measurement of adsorption equilibria (e.g. adsorption isotherms) are explained also.

The *Henry* coefficient which describes the adsorption isotherm of diluted gases depends on the properties of both the gaseous (adsorptive) and the solid (adsorbent) phase. However, the key parameter of the intermolecular interaction forces, the *Hamaker* constant, is unknown for most zeolites. In Chapter 3, an approximated *Hamaker* and *de Boer* model for predicting the *Hamaker* constant of microporous solids is developed on the basis of the refractive index.

The refractive index is determined by the *Clausius-Mosotti* relationship between the relevant optical and density parameters of the solid adsorbent. For zeolitic adsorbents, the optical parameters can be derived from the polarisability of ions in the zeolite crystal.

Experimental methods for the determination of adsorption equilibria are presented in Chapter 4 of this thesis. Besides classical techniques some novel ones are treated in detail, e.g. the zero length column method.

An important result of the thesis is the finding that the adsorption of unpolar as well as polar gases on energetical heterogeneous adsorbents is controlled by the *Hamaker* constant. Therefore, the dominant mechanism is the induced dipole – induced dipole interaction. For this case the dimensionless *Henry* curve was numerically evaluated because the differential equation cannot be solved analytically. The numerical results were correlated by an exponential function. The adsorption of polar gases on energetical heterogeneous adsorbents depends on more than two parameters. It was not possible to correlate the numerical results by simple regression. Nevertheless, a suited algorithm is presented in Chapter 5.

In Chapter 6, the prediction model for all cases was developed by integrating the fundamental differential equation under consideration of two boundary conditions, e.g.. the *Henry* coefficient and the saturation loading.

In Chapter 7 the novel model was compared with literature and experimental data. The *Toth* isotherm model was used to calculate the experimental Henry coefficients. The calculated *Henry* coefficients of the novel model fit very well with experimental data over six orders of magnitudes. As second step the predicted adsorption equilibria were compared with experimental data from the literature. The novel model fits the isotherms very well beginning at the *Henry* region and ending at the saturation region. Next in Chapter 7, the assumptions for the calculation of the adsorption model parameters, e.g. the refractive index, were verified. For engineering purposes it is important to know which attraction potentials are of theoretical interest only and which are dominant for calculating the *Henry* coefficient. As a result it was shown that the induced dipole – induced dipole interaction is always eminent. For polar gases additionally the permanent dipole – charge and/or the quadrupole moment – charge interaction have to be taken into account. All other induced dipole interactions have minimal impact and can be neglected.

In the appendix the set-up for own experimental data will be explained.

Appendix

Appendix A: Isotherms in transcendental form

Maurer [26] introduced a generalized empirical equation that allows for a priori predictions of complete adsorption isotherms for active carbon with

$$He\,p = n \exp\left(f(S_{BET}) \frac{T_c/K}{(p_c/bar)^2} \frac{n}{mol/kg} \right) \tag{A.1}$$

where He is the *Henry* coefficient in mol/(kg*Pa), p the adsorption equilibrium pressure in Pa, n the loading of the adsorbent in mol/kg, T_c the critical temperature of the adsorptive in K and p_c the critical pressure of the adsorptive in bar. $f(S_{BET})$ is a function of the BET surface area S_{BET} and follows from

$$f(S_{BET}) = -0{,}367 + \frac{6167 \frac{m^2}{g}}{S_{BET} \frac{m^2}{g}} \tag{A.2}$$

The *Henry* coefficient can be determined by the following equation for energetic homogeneous adsorbents, derived in Chapter 5 with

$$He = \frac{\sigma_{i,j}\, S_{BET}}{\Re\, T_{ads}} IL = \frac{\sigma_{i,j}\, S_{BET}}{\Re\, T_{ads}} \exp\left(p_1 IP^{p_2}\right) = \frac{\sigma_{i,j}\, S_{BET}}{\Re\, T_{ads}} \exp\left(p_1 \left(\frac{T_c}{T_{ads}} \sqrt{\frac{2\,Ha_j}{\pi \sigma_j^3\, p_c}} \right)^{p_2} \right) \tag{A.3}$$

where all the coefficients are in SI units and explained already in Chapter 5. The parameters are p_1 = 0.3313 and p_2 = 1.180. The loading n can be calculated by given partial pressure p.

Equation (A.2) cannot be solved analytically for n. The given function has the structure

$$y(x) = x \exp(u\,x) \tag{A.4}$$

The inverse function of equation (A.4) is the so-called *Lambert* function W with

$$x = \frac{W(u\,y)}{u} \tag{A.5}$$

where y is a substitution for

$$y = He\,p \tag{A.6}$$

and the parameter u a substitution for

$$u = f(S_{BET}) \frac{T_c / K}{(p_c / bar)^2} \tag{A.7}$$

Rechid [104] introduced a mathematical approach for describing the *Lambert* function with analytically solvable functions. It is therefore

$$n = \frac{1.0004 \ln(u\,y+1) - 2.1037 \ln(\ln(u\,y+1)+1) + 2.3948 \ln(\ln(\ln(u\,y+1)+1)+1)}{u} \tag{A.8}$$

The adsorption isotherm for active carbon can be calculated straight forward analytically only with knowledge of the properties of adsorptive and adsorbent. As example the isotherm of ethane on active carbon is shown in figure A.1. The parameters are listed in table A.1.

Table A.1: Parameters for the adsorption isotherm of ethane on active carbon.

Parameter	Value	Unit
Adsorption temperature T_{ads}	303.15	K
Critical temperature T_c of ethane	305.4	K
Critical pressure p_c of ethane	48.8	bar
Critical pressure p_c of ethane	4880000	Pa
Hamaker constant Ha_j of active carbon	6.0 E-20	J
Van-der-Waals diameter of active carbon σ_j	3.4 E-10	m
Van-der-Waals diameter of ethane σ_i	3.72 E-10	m
Minimum distance $\sigma_{i,j}$	3.56 E-10	m
Specific surface of the adsorbent	1.1 E+6	m^2/kg
Specific surface of the adsorbent	1.1 E+3	m^2/g
Toth isotherm parameter n_{max}, equation (3.81)	14.46	mol/kg
Toth isotherm parameter m, equation (3.81)	0.289	-
Toth isotherm parameter $1/K_T$, equation (3.81)	2.010	$(kPa)^m$

The experimental values of the adsorption isotherm are compared with the adjusted *Toth* isotherm and the predictive isotherm calculated with equation (A.8). The *Toth* isotherm parameter $1/K_T$ is given in the literature example in kPa [105], so the partial pressure p in the Toth isotherm has to be inserted also in kPa.

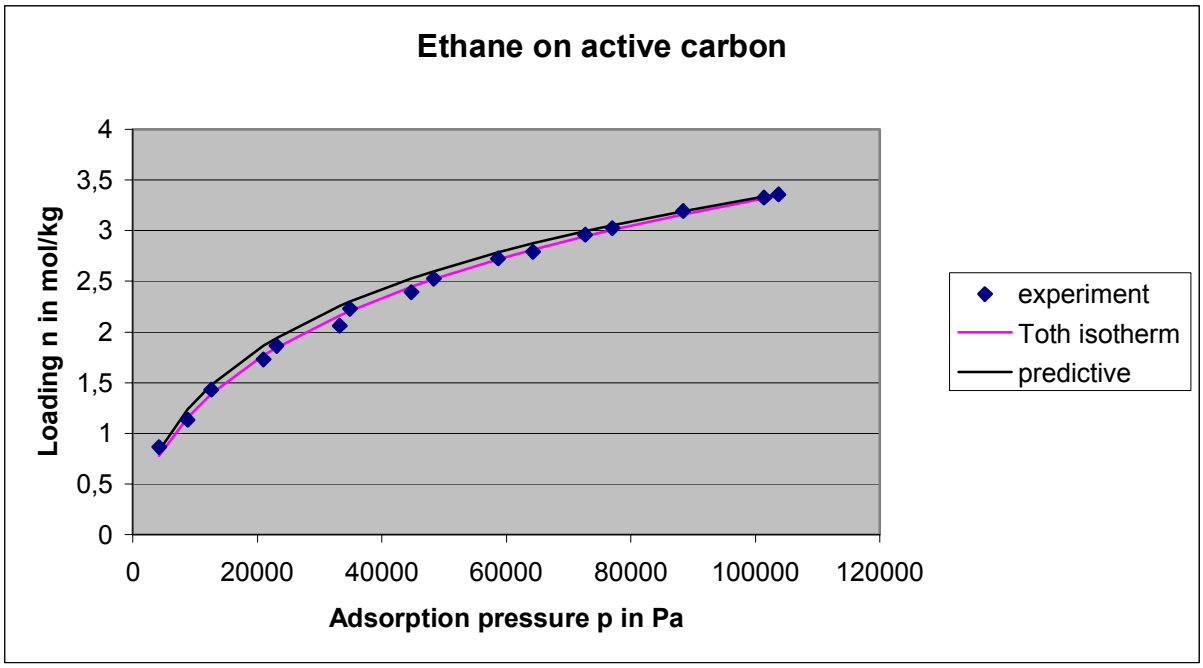

Figure A.1: Adsorption isotherm of ethane on active carbon at T_{ads} = 303.15 K.

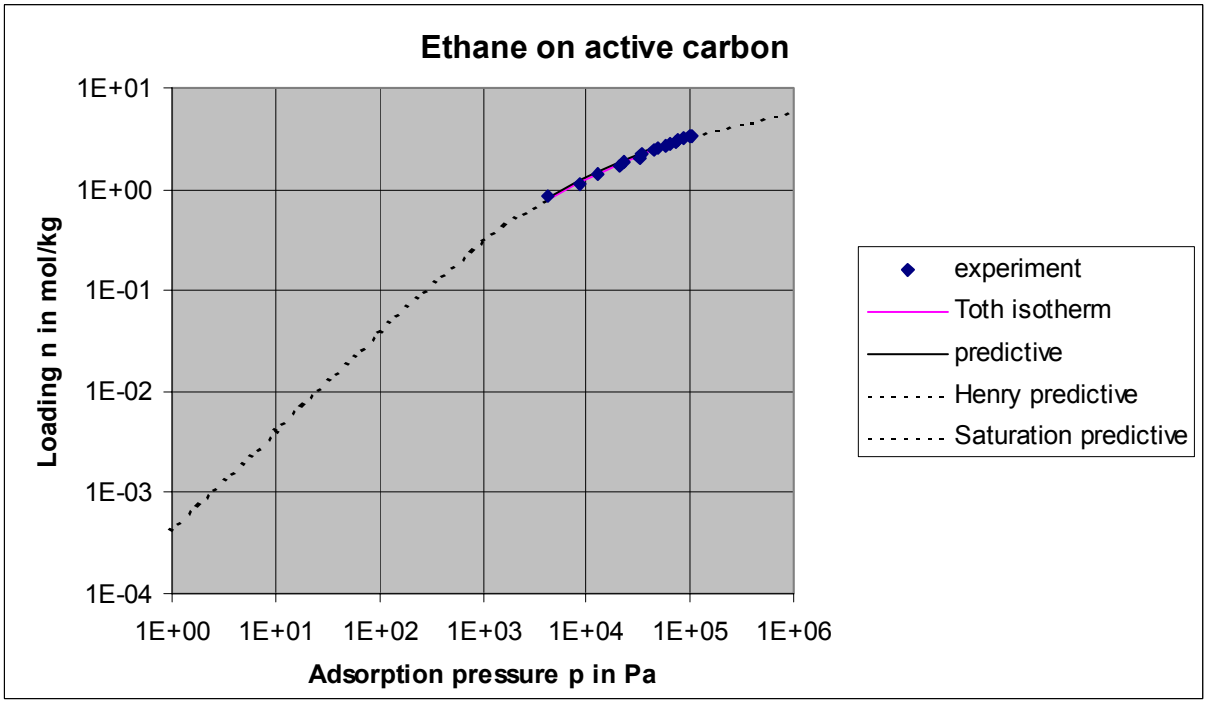

Figure A.2: Adsorption isotherm of ethane on active carbon at T_{ads} = 303.15 K in a double logarithmic plot.

With given loading n the partial pressure p of the adsorption isotherm can be calculated by

$$p = \frac{n \exp\left(f(S_{BET}) \frac{T_c/K}{(p_c/bar)^2} \frac{n}{mol/kg} \right)}{He} \qquad \text{(A.9)}$$

With equations (A.8) and (A.9) the adsorption isotherm of any adsorptive on activated carbon can be calculated analytically in both directions.

Appendix B: Materials and Methods

This study is based on both literature data and own adsorption experiments. Experimental *Henry* coefficients were calculated by *Langmuir* and *Toth* isotherm adaptations. *Henry* coefficients in the literature were taken from tables or calculated by regressing the isotherm data with *Langmuir* and *Toth* parameters.

B.1. Materials

B.1.1. Experimental data

Adsorption experiments were conducted at the Lehrstuhl für Technische Chemie II of the Technische Universität München in Garching and at the Institut für Nichtklassische Chemie e.V. at the Universität Leipzig. In tables B.1 and B.2 the used adsorptives and adsorbents and their relecant properties are listed.

Table B.1: Adsorptives used for adsorption isotherms with their properties.

Adsorptive	Methanol (CH_3OH)	Dichloromethane (CH_2Cl_2)
Molar mass M_i in kg/mol [106]	0.032042	0.084933
Critical temperature T_c in K [106]	512.6	510
Critical pressure p_c in Pa [106]	6300000	8090000
Normal boiling temperature T_b in K [106]	337.7	313
Van-der-Waals diameter σ_j in m (equation 5.19)	$3.74*10^{-10}$	$4.06*10^{-10}$
Critical molecule diameter in m	$3.6*10^{-10}$	$3.73*10^{-10}$
Dipole moment μ in debye (1 debye = $3{,}34*10^{-30}$ Cm) [106]	1.7	1.8
Polarisability α in $(C^2*m^2)/J$ [6] and equation (3.67)	$3.66*10^{-40}$	$7.21*10^{-40}$
Quadrupole moment Q in Cm^2 [107]	$4.337*10^{-40}$	$1.0*10^{-39}$

Table B.2: Adsorbents used for adsorption isotherms with their properties.

Adsorbent	NaY	MS5A	NaX (13X)
Specific surface S_{BET} in m^2/kg, measured	655400	464135	521977
Micropore volume v_{micro} in 10^{-3} m^3/kg, measured	0.2723	0.2323	0.2643
Bulk density ρ_b in kg/m^3 [108, 24]	650	700	675
Bulk porosity ε_b [24]	0.6	0.6	0.6
Apparent density ρ_{app} in kg/m^3, $\rho_{app} = \rho_b/\varepsilon_b$	1100	1166	1125
Refractive index n, equation (3.63)	1.61	1.58	1.63
Chemical structure [24]	Na_{56} $((AlO_2)_{56}(SiO_2)_{106})$	Ca_5Na_2 $((AlO_2)_{12}(SiO_2)_{12})$	Na_{86} $((AlO_2)_{86}(SiO_2)_{106})$
Effective pore opening in m, [108, 24]	$10*10^{-10}$	$5*10^{-10}$	$10*10^{-10}$
Van-der-Waals diameter σ_j in m, table 5.2	$4.2*10^{-10}$	$3.8*10^{-10}$	$3.9*10^{-10}$
Number density of atoms $\rho_{j,at}$ in $1/m^3$, equation (3.92)	$3.28*10^{28}$	$3.31*10^{28}$	$3.72*10^{28}$
$\frac{S_{BET}\sigma_j}{v_{micro}}$	1.01	0.76	0.75

The methanol had a purity of 99.9 mass-%. For experiments in Garching it was a Merck product with the trade name Uvasol® and is normally used for spectroscopy purposes. Methanol adsorption experiments in Leipzig were conducted with the Merck product LiChrosolv® which is suitable for liquid chromatography purposes. The dichloromethane had a purity of 99.8 mass-%. For experiments in Garching it was a Sigma-Aldrich product with the trade name AMD Chromosolv® and is normally used for chromatography purposes. Dichloromethane adsorption experiments in Leipzig were conducted with the Merck product pro analysi®. The adsorbents MS5A and NaX were from Grace Davison. MS5A has the trade name Sylobead® MS C 522 and NaX (13X) the trade name Sylobead® MS C 544. The adsorbent NaY were from Akzo Nobel.

Methanol is a high value chemical in many processes, e.g. the conversion to highly knockproofed gasoline via zeolite catalysts. Dichloromethane is a solvent for resins, fats and plastics. Both adsorptives have a medium dipole moment, high enough to dominate with their dipole/charge potential the *Hamaker* potential and small enough to get into the *Henry* region with a gravimetric experimental set-up when adsorbed on zeolites. The zeolites MS5A, NaX and NaY are standard adsorbents in many chemical processes like removal of pollutants.

B.1.2. Literature data

Literature data were collected and analyses was made for verifying the models derived in this study [1, 3, 5, 7, 8, 9, 11, 12, 13, 18, 20, 22, 23, 25, 28, 29, 31, 33, 34, 35, 36, 37, 38, 39, 40, 45, 60, 91, 92, 115, 116, 117]. *Henry* coefficients were tabulated in most of the cases, if not the adsorption isotherms were analysed by using the *Langmuir* plot explained in Chapter 3 or with *Langmuir* parameter regressing in the program Origin or with *Toth* isotherm regressing. The properties of the adsorptives were found in *Reid et al.* [106] and in the CRC Handbook [6]. Especially quadrupole moments were found in the Computational Chemistry Comparison and Benchmark Database [107] and in further literature [2, 14, 15, 16, 17, 42, 43, 103]. The examined adsorptives and adsorbents with their properties are listed in appendix C and appendix D, respectively.

B.2. Experimental set-up

B.2.1. Adsorption isotherm measurements

The adsorption equilibrium isotherms were measured at the Lehrstuhl für Technische Chemie 2 of the Technische Universität München gravimetrically in a modified SETARAM TG-DSC 111 microbalance (see figure B.1) which is able to measure differences in mass down to 10^{-6} g which is also the accuracy. The sample weight in the microbalance was applied between 13 to 22 mg in order to record precise measurement and better signal-to-noise ratio. The pressure inside the system can be reduced down to 10^{-7} mbar with a Pfeiffer turbo molecular pump and the temperatures can be applied within the range of 25°C to 750°C with an accuracy of 0.15°C. The high vacuum was measured with a Pfeiffer TPG 300 pressure transducer. The experiments were carried out in the pressure range from 10^{-3} to 13 mbar (0.1 Pa to 1300 Pa), measured with a BARATRON 122 A pressure transducer. The transducer has an accuracy of 0.5 % of reading [108]. For activation, the solid samples were heated in vacuum (p < 10-6 mbar) to 500 °C with 10 °C/min and held 4 h at 500 °C. After activation, the temperature was reduced to ca. 45°C. The liquid sorbates were added in pulses to the high vacuum system in which they vaporised. After each pulse the system was equilibrated. This was monitored by observation of the sample weight and pressure. The system was regarded to be in steady state or equilibrium, when changes in any of the parameters pressure, mass or heating flux were not observed any more [110]. Figure B.2 shows the experimental set-up.

Figure B.1: SETARAM TG-DSC 111 microbalance.

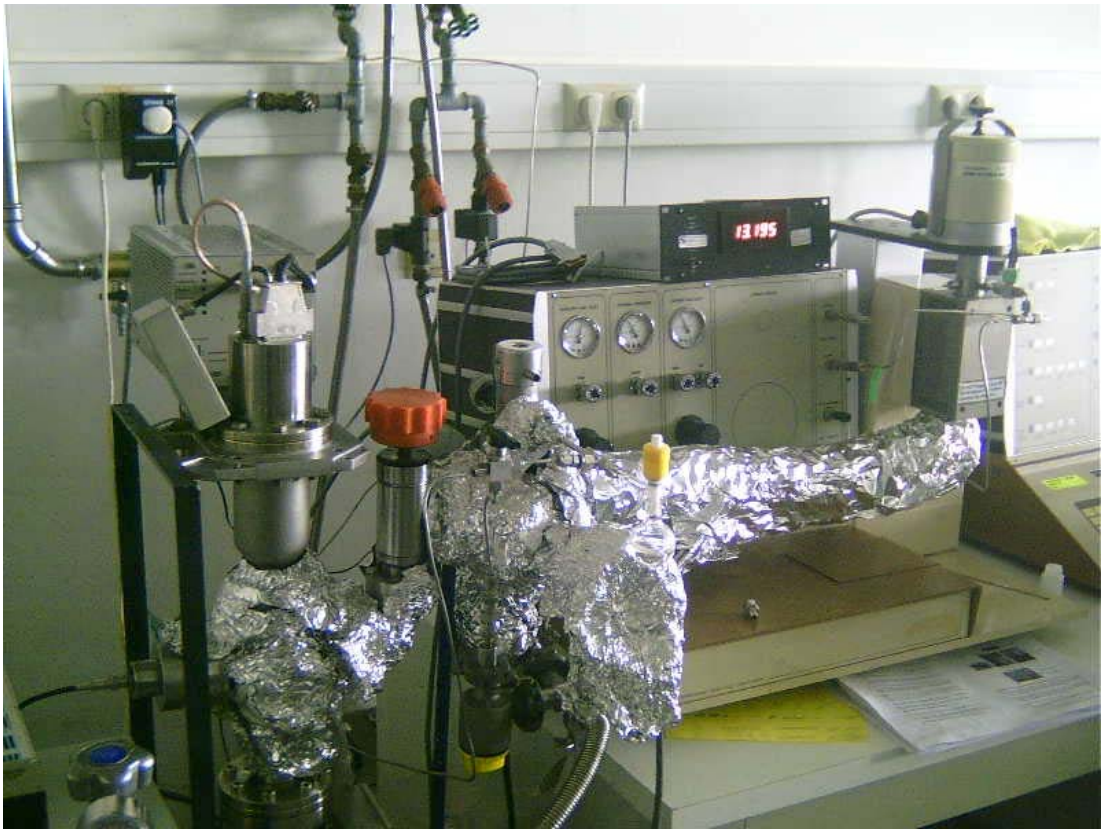

Figure B.2: Experimental set-up for adsorption isotherm measurements at the Institut für Technische Chemie 2 of the Technische Universität München.

The data for the adsorption isotherm graphs were calculated by the following method: The adsorbents are hold by a crucible in the microbalance. Its mass after activating is the so-called blank mass m_0. The mass of the crucible with activated adsorbent is the mass m_1. After equilibrium of the injected adsorptive with the adsorbent the new absolute mass m_{i+1} is measured. So one can calculate the equilibrium loading n_{i+1} of every adsorption step with its equilibrium pressure could be measured by

$$n_{i+1} = \frac{m_{i+1} - m_1}{m_0} \frac{1}{M_{adsorptive}} \quad for \;\; i > 1 \qquad \text{(B.1)}$$

where the masses are in kg and $M_{adsorptive}$ is the molar mass of the adsorptive in kg/mol. With equation (B.1) the equilibrium loading n in mol/kg regarding to the equilibrium pressure p in Pa is obtained.

The adsorption equilibrium isotherms at the Institut für Nichtklassische Chemie e.V. from the Universität Leipzig were measured gravimetrically with a high resolution magnetic suspension balance from Rubotherm Präzisionsmesstechnik GmbH which had a weighing instrument from Mettler-Toledo of type AT261. The sample weight in the microbalance was applied between 10 to 30 g. The relative error of this instrument is 0.002 % of the measured value and its resolution is 0.01 mg [113]. The pressure inside the system can be reduced down to 10^{-3} mbar with a Pfeiffer turbo molecular pump TMH 071P and the temperatures can be applied within the range of 25°C to 400°C with an accuracy of 0.15°C of the used PT100 sensor. The high vacuum was measured with an MKS pressure transducer, Baratron Model 627B, and the low vacuum with a Newport/Omega pressure transducer, Model SN2713. The experiments were carried out in the pressure range from 10^{-1} mbar to 1 bar (10 Pa to 100.000 Pa). The transducers had an accuracy of 0.12 % of reading for the MKS model and 0.03 % of the end value 1 bar for the Newport/Omega model [114]. For activation, the solid samples were heated in vacuum (p < 10-3 mbar) to 370°C with 1 K/min and held 10 h at 370°C. After activation, the temperature was reduced to 323 K. The liquid sorbates were degassed after condensing with liquid nitrogen with a vacuum pump from ATS Antriebstechnik GmbH. This was done several times. After this the sample was added in pulses to the high vacuum system in which they vaporised. After each pulse the system was equilibrated. This was monitored by observation of the sample weight and pressure. The system was regarded to be in steady state or equilibrium, when changes in any of the parameters were not observed. Figure B.3 shows the experimental set-up.

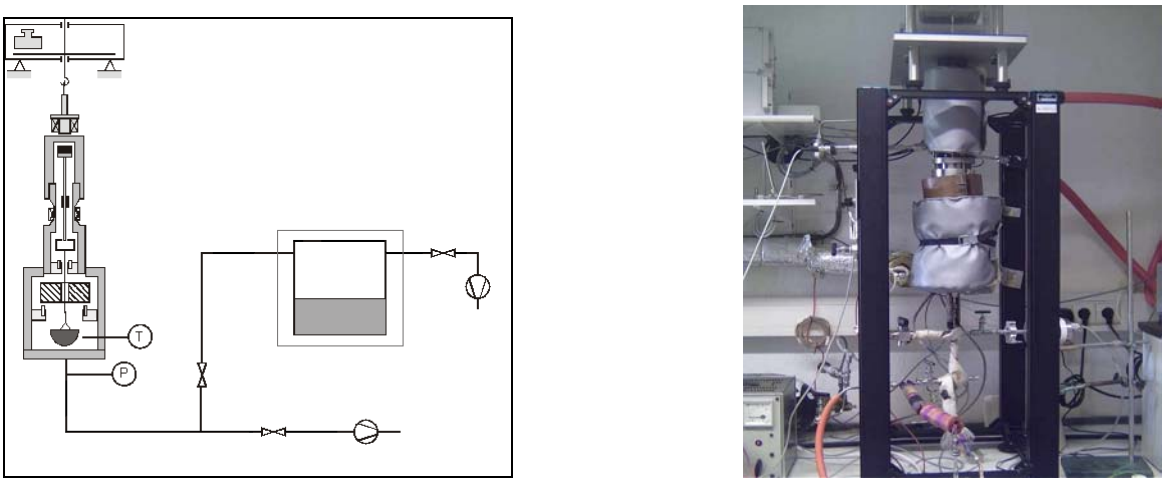

Figure B.3: Experimental set-up for adsorption isotherm measurements in Leipzig.

The data for the adsorption isotherm graphs were calculated by the same method as described above for equation (B.1).

In general the first set-up was taken for high-vacuum measurements from 0.1 Pa to 100 Pa and the second set-up for medium-vacuum measurements from 100 Pa to saturation pressure of the adsorptive at room temperature.

B.2.2. BET surface and micropore volume measurements

BET surface measurements were conducted with nitrogen at 77 K as described in Chapter 3. The micropore volume of the adsorbents were derived from t-plot analysis. Results are listed in table B.2.

B.2.3. Adsorptive data

Table B.4: Examined adsorptives and their relevant properties.

Adsorptive	Molar mass in 10^{-3} kg/mol	*Van-der- Waals* diameter σ_i in m	Dipole moment m_i in debye	Polarisability α_i in $(C^2*m^2)/J$	Quadrupole moment Q_i in Cm^2	Critical temperature T_c in K	Critical pressure p_c in Pa
N_2	28.01	3.13E-10	0	1.93E-40	5.07E-40	126.2	3390000
CO	28.01	3.15E-10	0.1	2.14E-40	9.87E-40	132.9	3500000
CH_4	16.04	3.24E-10	0	3.00E-40	0	190.4	4600000
O_2	31.99	2.93E-10	0	1.76E-40	2.70E-40	154.6	5040000
Kr	83.80	3.15E-10	0	2.76E-40	0	209.4	5500000
C_2H_4	28.05	3.59E-10	0	4.73E-40	1.44E-39	282.4	5040000
CHF_3	70.01	3.70E-10	1.6	3.95E-40	1.07E-39	299.3	4860000
C_3H_6	42.08	4.15E-10	0.4	6.91E-40	1.80E-40	364.9	4600000
NH_3	17.03	3.09E-10	1.5	3.13E-40	8.67E-40	405.5	11350000
H_2	2.016	2.76E-10	0	8.93E-41	1.33E-40	33.2	1300000
CO_2	44.01	3.24E-10	0.7	2.89E-40	1.50E-39	304.2	7380000
C_2H_6	30.07	4.78E-10	0	4.98E-40	2.47E-40	305.4	4880000
C_3H_8	44.09	4.15E-10	0	7.03E-40	1.80E-40	369.8	4250000
C_4H_{10} (n-Butane)	58.12	4.52E-10	0	9.06E-40	2.67E-40	425.2	3800000
C_4H_{10} (i-Butane)	58.12	4.52E-10	0.1	9.06E-40	2.67E-40	408.2	3650000
C_6H_{14} n-Hexane	88.18	5.18E-10	0	1.32E-39	0	507.5	3010000
C_6H_{12} (cyclohexane)	84.16	4.82E-10	0	1.22E-39	3.00E-40	553.5	4070000
C_6H_{14} (2methylpentane)	88.18	5.14E-10	0.1	1.31E-39	2.67E-40	497.5	3010000
SF_6	146.05	4.12E-10	0	7.28E-40	0	319	3760000
CH_2Cl_2	84.93	4.06E-10	1.8	7.21E-40	1.00E-39	510	6030000
C_2HCl_3	131.39	4.54E-10	0.9	1.12E-39	6.67E-40	572	5050000
He	4.0	2.66E-10	0	2.20E-41	0	5.19	227000

Table B.4: Examined adsorptives and their relevant properties.

Adsorptive	Molar mass in 10^{-3} kg/mol	*Van-der- Waals* diameter σ_i in m	Dipole moment m_i in Debye	Polarisability α_i in $(C^2*m^2)/J$	Quadrupole moment Q_i in Cm^2	Critical temperature T_c in K	Critical pressure p_c in Pa
C_6H_6 (benzene)	78.11	4.56E-10	0	1.11E-39	1.20E-39	562.2	4890000
C_2H_4 (ethene)	28.05	3.59E-10	0	4.73E-40	1.44E-39	282.4	5040000
CH_3OH (methanol)	32.04	3.74E-10	1.7	3.66E-40	4.34E-40	512.6	8090000
C_8H_{10} (p-xylene)	106.16	5.25E-10	0	1.57E-39	2.56E-39	616.2	3510000
$C_{10}H_8$ (naphtalene)	128.17	5.34E-10	0	1.94E-39	4.50E-39	748.4	4050000
Ar	39.95	2.94E-10	0	1.83E-40	0	150.8	4870000
HFC134a ($C_2H_2F_4$)	102.03	4.23E-10	2.1	4.87E-40	4.13E-39	374	4060000

B.2.4. Adsorbent data

Table B.5: Examined adsorbents from the literature and their relevant properties.

Adsorbent	Chemical structure	σ_j in 10^{-10} m	Number n_a of atoms in the solid molecule	Density ρ_{app} of the solid in kg/m^3	Molecular mass M_j of the solid in kg/mol	Number density $\rho_{j,at}$ of atoms in $1/m^3$	Refractive index of the solid	Average polarisability of the solid atoms $\overline{\alpha}_j$ in C^2m^2/J	Average number of valence electron bindings s	Hamaker constant Ha_j in J
MS4A	$Na_{12}((AlO_2)_{12}(SiO_2)_{12})$	3.80	84	1680	1.70	5.00E28	1.44	1.40E-40	2.30	6.50E-20
MS5A	$Ca_5Na_2((AlO_2)_{12}(SiO_2)_{12})$	3.80	79	1150	1.68	3.27E28	1.57	2.67E-40	2.43	7.66E-20
NaX	$Na_{86}((AlO_2)_{86}(Si0_2)_{106})$	3.86	662	1100	12.0	3.64E28	1.62	2.55E-40	2.32	8.70E-20
NaY	$Na_{56}((AlO_2)_{56}(SiO_2)_{136})$	4.20	632	1100	12.76	3.28E28	1.613	2.82E-40	2.43	8.40E-20
Silicalite-1	$Si_{96}O_{192}$	3.85	298	1760	5.80	5.58E28	1.46	1.32E-40	2.67	7.89E-20

Appendix C: Alternative way for deriving the potential factor $f_{quadcha}$

In Section 5.1 the assumption has been made that no permanent dipole or quadrupole in an adsorbent molecule is existing and inSection 5.2.1 it has been stated that the time avareged dipole moment is zero. However, a strong quadrupole moment Q_i with a certain structure can induce a dipole moment μ_i in an adsorbent molecule. The ratio between the moments μ_i and Q_i of an adsorptive molecule can be derived when equation (5.57) is divided by equation (5.51):

$$\frac{Q_i^2}{\mu_i^2\left(\sigma_{i,j}+z\right)^2} = 20 \qquad \text{(C.1)}$$

or for z = 0 (maximum value of Q_i for a given μ_i)

$$Q_i = \sqrt{20}\mu_i\sigma_{i,j} \qquad \text{(C.2)}$$

The only adsorptive molecule with a strong quadrupole moment but a rather dipole moment already often investigated with respect to adsorption isotherms is CO_2 (Q_i = 15*10^{-40} Cm^2, μ_i = 2.34*10^{-30} Cm). In the previous sections the potential factors f_{dipcha} = f_{indcha} = 1.35 $\left(\frac{Al}{Si}\right)_j$ have been found. These factors are supported by experimental data. Let us assume that the potential factor $f_{quadcha}$ is also 1.35*$\left(\frac{Al}{Si}\right)_j$. An agreement between experimental results for the system CO_2-MS4A is given if the dimensionless energy $-\frac{\Phi_{quadcha}}{kT_{ads}}$ in equation (5.57) is multiplied by the factor 8 which leads to $f_{quadcha}$ = 1,35/8 *$\left(\frac{Al}{Si}\right)_j$ =0.168*$\left(\frac{Al}{Si}\right)_j$. As a first approach it is further assumed that the induced dipole moment μ_j (permanent due to the close neighborship of an quadrupole moment Q_i) is related. Now an effective quadrupole moment $Q_{i,eff}$ is introduced which takes into account the interaction between Q_i and μ_i With $\sigma_{i,j}$ = 4.05*10^{-10} m and $\mu_i = \mu_j$ we find

$$Q_{i,eff} = \sqrt{20}\mu_i\sigma_{i,j} = 42.4 * 10^{-40}\, Cm^2 \qquad \text{(C.3)}$$

and finally

$$\left(\frac{Q_{i,eff}}{Q_i}\right)^2 = \left(\frac{42.4 * 10^{-40}}{15.0 * 10^{-40}}\right)^2 = 8 \qquad \text{(C.4)}$$

It is stressed here that the hypothesis here presented should be tested by experimental results, for instance by experimental data of the system $C_2H_2F_4$/zeolite.

References

[1] Azarenkov, A.N., Al'tshuler, G.B., Belashenkov, N.R. and S.A. Kozlov. 1993. Fast nonlinearity of the refractive index of solid-state dielectric active media. *Quantum Electronics* 23:633-655

[2] Benavides, A.L., Guevara, Y. and A.F. Estrada-Alexanders. 2000. A theoretical equation of state for real quadrupolar fluids. *Journal of Chemical Thermodynamics* 32:945–951.

[3] Bieske, E. J., Nizkorodov, S.A., Bennett, F.R. and J.P. Maier. 1995. Combined infrared and ab initio study of the H2-HN_2^+ complex. *International Journal of Mass Spectrometry and Ion Processes* 149/150:. 167–177.

[4] Braun, Björn. 2004. *Aggregation and Agglomeration in Percipitative Crystalization*. Dissertation at the Technical University of Munich.

[5] Choudhary, V. R. and S. Mayadevi. 1996. Adsorption of methane, ethane, ethylene and carbon dioxide on silicalite-1. *Zeolites* 17:501-507.

[6] Lide, David R., Editor-in-Chief. 2004-2005. *CRC Handbook of Chemistry and Physics, 85th Edition*. London, New York, Washington: CRC Press.

[7] Dunne, J. A., Rao, M., Sircar, S., Gorte, R.J. and A.L. Myers. 1996. Calorimetric Heats of Adsorption and Adsorption Isotherms. 2. O_2, N_2, Ar, CO_2, CH_4, C_2H_6 and SF_6 on NaX, H-ZSM-5, and Na-ZSM-5 Zeolites. *Langmuir* 12:5896-5814.

[8] Markmann, Birgitt. 1999. *Zur Vorhersagbarkeit von Adsorptionsgleichgewichten mehrkomponentiger Gemische.* Dissertation at the Technical University of Munich.

[9] Fox, J.P., Rooy, V. and Simon P. Bates. 2004. Simulating the adsorption of linear, branched and cyclic alkanes in silicalite-1 and $AlPO_4$-5. *Microporous and Mesoporous Materials* 69:9-18.

[10] Fried, J. R. and N. Hu. 2003. The molecular basis of CO_2 interaction with polymers containing fluorinated groups. *Polymer* 44:4363–4372.

[11] Giaya, A., and Robert W. Thompson. 2002. Single-component gas phase adsorption and desorption studies using a tapered element oscillating microbalance. *Microporous and Mesoporous Materials* 55:265-274.

[12] Grande, C.A., Gigola, C. and A.E. Rodrigues. 2002. Adsorption of Propane and Propylene in Pellets and Crystals of 5A Zeolite. *Industrial and Engineering Chemistry Research* 41:85-92.

[13] Grande, C.A., Gigola, C. and A.E. Rodrigues. Propane-Propylene Binary Adsorption on Zeolite 4A. *Adsorption* 9(4):321-329.

[14] Greenhow, C. and W.V. Smith. 1951. Molecular Quadrupole Moments of N2 and O2. *The Journal of Chemical Physics* 10:1298-1230.

[15] Halkier, A. and S. Coriani. 1999. On the molecular electric quadrupole moment of C_2H_2. *Chemical Physics Letters* 303:408–412.

[16] Heard, G. L. and R.J. Boyd. 1997. Density functional theory studies of the quadrupole moments of benzene and naphthalene. *Chemical Physics Letters* 277:252–256.

[17] Heard, G. L. and R.J. Boyd. 1997. Calculation of Quadrupole Moments of Polycyclic Aromatic Hydrocarbons: Applications to Chromatography, *Journal of Physical Chemistry A* 101:5374-5377.

[18] Helminen, J., Helenius, J. and E. Paatero. 2001. Adsorption Equilibria of Ammonia Gas on Inorganic and Organic Sorbents at 298,15 K. *Journal of chemical and engineering data*, 46:391-399.

[19] Hirschfelder, Joseph O., Curtiss, Charles F. and Bird R. Byron, eds. 1964. *Molecular Theory of Gases and Liquids.*, New York: John Wiley & Sons, Inc.

[20] Inel, O., Topaloglu, D., Askin, A. and F. Tümsek. 2002. Evaluation of the thermodynamic parameters for the adsorption of some hydrocarbons on 4A and 13X zeolites by inverse gas chromatography. *Chemical Engineering Journal* 88:255-262.

[21] Israelachvili, Jacob N. 1991. *Intermolecular and Surface Forces*, *2nd Edition*. San Diego, San Francisco, New York: Academic Press.

[22] Jaramillo, E. and M. Chandross. 2004. Adsorption of Small Molecules in LTA Zeolites. 1. NH_3, CO_2, and H_2O in Zeolite 4A. *The Journal of Physical Chemistry. B, Condensed Matter, Materials, Surface, Interfaces & Biophysical Chemistry.* 108(52):20155-20159.

[23] Vashchenko, L.A. and V.V. Katal´nikova. 1996. Adsorption of helium on zeolite NaA. *Russian Chemical Bulletin* 45(5):1230-1231.

[24] Kast, Werner. 1998. *Adsorption aus der Gasphase*. Weinheim, Germany: VCH Press.

[25] Klemm, E., Wang, J. and G. Emig. A comparative study of the sorption of benzene and phenol in silicalite, HAlZSM-5 and NaAlZSM-5 by computer simulation. *Microporous and Mesoporous Materials* 26:11-21.

[26] Maurer, Stephan. 2000. *Prediction of Single-Component Adsorption Equilibria*. Dissertation at the Technical University of Munich.

[27] Mersmann, A., Fill, B. and S. Maurer. 2002. Single and Multicomponent Adsorption Equilibria of Gases. *Fortschritt-Berichte VDI, Reihe 3 Verfahrenstechnik* 735.

[28] Moeller, A. and R. Staudt. 2005. *Personal communication*.

[29] Mohr, R. J., Vorkapic, D., Rao, M.B. and S. Sircar. 1999. Pure and Binary Gas Adsorption Equilibria and Kinetics of Methane and Nitrogen on a 4A Zeolite by Isotope Exchange Technique. *Adsorption* 5:145-158.

[30] Munataka, K., Fukumatsu, T., Yamatsuki, S., Tanaka, K. and M. Nishikawa. 1999. Adsorption Equilibria of Krypton, Xenon, Nitrogen and Their Mixtures on Molecular Sieve 5A and Activated Charcoal. *Journal of Nuclear Science and Technology* 36:818-829.

[31] Nam, G., Jeong, B., Kang, S., Lee, B. and D. Choi. 2005. Equilibrium Isotherms of CH_4, C_2H_6, C_2H_4, N_2 and H_2 on Zeolite 5A Using a Static Volumetric Method. *Journal of Chemical & Engineering Data* 50:72-76.

[32] Palik, Edward D. 1991. *Handbook of Optical Constants of Solids I, II, III*., New York: Academic Press, Inc.

[33] Rep, M., Palomares, A.E., Eder-Mirth, G., van Ommen, J.G., Rösch, N. and J.A. Lercher. 2000. Interaction of Methanol with Alkali Metal Exchanged Molecular Sieves. 1. IR Spectroscopic Study. *Journal of Physical Chemistry B* 104:8624-8630.

[34] Ruthven, D.M. and B.K. Kaul. 1993. Adsorption of Aromatic Hydrocarbons in NaX Zeolite. 1. Equilibrium. *Industrial & Engineering Chemistry Research* 32:2047-2052.

[35] Sander, Stefan. 2000. *Experimentelle Bestimmung von Adsorptionsgleichgewichten und Evaluation von Adsorptionsgleichgewichtsmodellen*. Dissertation at the Carl von. Ossietzky University, Oldenburg.

[36] Schweighart, Peter. 1994. *Adsorption mehrerer Komponenten in biporösen Adsorbentien*. Dissertation at the Technical University of Munich.

[37] Sievers, Werner. 1993. *Über das Gleichgewicht der Adsorption in Anlagen zur Wasserstoffgewinnung*. Dissertation at the Technical University of Munich.

[38] Sieperstein, F.R., Gorte, R.J. and A.L. Myers. 1999. Measurement of Excess Functions of Binary Gas Mixtures Adsorbed in Zeolites by Adsorption Calorimetry. *Adsorption* 5:8-12.

[39] Sieperstein, F.R. and A.L. Myers. 2001. Mixed-Gas Adsorption. *AIChE Journal* 47(5):1141-1159.

[40] Talu, O. and A.L. Myers. 2001. Reference potentials for adsorption of helium, argon, methane, and krypton in high-silica zeolites. *Colloids and Surfaces A: Physicochemical and Engineering Aspects.* 187:83-93.

[41] Van der Hoeven, Ph.C. 1991. *Electrostatic Stabilization of Suspensions in Non-Aqueous Media*. Dissertation at the Landbouwuniversiteit te Wageningen.

[42] Vrabek, J., Stoll, J. and H. Hasse. 2001. A Set of Molecular Models for Symmetric Quadrupolar Fluids. *Journal of Physical Chemistry* 105:12126-12133.

[43] Wan, Q., Ramaley, L. and R. Guy. 1997. Quadrupolar Effects on the Retention of Aromatic Hydrocarbons in Reversed-Phase Liquid Chromatography. *Analytical Chemistry* 69:4581–4585.

[44] Xu, K., Li, Y. and Liu, W. 1998. Application of perturbation theory to chain and polar fluids Pure alkanes, alkanols and water. *Fluid Phase Equilibria*, 142:55-66.

[45] Zhang, Y., Furukawa, S. and T. Nitta. 2004. Monte Carlo Simulation Studies on Adsorption of Propane/Propylene in NaX Zeolite. *Journal of Chemical Engineering of Japan* 37(4):563-568.

[46] Zhu, W., Kapteijn, F. and J.A. Moulijn. 2000. Equilibrium Adsorption of Light Alkanes in Silicalite-1 by the Inertial Microbalance Technique. *Adsorption* 6:159-167.

[47] Mersmann, A., Kind, M. and Johann Stichlmair. 2005. *Thermische Verfahrenstechnik*. Berlin Heidelberg: Springer Verlag.

[48] Ruthven, Douglas M. 1984. *Principles of Adsorption and Adsorption Processes*. New York: John Wiley & Sons, Inc.

[49] Götzinger, Martin. 2004. *Zur Charakterisierung von Wechselwirkungen partikulärer Feststoffoberflächen*. Dissertation at the Technical University of Munich.

[50] Mehler, Carsten. 2003. *Charakterisierung heterogener Feststoffoberflächen durch Erweiterung eines dielektrischen Kontinuumsmodells*. Dissertation at the Technical University of Munich.

[51] Groth, Thomas. 2002. *Die Bedeutung der Volumen- und Oberflächeneigenschaften von Biomaterialien für die Adsorption von Proteinen und nachfolgende zelluläre Reaktionen.* State doctorate at the University of Potsdam.

[52] Dabrowski, A. 2001. Adsorption - from theory to practice. *Advances in Colloid and Interface Science* 93:135-224.

[53] Matisova, E. and S. Skrabakova. 1995. Carbon sorbents and their utilization for the preconcentration of organic pollutants in environmental samples. *Journal of Chromatography A* 707:145-179.

[54] Yang, T and A. C. Lua. 2003. Characteristics of activated carbons prepared from pistachio-nut shells by physical activation. *Journal of Colloid and Interface Science* 267:408-417.

[55] Weitkamp, J. 2000. Zeolites and catalysis. *Solid State Ionics* 131:175-188

[56] Röhr, Caroline. 2005. *Siedende Steine*. Recitation Wissenschaftliche Gesellschaft. Internet site: http://ruby.chemie.uni-freiburg.de/Vorlesung/PDF_Demos/zeolithe.pdf.

[57] Staudt, Reiner. 1994. *Analytische und experimentelle Untersuchungen von Adsorptipnsgleichgewichten von reinen Gasen und Gasgemischen an Aktivkohlen und Zeolithen*. Dissertation at the Universität-Gesamthochschule-Siegen.

[58] Simon, Ulrich. 2000. Innere Werte Zeolithe: nanoporöse Materialien für vielfältige Anwendungsfelder. *Essener Unikate* 13:66-77.

[59] Kalipcilar, H. and A. Culfaz. 2000. Synthesis of Submicron Silicalite-1 Crystals from Clear Solutions. *Cryst. Res. Technol.* 35(8):933-942.

[60] Zhu, W., Kapteijn, F. and J.A. Moulijn. 2000. Adsorption of light alkanes on silicalite-1 : Reconciliation of experimental data and molecular simulations. *Physical Chemistry Chemical Physics* 2:1989-1995.

[61] Jentys, A. and J.A. Lercher. 2001. Chapter8: Techniques of zeolite chracterization. *Studies in Surface Science and Catalysis* 137:345-386.

[62] Brunauer, S., Emmett, P.H. and E. Teller. 1937. Adsorption of Gases in Multimolecular Layers. *Journal of the American Chemical Society* 60:309-316.

[63] Lercher, Johann A. 1999. Chapter 13: Adsorption methods for the assessment of the specific surface area, the pore size distribution and the active sites of heterogeneous catalysts. *Catalysis: An Integrated Approach.* Editors Van Santen, R.A. et al.

[64] Fletcher, Ashleigh. 2006. *Porosity and sorption behaviour*. Internet site: http://www.staff.ncl.ac.uk/a.j.fletcher.

[65] Westermarck, Sari. 2000. *Use of mercury porosimetry and nitrogen adsorption in characterisation of the pore structure of mannitol and microcrystalline cellulose powders, granules and tablets*. Dissertation at the University of Helsinki.

[66] Washburn, E.W. 1921. The dynamics of capillary flow. *Physical Review* 17(3):273-283.

[67] Micromeritics. 2005. *Data reduction methods*. Internet site http://www.micromeritics.com

[68] Lowell, S., Shields, J.E., Thomas, M.A. and M. Thommes. 2004. Characterization of Porous Solids and Powders: Surface Area, Pore Size and Density. *Particle Technology Series* Volume 16.

[69] Quantachrome. 2003. Dichtebestimmung von Feststoffen und neue Anwendungen mit dem ULTRAPYCNOMETER 1000T. *Partikelwelt, Aktuelle Fachbeiträge der Quantachrome GmbH* 2:7-8.

[70] Viana, M., Jouannin, P., Pontier, C. and D. Chulia. 2002. About pycnometric density measurements. *Talanta* 57:583-593.

[71] Zundu, L. and H. Yidong. 2004. Qualitative relationship between refractive index and atomic parameters of solid materials. *Journal of Rare Earths* 22(4):486-488.

[72] Marler, B. 1988. On the relationship between refractive index and density of SiO_2-polymorphs. *Physics and chemistry of minerals* 16:286-290.

[73] Susa, M., Kamijo, Y., Kusano, K. and R. Kojima. 2005. A predictive equation for the refractive indices of silicate melts containing alkali, alkaline earth and aluminium oxides. *Glass Technology* 46(2):55-61.

[74] Striebel, F. 2005. Physikalisch-Chemisches Praktikum für Fortgeschrittene. Versuch F32: Dielektrizitätskonstante, Dipolmoment und Molrefraktion. *Institut für Physikalische Chemie Universität Karlsruhe*.

[75] Hamaker, H.C. 1937. The London-Van der Waals attraction between spherical particles. *Physica* 4(10):1058-1072.

[76] Ackler, H.D., French, R.H. and Y. Chiang. 1995. Comparisons of Hamaker Constants for Ceramic Systems with Intervening Vacuum or Water: From Force Laws and Physical Properties. *Journal of Colloid and Interface Science* 179:460-469.

[77] Bergström, L. Hamaker constants of inorganic materials. 1997. *Advances in Colloid and Interface Science* 70:125-169.

[78] Brunauer, S., Deming, L.S., Deming, W.E. and E. Teller. 1940. *Journal of the American Chemical Society* 62:1723-.

[79] Czepirski, L., Balys, M.R. and E. Komorowska-Czepirska. 2000. Some generalization of Langmuir adsorption isotherm. *Internet Journal of Chemistry* 3(14).

[80] Langmuir, I. 1918. The adsorption of gases on plane surfaces of glass, mica and platinum. *Journal of the American Chemical Society* 40:1361-1402.

[81] Yang, Ralph T. 1987. *Gas separation by adsorption processes*. Stoneham: Butterworth Publishers.

[82] Kajszika, Holger. 1998. *Adsorptive Abluftreinigung und Lösungsmittelrückgewinnung durch Inertgasregenerierung*. Dissertation at the Technical University of Munich.

[83] Toth, J. 1971. State equations of the solid-gas interface layers. *Acta Chim. Acad. Sci. Hung.* 69:311-328.

[84] Polanyi, M. 1916. Adsorption von Gasen (Dämpfen) durch ein festes nichtflüchtiges Adsorbens. *Verhandlungen der Deutschen Physikalischen Gesellschaft* 18(4):55-80.

[85] Dubinin, M.M. 1967. Adsorption in Micropores. *Journal of Colloid and Interface Science* 23:487-499.

[86] Dubinin, M.M. 1960. The Potential Theory of Adsorption of Gases and Vapors for Adsorbents with energetically nonuniform surfaces. *Chem. Rev*. 60:235-241.

[87] Jentz, M.A. 2005. *Molecular Modeling of Separations in Silicalite and Crystalline Silicotitanate Systems*. Research Thesis at the University of Notre Dame, Department of Chemical and Biomolecular Engineering in Hall.

[88] Smit, B. and R. Krishna. 2001. Monte Carlo simulations in zeolites. *Current Opinion in Solid State and Materials Science* 5:455-461.

[89] Brandani, F., Ruthven, D. and C.G. Coe. 2003. Measurement of Adsorption Equilibria by the Zero Length Column (ZLC) Technique Part 1: Single-Component Systems. *Industrial & engineering chemistry research* 42(7):1451-1461.

[90] Brandani, F., Ruthven, D. and C.G. Coe. 2003. Measurement of Adsorption Equilibria by the Zero Length Column (ZLC) Technique Part 2: Binary Systems. *Industrial & engineering chemistry research* 42(7):1462-1469.

[91] Harlick, P.J.E. and F.H. Tezel. 2003. Use of Concentration Pulse Chromatography for Determining Binary Isotherms: Comparison with Statically Determined Binary Isotherms. *Adsorption* 9:275-286.

[92] Harlick, P.J.E. and F.H. Tezel. 2004. An experimental adsorbent screening study for CO_2 removal from N2. *Microporous and Mesoporous Materials* 76:71-79.

[93] Levenspiel, Octave. 1972. *Chemical Reaction Engineering Second Edition*. New York: John Wiley & Sons, Inc.

[94] Dilger, H. 2006. *Physikalisch-Chemisches F-Praktikum, Dipolmoment*. Praktikum at the University of Stuttgart, Institut für Physikalische Chemie.

[95] Kuchling, H. 1986. *Taschenbuch der Physik*. Thun and Frankfurt/Main: Verlag Harri Deutsch.

[96] Knerr, R. 1999. *Goldmann Lexikon, Physik, Vom Atom zum Universum*. München: Wilhelm Goldmann Verlag.

[97] Borisover, M.D. and E.R. Graber. 1997. Specific interactions of organic compounds with soil organic carbon. *Chemosphere* 34(8):1761-1776.

[98] van Oss, C.J., Chaudry, M.K. and R.J. Good. 1988. Interfacial Lifshitz-van der Waals and polar interactions in macroscopic systems. Chem. Rev. 88:927-941.

[99] Salem, L. 1960. The calculation of dispersion forces. *Molecular Physics* 3:441-452.

[100] Slater, J.C. and J.G. Kirkwood. 1931. The Van-der-Waals forces in gases. *The physical review* 37(6):682-697.

[101] Bloeß, Harald. 2001. *Erzeugung und Charakterisierung von SiO_2 Nanostrukturen auf Silizium*. Dissertation at the Heinrich-Heine-University Düsseldorf.

[102] Pierotti, R.A. and H.E. Thomas. 1971. Physical adsorption: The interaction of gases with solids. *Surface and Colloid Science* 4:93-259.

[103] Halkier, A. and S. Coriani. 2001. State-of-the-art ab initio calculations of the molecular electric quadrupole moments of hydrogen fluoride. *Chemical Physics Letter* 346:329-333.

[104] Rechid, Juan. 2000. *Elektrische Mikrocharakterisierung von elektrochemisch hergestellten CIS-Solarzellen mittels EBIC*. Dissertation at the University of Oldenburg.

[105] Valenzuela, D.P. and A.L. Myers. 1989. *Adsorption Equilibrium Data Handbook*. New Jersey: Prentice Hall, Englewood Cliffs.

[106] Reid, R.C., J.M. Prausnitz and B.E. Polling. 1988. *The Properties of Gases & Liquids*. Singapore: McGraw-Hill Book Co.

[107] National Institute of Standards and Technology. 2006. *Computational Chemistry Comparison and Benchmark Database*. http://www.nist.gov/ and http://srdata.nist.gov/cccbdb/.

[108] Grace Davison. 2006. *Product Information Sheets for MS5A (Sylobead MS C 522) and 13X (Sylobead MS C 544)*.

[109] University of Wisconsin. 2006. Range of alphas. *Advances Laboratory, Physics* 407.

[110] Sievers, C. 2006. Personal communication: *Experimental set-up for adsorption isotherm measurements at the Department for Technical Chemistry 2 at the Technical University of Munich*.

[111] Al-Baghli, N.A. and K.F. Loughlin. 2006*. Pure and Mixture Gas Adsorption of Light Hydrocarbon on ETS-10 Zeolite*. Chemical Engineering Department, King Fahd University of Petroleum & Minerals.

[112] Klank, D. 2005. Oberflächen- und Porencharakterisierung mit Hilfe von Gassorption und Quecksilberporosimetrie, Teil 5: Die Verwendung alternativer Messgase bei Gassorptionsmessungen. *Partikelwelt, Aktuelle Fachbeiträge der Quantachrome GmbH* 5:8-11.

[113] Lösch, W. *Magnetic Suspension Balances*. Rubotherm Präzisionsmesstechnik GmbH.

[114] Möller, A. 2006. *Personal communication*. Institut für Nichtklassische Chemie, Universität Leipzig.

[115] Talu, O., Zhang, S. and D.T. Hayhurst. 1993. Effect of Cations on Methane Adsorption by Nay, MgY, Cay, SrY, and BaY Zeolites. *Journal of Physical Chemistry 97*:12894-12898.

[116] Bellat, J., Simonot-Grange, M. and S. Jullian. 1995. Adsorption of gaseous p-xylene and m-xylene on NaY, KY, and BaY zeolites: Part 1, Adsorption equilibria of pure xylenes. *Zeolites* 15:124-230.

[117] Choudhary, V.R., Mayadevi, S. and A.P. Singh. 1995. Sorption isotherm of methane, ethane, ethene and carbon dioxide on NaX, NaY and Na-mordenite zeolites. *Journal of the Chemical Society, Faraday Transactions I* 91(17):2935-2944.

[118] Morishige, K., Kittaka, S. and S. Ihara. 1985. Adsorption of methylamines on dehydrated NaX, NaY and KY zeolites. *Journal of the Chemical Society, Faraday Transactions I* 81:2525-2539.

[119] Nitta, T., Suzuki, T. and T. Katayama. 1991. Gas-Phase Adsorption Equilibria for Acetone, Diethylether, methanol, and water on activated carbon fiber. *Journal of Chemical Engineering of Japan* 24(2):160-165.

[120] Klank, D. 2005. Oberflächen- und Porencharakterisierung mit Hilfe von Gassorption und Quecksilberporosimetrie, Teil 5: Die Verwendung alternativer Messgase bei Gassorption. *Partikelwelt, Aktuelle Fachbeiträge der Quantachrome GmbH* (5):8-13.

[121] Suk, Y. 2000. *Characterization of the Physical, Thermal and Adsorption Properties of a Series of Activated Carbon Fiber Cloths*. M. S. Thesis, University of Illinois at Urbana–Champaign.

[122] Mersmann, A. 2006. *Personal Communication*. (TU München, Germany).

[123] Laurin, M. 2005. *Diffusion und Fluktuationen bei der CO-Oxidation an Pd-getraegerten Nanopartikeln*. FU Berlin Digitale Dissertation, http://www.diss.fu-berlin.de/2006/13/index.html.

[124] B.P. Russell and M.D. LeVan. 1997. Coadsorption of Organic Compounds and Water Vapour on BPL Activated Carbon. 3. Ethane, Propane, and Mixing Rules. *Ind. Eng. Chem. Res.* 36:2380-2389.

[125] R. W. Morrison. Overview of Current Collective Protection Filtration Technology. *Guild Associates Inc.Baltimore, Maryland*.

[126] F. Eder and J.A. Lercher. 1997. Alkane sorption in molecular sieves: the contribution of ordering intermolecular interactions, and sorption on Bronsted acid sites. *Zeolites* 18:75-81.

[127] Carbon Materials Research Group from the Center of Applied Energy Research from the University of Kentucky. 2006. *Historical production and*

use of carbonic materials. Internet site http://www.caer.uky.edu/carbon/history/carbonhistory.shtml.

[128] V.L. Lorenz. 1880. *Annualen der Physik* 11:70.

[129] H.A. Lorentz. 1880. *Annualen der Physik* 9:641.

[130] M.M. Dubinin and V.V. Astakhov. 1971. Description of Adsorption Equilibria of Vapors on Zeolites over Wide Ranges of Temperature and Pressure. *Advances in Chemistry Series* 102:69-85.

[131] U. Münstermann. 1984. *Adsorption von CO_2 aus Reingas und aus Luft am Molekularsieb-Einzelkorn und im Festbett - Berücksichtigung von Wärmeeffekten und H_2O-Präadsorption*. Dissertation at the Technical University of Munich.

[132] Gerthsen, Kneser, Vogel. 1977. Gerthsen Physik. Berlin Heidelberg New York Tokio: Springer.

[133] D. Pan. 1992. *Untersuchungen zur Adsorption von Gasen am Zeolith ZSM-5*. Dissertation at the Technical University of Munich.